

NOISE IN NONLINEAR MICRO-RESONATORS

By

Nicholas Miller

A DISSERTATION

Submitted to  
Michigan State University  
in partial fulfillment of the requirements  
for the degree of

DOCTOR OF PHILOSOPHY

Mechanical Engineering  
Physics

2012

**ABSTRACT**  
**NOISE IN NONLINEAR MICRO-RESONATORS**

By  
**Nicholas Miller**

In this work we examine several noise-induced phenomena that are found in nano- and micro-electromechanical systems. Our aim is to exploit these phenomena, where possible, for system identification and sensing applications. The exception being our discussion of nonlinear oscillators, where our goal is to remove the effect of noise as much as possible. In general, however, our viewpoint is one of embracing the noise and nonlinearity that are an inevitable part of miniaturization and seek new modes of micro- and nano-system operation applicable where noise and nonlinearity are fundamentally unavoidable.

In this work we discuss three different, but related, topics. First, we discuss the dynamics of a system subject to a parameter sweep through a bifurcation in the presence of noise. We develop approximate distributions for the time at which a system swept through a subcritical pitchfork or a saddle-node bifurcation will leave the local region of phase space, leading to a sudden jump in response amplitude. These distributions are developed in the limit of “fast” sweeping, where the sweep rate is large compared to the noise strength, which is relevant to most MEMS applications. We then present the results of sweeping experiments performed on a MEMS resonator and show the value of our analytic predictions. Our primary conclusion is that delayed bifurcation is prominent in MEMS devices, and we provide predictive tools for predicting the resulting distribution of jump events.

Next, we consider a novel dynamical bridge sensing paradigm. This sensing methodology employs a vibrating bistable system arranged, by tuning of parameters, such that the rate of noise-activated escape out of the two stable basins of attraction are identical. The ratio of occupation probabilities can become extremely sensitive at

this point when the noise is weak. We calculate the sensitivity and detection time of the balanced dynamical bridge for use as a general use detector and we develop the conditions required and demonstrate its application as a detector of non-Gaussian noise. We illustrate the measurement of the parameters of a shot-noise process using a one-dimensional bridge model.

Finally, we discuss phase noise in oscillators employing nonlinear frequency selective elements. We employ the method of averaging to develop an expression for the spectrum of fractional frequency fluctuations in an oscillator. The expression for the spectrum of frequency fluctuations is quite general, although it neglects dynamics in the feedback elements of the oscillator. The expression contains elements of the noise model and the nominal limit cycle shape of the oscillator. We demonstrate the utility of the results by exploring the parameter space of a prototypical oscillator modeled by a biased Duffing equation. We find that one can reduce the phase diffusion constant of the oscillator by tuning the system to a zero-dispersion point of the resonator element, thus eliminating the action-angle coupling at zero-dispersion points of the resonator frequency can lower the phase diffusion constant.

## ACKNOWLEDGMENT

First and foremost, this work could not have been accomplished without the efforts of my advisors: Professor Steven W. Shaw and Professor Mark I. Dykman. Beyond the technical guidance and instruction Professors Shaw and Dykman have been mentors and exemplars of scientific integrity. I am honored to have had the opportunity to work with them both. The example set by these gentlemen will continue to guide me for the remainder of my career. Thanks also to the committee who oversaw this work; Professor Brian Feeny, Professor Norman Birge, and Professor Jongeun Choi. I have had the good fortune to collaborate with Professor Kimberly L. Turner and Chris Burgner of UCSB. I would like to thank Chris for his creativity, grounding practicality, and hard work. Collaborating with him has been very educational and enjoyable. I am indebted to my fellow lab-mates and former lab-mates for many meaningful discussions about various interesting academic problems. These include Jeff Rhoads, Umar Farooq, Ryan Monroe, Brendan Vidmar, Venkat Ramakrishnan, and Pavel Polunin. I would especially like to thank Scott Strachen who is always ready to discuss some sticky point of condensed matter physics or philosophy or anything else. Our conversations have been particularly useful and enjoyable. Finally, I would like to thank the funding agencies that made this work possible. The National Science Foundation under grants CMMI-0758419 and CMMI-0900666 and the Defense Advanced Research Agency under the DARPA-MTO-DEFYS project.

# TABLE OF CONTENTS

<b>List of Figures</b>	vii
<b>1 Introduction</b>	<b>1</b>
1.1 MEMS and NEMS	2
1.2 Noise and Nonlinearity	4
1.3 Noise-Induced Phenomena	6
1.4 Summary of Results	16
<b>2 Escape Statistics for Parameter Sweeps Through Bifurcations</b>	<b>19</b>
2.1 Stochastic Normal Forms	21
2.2 Kramers Escape Rate	26
2.3 Escape Near a Saddle-Node Bifurcation	30
2.4 Escape Near a Subcritical Pitchfork Bifurcation	39
2.5 Subcritical Pitchfork Bifurcation in a MEMS Resonator	47
2.6 Outlook	54
<b>3 The Dynamical Bridge</b>	<b>56</b>
3.1 Activated Escape	59
3.2 Dynamical Bridge Sensitivity	61
3.3 Detection of Non-Gaussian Noise	64
3.4 The Duffing Resonator Bridge	67
3.5 Shot Noise Measurement	71
3.6 Outlook	76
<b>4 Phase Noise in Nonlinear Oscillators</b>	<b>78</b>
4.1 Action-Angle Coordinates	81
4.2 Microscopic Resonator Model	84
4.3 Oscillator Frequency Fluctuations	92
4.4 The Biased Duffing Oscillator	100
4.5 Outlook	109
<b>5 Conclusions</b>	<b>110</b>
<b>A Stochastic Processes</b>	<b>114</b>
A.1 The Kinetic Equation for a Stochastic Process	114
A.2 The Langevin Equation	118
A.3 Ito and Stratonovich Integrals	121

<b>B Stochastic Averaging</b>	<b>126</b>
B.1 A Near-Identity Coordinate Transformation	128
B.2 Stochastic Averaging Part I: $\mathcal{O}(\epsilon^{1/2})$	129
B.3 Stochastic Averaging Part II: $\mathcal{O}(\epsilon)$	132
B.4 Time Scaling	134
B.5 Approximation by a Markov Process	136
<b>C Derivation of Equation (2.65)</b>	<b>140</b>
Bibliography	150

## LIST OF FIGURES

1.1	Activated escape in one dimension. . . . .	6
1.2	Most probable paths (dashed lines) of activated escape in a two dimensional system. Invariant stable and unstable manifolds (solid lines) represent underlying noise free dynamics. . . . .	10
2.1	Example potential governing normal form dynamics. . . . .	26
2.2	Illustration of the evolution of the potential (a), and the standard bifurcation diagram (b), for a saddle-node bifurcation. . . . .	30
2.3	$c_\infty$ boundary for linear sweeping, $\mu(t) = \mu_0 + rt$ , with $\mu_0 < 0$ . The first two branches are shown along with the variance (shaded region) of $c$ for $\epsilon^2 = 0.05$ . . . . .	35
2.4	Mean (a), variance (b), and sample distributions (c) of the escape time away from a swept saddle-node bifurcation. Numeric solution (solid line) and approximations (dashed) for fast and slow sweeping are shown. . . . .	38
2.5	Illustration of the evolution of the potential (a), and the standard bifurcation diagram (b), for a subcritical pitchfork bifurcation. . . . .	39
2.6	Mean (a), variance (b), skewness (c), and example distributions (d) of the distribution of escape times away from a swept subcritical pitchfork bifurcation. Numeric solution (solid lines) and approximations (dashed) for fast and slow sweeping are shown. Dots represent data points from Monte-Carlo simulations of the nonlinear Mathieu equation, equations (C.17) and (C.17), swept through the subcritical pitchfork bifurcation. . . . .	46

2.7	(a) SEM of MEMS gyroscope [89]. (b) Amplitude and phase of drive axis vibration during an example escape event under parameter sweep. For interpretation of the references to color in this and all other figures, the reader is referred to the electronic version of this dissertation. . . . .	48
2.8	(Top) Frequency response for the MEMS resonator. Blue data points track the sweep up and red data points track the sweep down. The green data points represent the mean jump frequency for various sweep rates. Black lines represent fitted stable (solid) and unstable (dashed) frequency response branches. (Bottom) Real and imaginary parts of the eigenvalues belonging to the fixed point at zero. Dashed line represents the linear sweep approximation. . . . .	51
2.9	Experimentally measured distributions of escape events for ambient noise and sweep rates ranging from 0.005 to 0.3 Hz/sec. The inset shows one such distribution, artificially shifted, and compared against the theoretical distribution. The purpose of the shift is discussed in the text. The three distributions in the inset correspond each to different sweep rate and noise intensities yet all three with the same ratio. This illustrates that, while the normalized statistics depend only on the ratio, the true statistics depend on both values. . . . .	52
2.10	Normalized mean (a) and variance (b) of the bifurcation parameter at escape. The solid line represents the mean of the distribution for a linear sweep predicted from the normal form, as given in equation (2.62). The data points were calculated from the measured distributions shown in figure 2.9. . . . .	54
3.1	The blue and magenta lines depict heteroclinic solutions connecting the operation points to the saddle point for system (3.43), as projected onto the $(q_1, q_2)$ plane. Solid lines represent the $p \neq 0$ solutions and the dashed lines are the noise-free ( $p = 0$ ) stable and unstable manifolds of the saddle point. Parameter values: $\Omega = 4.706182$ and $\beta = 8.501802$ . . . . .	70
3.2	Heteroclinic solutions for system (3.43) projected onto the $(p_1, p_2)$ plane. For the solution with $\Omega = 4.706182$ and $\beta = 8.501802$ . Note that these heteroclinics start and end at noise-free points where $p_1 = p_2 = 0$ . . . . .	71



3.3	Two dimensional parameter space for the Duffing resonator. Solid lines are saddle-node branches which enclose the bistable region. The dashed line is the balance curve on which the escape actions for two stable states are equal, $S_1 = S_2$ . In the weak noise limit this line is very close to the line where the escape rates are equal. . . . .	72
3.4	Double-well potential of equation (3.45); $q_1$ and $q_2$ denote positions of stable fixed points, while $q_S$ refers to the unstable fixed point. Poisson pulses with positive area $g$ change the switching rates such that $r_1 > r_2$ , resulting in a shift of the occupation probability from $q_1$ towards $q_2$ . 73	73
3.5	Change in probability ratio due to the addition of zero mean shot noise, equations (3.53). Data are results from Monte-Carlo simulations with $D = 0.04$ and $\nu = 0.5$ . The inset shows the same quantities over a larger range. . . . .	75
4.1	Noise roadmap (a) illustrating the different routes by which fluctuations may affect the angle. Prototypical oscillator block diagram (b). 79	79
4.2	Illustration depicting how noise is filtered and down-converted. The noise is selected near the oscillator harmonics, that is, in the shaded regions, weighted by the Fourier coefficients in equation (4.51), and modulated down to baseband by the oscillator motion. . . . .	97
4.3	Frequency dispersion for the biased Duffing resonator for several values of the bias. Red dashed line is the locus of critical (zero dispersion) points. . . . .	101
4.4	Several closed orbits belonging to the potential (4.65) with (a) $\lambda = 0$ and (b) $\lambda = 4$ . . . . .	102
4.5	The logarithm of the normalized long term phase diffusion coefficient, $\log_{10}(S_y(0)/D_{\text{env}})$ , as a function of operating action and bias force. Dashed white line is the locus of zero dispersion ( $\partial_I \omega(I) = 0$ ) points. For interpretation of the references to color in this and all other figures, the reader is referred to the electronic version of this dissertation. . .	108
4.6	Mean oscillator frequency as a function of operating action and bias force. Dashed white line is the locus of zero dispersion ( $\partial_I \omega(I) = 0$ ) points. For interpretation of the references to color in this and all other figures, the reader is referred to the electronic version of this dissertation. 109	109

# Chapter 1

## Introduction

It is well known that small fluctuations in nonlinear systems can have large repercussions in terms of the system response. One means by which this occurs is noise activated escape, where a series of pulses from a weak noise source may conspire in such a way as to push a system out of a potential well. For small noise, this process is a rare event which can be described by an average rate of occurrence. For classical systems the rate,  $W$ , of activated escape is given by the Arrhenius law [100]

$$W \propto \exp(-R/D), \tag{1.1}$$

where  $R$  is the activation energy and  $D$  is the noise strength. From this expression, we can see, for small noise (small  $D$ ), that a small change in the activation energy,  $\Delta R$ , corresponding to a small change in the system or its environment, can produce a large change in  $W$  if the ratio  $\Delta R/D$  is not small. This change in escape rate is described as a logarithmic susceptibility [100], a nomenclature which implies that the logarithm of  $W$  changes linearly with respect to a small perturbation acting on the system. Thus highly sensitive measurements can be, and have been [2, 91, 116, 77], made using the principle of activated escape. However, the full utility of such measurements in

the field of MEMS and NEMS has yet to be explored. The aim of this work is to investigate noise phenomena in micro- and nano- electromechanical systems (MEMS and NEMS). This includes the investigation of noise activated escape in N/MEMS resonators for sensing, analysis of noise-dispersed delayed bifurcations for bifurcation point detection, and phase diffusion in N/MEMS based nonlinear oscillators.

In this chapter we provide motivation and a brief overview of the main contributions described in this dissertation. In section 1.1 MEMS and NEMS are introduced and demonstrated to be a rich and interesting area of research. In section 1.2 we discuss the intrinsic nature of noise and nonlinear dynamics in MEMS and NEMS that makes them an appropriate area in which to exploit noise induced phenomena in nonlinear dynamic systems. In section 1.3 we give introductions to the phenomena that are the primary foci of this work: noise activated escape, delayed bifurcations, noise in slow-fast systems, etc. In section 1.4 we give a summary of the major contributions of this work.

## 1.1 MEMS and NEMS

The field of microelectromechanical systems (MEMS) emerged during the years between the 1960s to 1980s, arising from the integrated circuit industry [75]. It has since expanded rapidly, driven by commercial successes and the development of new enabling technologies. The ability to fabricate even smaller and smaller devices has led to the related field of nanoelectromechanical systems (NEMS) [26, 41]. The ability to batch fabricate such small mechanical structures and integrate them with electronics has had a large impact on both commercial electronics and research in fundamental physics alike. Devices such as pressure sensors, accelerometers, gyroscopes, ink jet printer nozzles, and DLP projectors have found a great deal of success in the commercial arena [75]. Devices such as cell sorters, retinal and cochlear implants, neural

probes, and other *in vivo* sensors have had significant impact on biological research [51]. Atomic force microscopy [13] and the use of nanoresonators to probe mesoscopic electrical systems [24, 116, 6] have had significant impact on fundamental and applied physics research. The list goes on, but this is sufficient to make the point that the field of MEMS and NEMS is rich and promising.

MEMS and NEMS can generally be split up into various subfields including sensors, actuators, and signal processing devices such as filters and oscillators. In this work, we focus on sensors and oscillators, specifically, systems that rely on vibration for operation.

The oscillators we consider employ nonlinear resonators as frequency selective devices. These resonators are models of N/MEMS devices. Our goal is to optimize the oscillator performance, in terms of phase noise, by tuning the feedback parameters and designing the nonlinearity in the N/MEMS resonators.

The sensors we consider are parametric sensors. A parametric sensor is a general type of sensor in which the signal to be detected influences the dynamic behavior of the sensing device. The system is then interrogated to retrieve the signal. Examples include gyroscopes [71] and resonant chemical mass sensors [118]. Gyroscopes encode the rotation rate in a coupling parameter that governs the interaction between two resonant modes of vibration. These two modes are designed to have identical natural frequencies and to be uncoupled save for the coupling arising from Coriolis effects. One mode is driven, and the other is monitored, or sensed. The amplitude of vibration of the sensed mode is then correlated with the rotation rate of the gyro. Resonant chemical mass sensors encode the mass of the substance being detected in the natural frequency, specifically by shifts in the natural frequency, of a resonator. This is typically monitored using a self-excited oscillator scheme based on a phase locked loop [40, 49]. In such a setup, the resonator is made to oscillate at its natural frequency via feedback, and the frequency of oscillation is monitored and correlated with the

measured mass.

While the above examples of dynamical sensors employ linear dynamic systems, nonlinear dynamics systems are often exploited for properties that might either avoid the problems inherent in the linear systems, attain more sensitivity, or simply provide functionality that is not possible with linear systems. For example, Oropeza-Ramos *et al.* constructed a gyroscope that employs nonlinear dynamics to circumvent the difficulty of matching the modal frequencies of its drive and sense modes [89]. Buks and Yurke explored the idea of using nonlinear dynamics in a chemical mass sensor to increase sensitivity by operating at a point of infinite slope in the frequency response curve [15]. A frequency response with infinite slope can only be produced by a nonlinear system. It was found that the increase in sensitivity came at the price of a slower response time. For a more complete review of applications of nonlinear dynamics in MEMS and NEMS, see [73, 92].

## 1.2 Noise and Nonlinearity

The use of nonlinear dynamics in MEMS and NEMS is in no way artificial. Such small devices are subject to significant thermal and electrical noise forces. Accordingly, it is often necessary to drive the devices hard enough to elicit a nonlinear response in order to obtain a response with good signal to noise ratio. It is by virtue of the smallness of these devices that the linear dynamic range is made small and one must account for the noise and nonlinear effects. To illustrate this, consider the following simple example. The equation describing a simple harmonic oscillator coupled to a thermal bath is [26]

$$m\ddot{x} + m\omega_0^2 x = -\frac{m\omega_0}{Q}\dot{x} + \sqrt{\frac{2m\omega_0 k_B T}{Q}}\xi(t), \quad (1.2)$$

where  $x$  is the displacement,  $m$  is the mass,  $\omega_0$  is the natural frequency,  $Q$  is the quality factor,  $k_B$  is Boltzmann's constant,  $T$  is the temperature, and  $\xi(t)$  is a white Gaussian noise force with  $\langle \xi(t)\xi(t') \rangle = \delta(t - t')$ . The noise force,  $\xi(t)$ , and the dissipative force,  $-\frac{m\omega_0}{Q}\dot{x}$ , result from coupling of the resonator to the environment and are responsible for keeping the oscillator in a state of thermal equilibrium. Dividing equation (1.2) through by  $m$  gives

$$\ddot{x} + \omega_0^2 x = -\frac{\omega_0}{Q}\dot{x} + \sqrt{\frac{2\omega_0 k_B T}{mQ}}\xi(t). \quad (1.3)$$

As devices are made smaller the mass,  $m$ , clearly must decrease if we continue to use the same materials. The quality factor,  $Q$ , also tends to decrease [81, 74, 43]. Meanwhile, the natural frequency,  $\omega_0$ , tends to increase. Thus, we can see from (1.3) that as devices decrease in size, the effective noise strength increases. Meanwhile, for a fixed-fixed beam, for example, the amplitude of vibration corresponding with the onset nonlinearity goes as  $tQ^{-1/2}$ , where  $t$  is the thickness of the beam [41]. This upper limit of linear dynamic range will decrease with device size if  $t$  decreases faster than  $Q^{1/2}$ . While it is unclear what the result of this competition is in general, we can concede that for many small devices the linear dynamic range is not large. Thus, in order to take advantage of the many attractive properties of small devices, one must consider models that go beyond the linear dynamic range and account for both nonlinear effects and random forcing. In this simple example, we have only considered thermal noise acting on the oscillator. However, MEMS and NEMS devices are often subject to additional noise sources. The reader is referred to [41] for a more complete discussion of linear dynamic range in NEMS, and to [25, 82] for a review of noise in MEMS and NEMS.

The host of phenomena created by the interplay of random fluctuations and nonlinearity in dynamic systems is quite large. In this work we will only touch on a

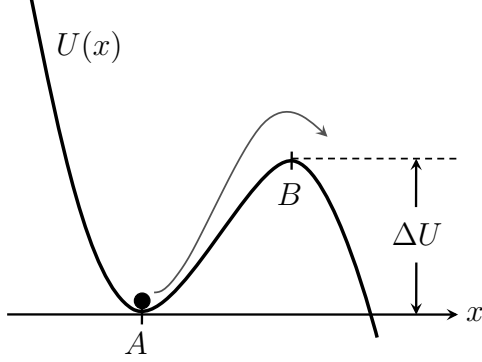


Figure 1.1: Activated escape in one dimension.

few examples, all of which can be found in nonlinear MEMS or NEMS resonators subject to noise, but they are also relevant to other physical systems of interest. In the following section we will introduce the phenomena of interest and cite some of the other interesting contexts in which they arise.

### 1.3 Noise-Induced Phenomena

Perhaps the most basic noise-induced phenomenon is diffusion. Diffusion arises from the sum of a large number of random variables. The value taken by this sum is itself random with a variance that grows with the number of variables in the sum. Brownian motion is one example [39]. Brownian motion can be illustrated by a particle suspended in a fluid. The random force acting on the particle resulting from many collisions with the fluid molecules is integrated in time to produce a wandering trajectory. A similar situation occurs in clocks [72]. A clock cannot have knowledge of a reference point in true time and so random perturbations on the clock accumulate causing the phase to diffuse. This results in the clock's estimate of true time drifting. Quartz and MEMS clocks are ubiquitous in electronic devices and the reduction of phase noise in these clocks can have significant impact on communication and navigation for example.

Another very important noise-induced phenomenon is activated escape. As men-

tioned above, activated escape is a rare event where a series of noise pulses drives a system out of a confining potential well, or metastable state. To understand this in more detail, but still from a qualitative perspective, it is helpful to consider a simple one dimensional case. Suppose we have a particle trapped in a potential well, as illustrated in figure 1.1, and subject to a random force. In the overdamped limit, the particle behaves as if it has no inertia and its dynamics are captured by the Langevin equation

$$\dot{x} = -U'(x) + \xi(t) \quad (1.4)$$

where  $U(x)$  is the potential and  $\xi(t)$  is the random force. If the noise,  $\xi$ , is small, and the particle starts inside the potential well, then it will very likely relax to near the bottom of the well at point  $A$ . The particle will then rattle around the vicinity of point  $A$  for some time as the noise pushes it back and forth. On occasion a rare large outburst of noise may overcome the potential force,  $-U'(x)$ , and push the particle up and over the hill, past point  $B$ . It will then roll down the hill and will have thus escaped the potential well. If the probability of such an outburst is nonzero, then it will inevitably occur, if one waits long enough. The question is: what are the statistics of the escape times for a given noise process? We can answer this question for a few cases. The simplest of which is where  $\xi(t)$  is a white Gaussian noise. Considering this case, we take  $\langle \xi(t) \rangle = 0$  and  $\langle \xi(t)\xi(t') \rangle = 2D\delta(t - t')$ . This is just restating that  $\xi$  is white and adding that it has zero mean and the strength of this noise is  $2D$ , which we assume to be small. The escape rate,  $W$ , in this case is given by the celebrated Kramers result [64, 93]

$$W = \frac{1}{2\pi} \sqrt{U''(x_A)|U''(x_B)|} \exp \left[ -\frac{\Delta U}{D} \right]. \quad (1.5)$$



A rate of this form is often referred to as an Arrhenius equation, or Arrhenius law, which gives the rate constant,  $k$ , of chemical reactions in terms of the temperature,  $T$ , and activation energy,  $E_a$ ,

$$k = A \exp \left[ -\frac{E_a}{RT} \right] \quad (1.6)$$

where  $A$  is the prefactor and  $R$  is the gas constant.

Near a simple bifurcation point with a zero eigenvalue the dynamics of a system, e.g., a noisy nonlinear resonator, squeeze down onto a one dimensional slow manifold, under certain conditions [62, 19]. If a resonator is operated just before a saddle-node bifurcation, for example, the dynamics are governed by a one dimensional equation with a potential similar to that shown in figure 1.1. Such systems are used in the readout of superconducting quantum bits, or *qubits*. Readout of qubits is difficult with conventional amplifiers because the amplifier must minimally disturb the system while maintaining high sensitivity [98]. However, a method proven to be successful is to employ what is called a *Josephson junction bifurcation amplifier* [98, 97, 116, 78, 76]. The method is to operate a Josephson junction in a bistable regime near a saddle-node bifurcation. The Josephson junction is used because “the superconducting tunnel junction is the only electronic dipolar circuit element whose nonlinearity remains unchanged at arbitrary low temperatures” [98]. The resonator is coupled to the qubit so that the actual position of the bifurcation point depends on the qubit state. In other words, the height of the energy barrier preventing escape depends on the qubit state. The resonator is operated in one of its states near the bifurcation point, held there for some time. It is then backed away from the bifurcation point, after which the state of the resonator is measured. If activated escape occurs in the resonator, that is, the response switches from one metastable state to the other, the amplitude and phase of the resonator will be found to have been changed. Because the probability

of such a state switch in the resonator by activated escape is related to the state of the measured qubit through the energy barrier, the state of the qubit can be inferred with some degree of confidence by determining whether or not the resonator switched during the measurement time.

Josephson junctions are commonly used in many practical uses of activated escape, because this switching phenomenon is intrinsic in their behavior. In the early study of the Josephson junction, it was found that the low current features of the current-voltage relationship across the junction, which are not predicted by a noise-free theory, are the result of activated escape events in a potential shaped like a tilted washboard [4, 102]. Thus, Josephson junctions make excellent test-beds for experimental observation of escape phenomena, including so-called resonant activation [28], and switching between dynamic states over a dissipation barrier [117]. The washboard potential of a current biased Josephson junction is of the form

$$U(x) = -ax - \cos x, \tag{1.7}$$

which is analogous to a classical pendulum subject to a constant torque. When operated in the overdamped regime, these devices exhibit activated escape in one dimension, similar to the discussion above. The use of these junctions was proposed for the experimental measurement of the full counting statistics of electrical current [109]. However, the details of such an experiment prevent the use of the overdamped regime, requiring underdamped junctions to be used instead [105, 88]. Nevertheless, the third cumulant of the current fluctuations can be measured from one dimensional escape event statistics [56, 70] using the asymmetry of the switching rate with respect to the bias current. In the study of current fluctuations using activated escape, the random force is no longer white and Gaussian, but has an arbitrary set of cumulants that we are trying to measure. The problem of escape due to an arbitrary noise force

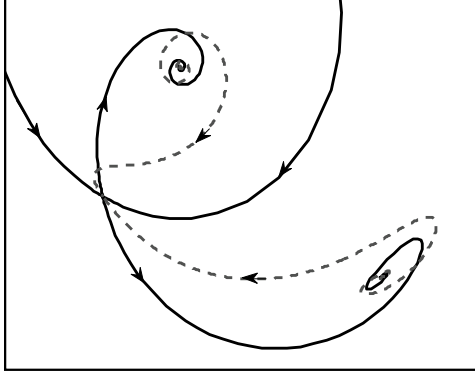


Figure 1.2: Most probable paths (dashed lines) of activated escape in a two dimensional system. Invariant stable and unstable manifolds (solid lines) represent underlying noise free dynamics.

is still open. However, the problem of poisson noise induced escape in one dimension has been recently solved [31].

Activated escape out of a multidimensional basin of attraction, as in the case of the underdamped Josephson junction, is more complex than escape in one dimension. For the underdamped Josephson junction the basin is two-dimensional, where the dimensions are the system coordinate and conjugate momentum. The coordinate in this case is the phase difference of the superconducting order parameters across the junction. The added complexity in the multi-dimensional case comes from the necessity to consider the path of escape in the higher dimensional phase space. In the one dimensional case we know the system must travel from point  $A$  to point  $B$ , from the local potential minimum to the local maximum, and it can only do so in a straight line. In the multidimensional case the escape event occurs along some path through phase space [37]. In the case of small noise, these paths are tightly packed around an optimal path which can be found by solving the variational problem for the most probable path. Such paths have been experimentally observed in MEMS resonators [21, 20]. Nevertheless, there are details that prevent a complete solution of the escape problem. The escape rate can only be found up to an approximately constant pre-factor. Escape in distributed systems amounts to escape in infinite dimensions. This

phenomenon arises in nucleation [100] at the onset of changes in thermodynamic phase, for example, in boiling. Figure 1.2 shows an example of optimal paths of escape for a bistable two dimensional system (described in more detail in Chapter 3). The figure shows the invariant manifolds (solid lines) of the saddle point in a system containing one saddle and two stable foci. The invariant manifolds give a picture of the underlying noise free dynamics. The stable manifold of the saddle point divides the phase space into the basins of attraction of the two stable points. Escape occurs when noise drives the system across this line. For weak noise, the escape events traverse paths very close to the optimal escape paths, the first segments of which are shown as dashed lines in the figure. Once the neighborhood of the saddle point is reached along such a path, the system will ride a trajectory close to one of the branches of the unstable manifold of the saddle point, and either escape or return to the region from which it started.

An interesting situation, related to the above, is escape out of a time varying potential well. Examples include periodically modulated systems [32] and systems swept through a bifurcation, where the potential well may vanish, as in the saddle-node or subcritical pitchfork bifurcations, or split into two wells, as in the supercritical pitchfork. Stochastic-dynamic bifurcations are particularly interesting candidates for application in MEMS and NEMS devices as they can easily be employed for device interrogation by setting up simple parameter sweeping experiments. The concept of a bifurcation in a stochastic system must be treated somewhat delicately, however. The reason is that, unlike a deterministic system, the solution of a stochastic system, described by a probability distribution over phase space, does not undergo any sudden change in form or structure as a function of the system parameters. Therefore, in some sense, the concept of a bifurcation point in a stochastic system is meaningless and the notion must be replaced with a bifurcation region [79]. Still, the underlying deterministic drift in a stochastic system still retains the structure of a deterministic

system, and so we can speak of the bifurcation points of a corresponding noise free system. In this work this is the perspective we take. When we speak of an escape event occurring before or after the bifurcation point, we mean that it occurs at a time during the sweep before or after the bifurcation of the deterministic drift term. For the present investigation, a suitable partition of stochastic-dynamic bifurcations is to distinguish between the concepts of escape before (activated escape) or after (delayed bifurcation) the noise-free bifurcation point is reached.

Escape before the bifurcation point in a swept system occurs with very high probability when the system is swept in a quasi-static fashion. That is, when the time-rate of change of the potential well is much slower than the escape attempt frequency. For small noise intensity a system will form a quasi-stationary distribution at the bottom of a potential well. Only rarely does a large noise pulse come along that pushes the system farther away from the minimum than the width of this quasi-stationary distribution. The escape attempt frequency is the rate of occurrence of these large noise pulses. Only a few of these large pulses will be large enough to cause escape. In this limit of slow change with respect to the escape attempt frequency, the escape rate in a time-varying potential can be well approximated by the quasi-static rate. For example, if we have a time-varying quasi-static escape rate,  $W(t)$ , then the probability to escape at time  $t$ ,  $P_e(t)$ , is governed by the differential equation

$$\dot{P}_e(t) = W(t)(1 - P_e(t)). \quad (1.8)$$

If we take initial conditions  $P_e(t_0) = 0$ , i.e. assume that the system starts inside the potential well, then the solution to equation (1.8) is

$$P_e(t) = 1 - \exp \left[ - \int_{t_0}^t W(t') dt' \right]. \quad (1.9)$$

Measuring the distribution  $P_e(t)$  by many repeated sweeping experiments can be a useful tool for gaining information about a system in the vicinity of a bifurcation point. For example, this experimental technique has often been employed in the study of switching fields in magnetic material, which has applications in magnetic recording media [115], high speed magnetoelectronics [63], and magnetic RAM cells [106] among other things. In the late 1980s a fundamental question was determining the power law dependence of a coercive field strength, as measured from the critical field, on the switching rate for a single particle magnet. The original model, due to Néel [115], suggested a power law dependence of  $(\Delta H)^2$ . However, the refined Néel-Brown model, suggested a dependence of  $(\Delta H)^{3/2}$  [120]. Another relevant issue is whether switching dynamics actually follow a simple Arrhenius law, or is it more complicated? Experimental confirmation of the  $3/2$  dependence and agreement with Arrhenius law was obtained using sweeping experiments [120] following the theory of Kurkijärvi [67]. However, in submicron-sized magnetic thin films a different behavior is observed. Activated escape experiments, where the system is placed close to the bifurcation point, and then the time until switching is recorded, showed that the behavior in magnetic thin films can be explained as an “energy ladder” wherein the system climbs through repeated thermally activated escape events up a ladder of states of increasing energy [63]. In [106] the authors use sweeping experiments to characterize the switching dynamics of submicron magnetic tunneling junctions, used in magnetic RAM cells, and found the Arrhenius law to hold. In [84, 65] the authors use thermally activated escape to experimentally investigate magnetic reversal due to spin-polarized currents. In [119] the authors use sweeping experiments based on the theory of Kurkijärvi [67] to determine the magnetic properties of single-molecule magnets: the energy barrier, magnetic anisotropy constant, spin, and crossover temperature from classical to quantum regime.

Similar sweeping experiments have also been used to study superconducting inter-

ference devices (SQUIDs), atomic friction, and rare molecular events such as protein unfolding and ligand dissociation. The study of escape is important in determining limits of sensitivity of weak link superconducting devices [47], such as SQUIDs, which are very sensitive magnetometers. In a superconducting ring with a weak link junction, however, the fluctuations in the internal flux can be very small. Thus, it proves convenient to investigate such systems through dynamic bifurcation or sweeping experiments [67, 58]. In experimental studies of friction between two surfaces, a friction microscope is used where a tip is dragged at constant slow velocity across a surface. The tip exhibits stick-slip behavior which can be described by activated escape out of a diminishing potential well [95, 83], similar to the magnetic and superconducting ring experiments mentioned above. This rate-state model for atomic friction is, of course, just one of many models for friction [113]. In the study of rare molecular events, pulling experiments are often used [57]. The technique is also referred to as dynamic force spectroscopy [29]. These experiments are carried out by using an atomic force microscope or laser tweezers to pull on an anchored molecule via a pulling spring, possibly a linker molecule, until some molecular transition occurs, e.g. unfolding, unwrapping, or dissociation. These experiments are also analogous to the sweeping experiments discussed above.

Escape after the bifurcation point occurs with high probability when the sweep rate is sufficiently fast such that the time it takes the system to respond in a significant way is greater than the time it takes to sweep past the bifurcation point. This occurs with certainty in situations where the bifurcating fixed point is stable and not metastable before the bifurcation point [87]. The concept of escape, when discussing escape after the bifurcation point, is, however, somewhat poorly defined because after the bifurcation point there is typically no longer a well defined region from which the system can be said to have escaped. This phenomenon is also called delayed bifurcation, though this term is usually used in the literature to refer to

the noise free situation. The term delayed bifurcation is also ambiguous as there is no well defined counter-part to the static bifurcation point in the swept (time varying) system. Thus multiple different definitions for the bifurcation time have been suggested. These include first threshold crossing time [104, 110], last threshold crossing time [59], time at which the variance of escape trajectories reaches a threshold [122, 14], and time of escape to infinity. The latter definition is employed in the present investigation, and to our knowledge, it is not used by anyone else. One reason for this might be that the bulk of the literature addresses delayed bifurcation in noisy systems that are globally bounded, since the systems considered exhibit supercritical pitchfork or Hopf bifurcations. Both of these bifurcations have one stable equilibrium before the bifurcation, and after the bifurcation this equilibrium is unstable, and there exist stable states that emerge from this equilibrium at the bifurcation. In the case of the supercritical pitchfork, the stable post-bifurcation states are a symmetric pair of stable equilibria, as in bucking of a symmetric elastic beam. In contrast, the supercritical Hopf bifurcation gives rise to a stable periodic orbit. The literature focuses on these supercritical bifurcations because they describe the important problem of laser turn-on [107, 103, 104, 122, 110, 111, 14]. These bifurcations can also be used to describe the firing of neurons [59]. In contrast, the saddle-node and subcritical pitchfork bifurcations we consider in this work both exhibit metastable states before the bifurcation and escape from the region of this state after the bifurcation. The time of escape to infinity is finite for the generic local models of these bifurcations. Since these bifurcation models describe a local picture of the dynamics of the full system model in the region of interest (in both the phase space and parameter space), the (finite) time of escape to infinity for the local models provide good estimates of the times of escape from the local region.



## 1.4 Summary of Results

In this work we discuss three different, but related, topics. The first topic is the dynamics of a system subject to a parameter sweep through a bifurcation in the presence of noise. This topic is examined in chapter 2. In this chapter we review the normal form models of dynamic systems near bifurcation points. We then review noise-activated escape in one-dimensional systems subject to white Gaussian noise. Our primary contributions follow this review material. We first develop approximate distributions for the time at which a system swept through a subcritical pitchfork or a saddle-node bifurcation will leave the local region of phase space. The general problem must be solved numerically, and we do so for comparison with the approximate solution. Our approximate expressions for these distributions are developed in the limit of “fast” sweeping. We determine that the ratio of sweep rate to noise strength is the important parameter condition that separates fast and slow sweeping. These results are compared with the numerical solution of the general case. We then present the results of sweeping experiments performed on a MEMS resonator, carried out in collaboration with colleagues at the University of California-Santa Barbara. Our primary conclusion is that delayed bifurcation is prominent in MEMS devices. While small, the noise levels we expect to see in MEMS devices is not large enough to cause an activated escape event before the bifurcation is reached, unless the sweep rate is extremely slow, to the point of being infeasible for some devices. Therefore, understanding this phenomenon is important if one wishes to locate the bifurcation point for system identification, sensing, or for use as a bifurcation amplifier. We however also conclude from our study that performing many sweeping experiments is an overly time-consuming way to retrieve information from a MEMS resonator. Ongoing work makes use of feedback to track the bifurcation point for bifurcation-based sensing strategies [17].

Our second topic is the novel dynamical bridge sensing paradigm, which we discuss in chapter 3. This sensing methodology employs a bistable system arranged such that the rate of noise-activated escape out of each stable basin of attraction is identical. The ratio of occupation probabilities can become extremely sensitive at this point if the noise is weak. Our contributions to this sensing concept are divided into two parts. First, we calculate the sensitivity and detection time of the dynamical bridge for use as a general use detector. Second, we develop the conditions required and demonstrate the application of the dynamical bridge as a detector of non-Gaussian noise. We illustrate the measurement of the parameters of a shot-noise process with a one-dimensional bridge model. In terms of the bridge as a general use detector, we conclude that it is a time-consuming sensing method. The reason is that the bridge sensitivity scales with the inverse of the noise strength while the measurement time is exponential in this same quantity. As a detector of the full-counting statistics of a shot-noise process, the bridge should perform comparable to other methods with the added convenience that one does not need to reset the system.

Our third topic is phase noise in oscillators employing nonlinear frequency selective elements. This is discussed in chapter 4. We review the theory of a nonlinear oscillator coupled to a medium [36], and employ this microscopic resonator model to gain insight into the origin of phase noise. Our primary contribution is the use of the method of averaging to develop an expression for the spectrum of fractional frequency fluctuations in an oscillator. The method of averaging applied to a noisy system is discussed in appendix B. The expression for the spectrum of frequency fluctuations is quite general, although it does ignore dynamics in the feedback elements of the oscillator. The expression contains elements of the noise model and nominal limit cycle shape of the oscillator. We demonstrate its utility by exploring the parameter space of a prototypical oscillator. It is shown that the action-angle decoupling at zero-dispersion points of the resonator frequency provide an operating point that

reduces the phase diffusion constant. Our conclusion is that these zero dispersion points are near the optimal operating points for strongly nonlinear oscillators. The reduction in phase noise gleaned from oscillator tuning should be complimented by the reduction of noise influence at the source. These results are relevant to the design of high performance N/MEMS frequency sources.

## Chapter 2

# Escape Statistics for Parameter Sweeps Through Bifurcations

In this chapter we discuss the dynamics of nonlinear N/MEMS resonators near co-dimension one bifurcation points that result in large changes in system response. Of the phenomena discussed in this dissertation, we choose to begin with this because the one-dimensional models we use provide ease of visualization and yield more complete solutions than the more complicated systems considered in later chapters. Our primary purpose is to examine the initial transient that occurs when the parameters of a system are swept through a saddle-node or subcritical pitchfork bifurcation. Since these bifurcations exhibit a loss of local stability, and have no stable states emerging from the bifurcation, we can qualitatively say that the system will undergo a transient, a “jump,” or an “escape”, to another region in phase space. These escape events are highly visible transient processes and therefore useful for detection. However, they can also be strongly influenced by noise and therefore must be understood as random events. In this chapter we formulate the general problem, determine conditions which separate fast and slow sweeping, and then develop the distribution of escape times in the limit of fast sweeping through a saddle-node or a subcritical

pitchfork bifurcation. These are new results, relevant for many N/MEMS resonators, and possibly for other systems as well.

This work is motivated by the applications of escape statistics to sensing, parameter fitting, and system identification. For example, circuits containing Josephson junctions often exhibit saddle-node bifurcations. Interrogating such systems by sweeping through the bifurcation point has been used to fit the critical current parameter of the junction [67, 47, 58]. In the study of nanomagnetic systems, the measured distribution of escape events was used to determine the type of bifurcation occurring in the the system, leading to support for certain system models [115, 120]. More recently escape due to a parameter sweep trajectory approaching a bifurcation has been used as a method for reading the state of a qubit coupled to a nonlinear resonator [116]. Another important example is the supercritical pitchfork or Hopf bifurcation encountered during parameter sweeps during laser turn-on [14, 110, 122, 8]. This example, however, does not exhibit loss of local stability and so differs qualitatively from the others.

As one might expect from these example applications, noise-activated escape near bifurcations has been the subject of many previous investigations. Many of these focus on systems in which parameters remain fixed [85, 108] or vary slowly [67, 48, 44, 116, 44, 54]. However, systems with comparatively weak noise typically exhibit delayed bifurcation during parameter sweeps [16]. It is this regime in which we are primarily interested. Berglund and Gentz [9] developed scaling laws which are applicable to the distribution of delayed bifurcation trajectories. However, more quantitative results are required for bifurcation-based sensing schemes, for example, in dynamic M/NEMS [16, 66].

We will begin, in section 2.1, by discussing the modeling of a nonlinear N/MEMS resonator by a reduced model, the normal form, near the bifurcation point. This section concludes by recalling the normal forms for the saddle-node and subcritical

pitchfork bifurcations. We then discuss, in section 2.2, how noise can cause the system to escape from the region of the bifurcating equilibria by reviewing Kramers [64, 93] escape formulation, which is valid in the limiting case of slow (adiabatic) sweeping. We then proceed with our solution to the problem of delayed saddle-node and subcritical pitchfork bifurcations. The saddle-node is discussed in section 2.3 and the pitchfork in section 2.4. Experimental demonstration of a delayed subcritical pitchfork bifurcation is presented in section 2.5 and future research directions related to this subject are discussed in section 2.6.

## 2.1 Stochastic Normal Forms

In this section we sketch the transformation of a weakly nonlinear resonator to a reduced one-dimensional stochastic differential equation that describes the resonator dynamics close to a bifurcation point. It is well known that the resonantly forced Duffing and nonlinear Mathieu resonators exhibit saddle-node and pitchfork bifurcations of equilibria, respectively, in an averaged rotating frame in which equilibria represent nearly-harmonic periodic system responses. In appendix C we develop the pitchfork normal form arising in the nonlinear Mathieu type resonator. In this section, however, we leave our discussion more general. For more background material, the reader is directed to [52] for the noise-free case. For additional discussion of stochastic normal forms, see [62].

A resonator with weak damping and weak nonlinearity can be described by

$$\ddot{q} + \omega_0^2 q = F(q, \dot{q}, t), \quad (2.1)$$

where  $q$  is the resonator coordinate and the function  $F$  represents small forces acting on the resonator including damping, nonlinear effects, periodic forcing, stochastic

processes, etc. From equation (2.1) we proceed to make a series of approximations based on the relative size of various terms. The first step is to transform equation (2.1) into a set of coupled first order equations with small right hand side. This can be done with the well-known Van der Pol transformation. A polar form of the transformation is given by

$$\begin{aligned} q &= a(t) \cos(\omega t + \phi(t)), \\ \dot{q} &= -\omega a(t) \sin(\omega t + \phi(t)), \end{aligned} \tag{2.2}$$

where  $\omega$  is the frequency of the harmonic excitation in  $F$ . This transformation is analogous to the method of variation of parameters. Applying equations (2.2) to (2.1) gives

$$\begin{aligned} \dot{a} &= -\sin(\omega t + \phi) \left[ \sigma a \cos(\omega t + \phi) + \frac{F(a, \phi, t)}{\omega} \right], \\ \dot{\phi} &= -\cos(\omega t + \phi) \left[ \sigma \cos(\omega t + \phi) + \frac{F(a, \phi, t)}{\omega a} \right]. \end{aligned} \tag{2.3}$$

where  $\sigma = (\omega^2 - \omega_0^2)/\omega$  is the detuning, which is assumed small, and  $F(a, \phi, t)$  is understood to imply  $F(q(a, \phi, t), \dot{q}(a, \phi, t), t)$ . Owing to the smallness of the right hand side, equations (2.3) imply that  $a$  and  $\phi$  change on a much longer time scale than the period of oscillation  $2\pi/\omega$ . Accordingly, fast oscillating periodic terms in (2.3) integrate to approximately zero and can be ignored. A more complete discussion of this approximation, called the method of averaging, is given in appendix B, where particular attention is given to dealing with stochastic processes. The result is an approximate set of envelop equations describing the slow variation of the resonator's amplitude and phase. We may assume that the equations (2.3) can be approximated by (see appendix B)

$$\dot{\mathbf{x}} = \mathbf{f}(\mathbf{x}, \mu) + G(\mathbf{x}, \mu)\boldsymbol{\xi}(t), \tag{2.4}$$

where we have lumped  $a$  and  $\phi$  into a state vector,  $\mathbf{x}$ ,  $\mu$  is some resonator parameter,  $\boldsymbol{\xi}(t)$  is an  $n$ -dimensional vector of zero mean stochastic processes, and  $G$  is a 2-by- $n$  dimensional matrix. Now, suppose there exists a point,  $\mathbf{x}^*$  and a corresponding parameter value,  $\mu^*$  such that  $\mathbf{f}(\mathbf{x}^*, \mu^*) = 0$  and the Jacobian at this point,  $D\mathbf{x}\mathbf{f}(\mathbf{x}^*, \mu^*)$ , has one zero eigenvalue and one negative eigenvalue,  $-\lambda$ . The *bifurcation point* is understood to be the pair  $(\mathbf{x}^*, \mu^*)$ . The *bifurcation value* is  $\mu^*$  alone, and the term *bifurcation* describes a change in the sign of the real part of an eigenvalue of an equilibrium point resulting from a change of the parameter  $\mu$  near  $\mu^*$ .

Let  $u$  be the deviation from  $\mathbf{x}^*$  along the stable eigenvector, i.e., the eigenvector associated with eigenvalue  $-\lambda$ , and let  $v$  be the deviation from  $\mathbf{x}^*$  along the marginally stable eigenvector, i.e., the eigenvector associated with the zero eigenvalue. We express equation (2.4) in the  $(u, v)$  coordinate system and expand in both the coordinates and the parameter about  $(u, v, \mu) = (0, 0, \mu^*)$ . Keeping leading order terms, the equations for  $u$  and  $v$  take the form

$$\dot{u} = -\lambda u + a_1 \xi_1(t) + \cdots, \quad (2.5)$$

$$\dot{v} = b_1 v^2 + b_2 u v + b_3 u^2 v + c v^3 \delta\mu + a_2 \xi_2(t) + \cdots, \quad (2.6)$$

where  $a_i \xi_i$  are the weighted projections of  $\boldsymbol{\xi}$  onto the two eigenvectors and  $\delta\mu = \mu - \mu^*$ . For sufficiently small noise and small  $u$ ,  $v$ , and  $\delta\mu$  the  $u$  dynamics evolve much faster than the  $v$  dynamics owing to the nonzero eigenvalue  $-\lambda$ . Thus we assume that  $u$  is quite small. Accordingly, we keep the mean contribution from those terms containing powers of  $u$  in equation (2.6), that is the terms that arise in the deterministic normal form [52], but ignore the fluctuating parts of  $u$ , as it is dominated by the fluctuating term  $a_2 \xi_2(t)$ . This amounts to simply averaging equation (2.6) over  $u$ , and it results



in the stochastic normal form

$$\dot{v} \approx b_1 v^{n_1} + b_3 \langle u^2 \rangle v^{n_3} + c v^{n_4} \delta\mu + a_2 \xi_2(t). \quad (2.7)$$

Expanding equation (2.4) in powers of  $u$  and  $v$  is called the tangent space approximation since  $u$  and  $v$  describe a deviation in the eigenspace of the bifurcation point. A more detailed reduction can be performed by seeking the deterministic center manifold  $u = h(v) + \epsilon$  such that  $\dot{u} = h'(v)\dot{v}$  for  $\xi = 0$ .  $h(v)$  can be found by expressing it as a series in  $v$  and then using the condition  $\dot{u} = h'(v)\dot{v}$  to solve for the coefficients by matching like powers. This provides a more complete picture of the slow manifold in phase space. We take this approach when we consider the nonlinear Mathieu equation in appendix C.

The exponents  $n_i$  in equation (2.7) define the type of bifurcation. The coefficients  $b_i$  and  $c$  can be given standard values by a scaling of the coordinate  $v$  and time and re-normalizing the bifurcation parameter, yielding a normal form with minimal parameters.

For the saddle-node bifurcation  $n_1 = 2$  and  $n_4 = 0$ . For the pitchfork bifurcation  $n_1 = 3$  and  $n_4 = 1$ . In the nonlinear Mathieu resonator we also have  $n_3 = 1$ , which simply shifts the bifurcation point, an effect that can be accounted for by re-defining the bifurcation parameter,  $\delta\mu$  [85, 86]. This effect can also be neglected if the noise is sufficiently weak. Thus, in the saddle-node and pitchfork bifurcations, only the value of  $a_2$  and the relationship between  $\delta\mu$  and the original resonator parameters are specific to any given system undergoing such a bifurcation. For this reason the model is very general and valid for a wide class of systems undergoing the bifurcations of interest.

There are two types of pitchfork bifurcations, the supercritical, for which  $b_1 > 0$ , and the subcritical, for which  $b_1 < 0$ . As mentioned above the supercritical pitchfork

arises in laser dynamics, but also in parametric resonance of the nonlinear Mathieu resonator, when the system restoring force is hardening. The subcritical pitchfork likewise can be found in parametric resonance, for systems with softening restoring force. Again, we are interested in the subcritical bifurcation because it results in a loss of local stability and an escape event.

Since the normal form, equation (2.7), is one-dimensional, we can write

$$\dot{v} = -U'(v) + \sqrt{D}\xi(t), \quad (2.8)$$

where  $U$  is an effective potential,  $D$  is the effective noise strength, and  $\xi(t)$  is the effective noise on the slow manifold arising from a combination of the components of  $\xi$ . As we mentioned above, we have neglected any parametric noise terms by appealing to an appropriate scaling, c.f. appendix C. Coordinate  $v$  can be understood as describing the position of an overdamped particle in the potential  $U$ . We are particularly interested in bifurcations for which  $U$  presents a finite barrier for the system to escape to  $v \rightarrow \pm\infty$ . The finite barrier allows the system to escape from the local region of phase space and exhibit a highly visible transient that can be used for sensing or system identification, as discussed above. Two examples are the saddle-node and the subcritical pitchfork. The supercritical pitchfork does not have this property, since responses stay in the neighborhood of the bifurcation point.

Now, we wish to consider the parameter sweeping experiments described above. Thus, we will let  $\delta\mu$  vary in time according to a prescribed parameter sweep trajectory. In order for the reduced model to remain valid, this variation, as well as other effects, including the noise, should not push the system far from the slow manifold. This should be the case so long as the time rate of change of the eigenvectors is much smaller than  $\lambda$  and the noise is sufficiently weak. For the remainder of the analysis, we assume these assumptions hold. As we will see, when sweeping the bifurcation

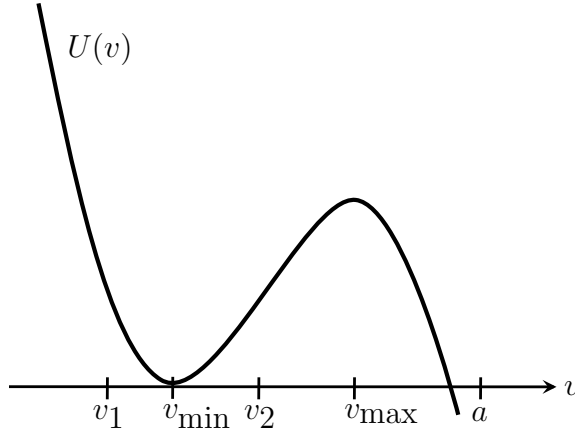


Figure 2.1: Example potential governing normal form dynamics.

parameter linearly in time, only the ratio of the sweep rate to the noise strength is important. Therefore we speak of fast and slow sweep rates according to whether this ratio is large or small, but always assume the sweep rate is sufficiently slow (i.e., noise sufficiently small) so that the normal form model holds.

## 2.2 Kramers Escape Rate

Consider equation (2.8) and suppose that the potential  $U$  presents a finite barrier beyond which the system response will become unbounded. For example, see figure 2.1. Since the barrier height is finite, there is some chance that the noise will push the system out of the potential well and it will escape to  $\infty$ . Of course, equation (2.8) is only a local model of the full system dynamics, obtained from the reduction to the slow mode. As  $v$  grows, this model will eventually become invalid, and rather than escape to  $\infty$ , the resonator state will move to another region of phase space that is outside the domain of this local picture.

The probability per unit time of escape out of the well was first derived in the classic 1940 work of Kramers [64]. This result applies to a time-independent potential, but can be applied to a slowly varying potential via an adiabatic approximation.

This important result is the counterpoint to the new results we develop in sections 2.3 and 2.4. These new fast sweeping solutions complement the slow sweeping (adiabatic) solutions since they are the two asymptotic cases that bracket the complete picture. For this reason we review the celebrated Kramers' result and the corresponding adiabatic approximation in this section. Our development of Kramers' escape rate comes from Risken [93]. We assume that  $U$  is time independent,  $D$  is constant, and  $\xi$  is a zero mean white Gaussian noise with  $\langle \xi(t)\xi(t') \rangle = 2\delta(t - t')$ . Under the white noise assumption, the probability distribution,  $\rho$ , for  $v$  is governed by the Fokker-Planck (FP) equation [93]

$$\frac{\partial \rho}{\partial t} = -\frac{\partial S}{\partial v}, \quad (2.9)$$

$$S = -De^{-U/D} \frac{\partial}{\partial v} [e^{U/D} \rho], \quad (2.10)$$

where  $S$  is the probability current. If the potential barrier is high, it is unlikely that the system will escape and  $\rho$  will settle into a quasi steady state distribution. Accordingly,  $\partial_t \rho$  is small and  $S$  is approximately constant. Making this assumption, we integrate equation (2.10) over the interval  $[v_{\min}, a]$  (see figure 2.1)

$$S \int_{v_{\min}}^a e^{U/D} dv \approx D \left[ e^{U(v_{\min})/D} \rho(v_{\min}) - e^{U(a)/D} \rho(a) \right], \quad (2.11)$$

where  $a$  an arbitrary point sufficiently beyond the barrier peak. We can also assume that the probability of finding the system at point  $a$  is small. We therefore drop the second term on the right hand side of equation (2.11). Thus, the probability current is approximately given by

$$S \approx De^{U(v_{\min})/D} \rho(v_{\min}) \left[ \int_{v_{\min}}^a e^{U/D} dv \right]^{-1}. \quad (2.12)$$

Returning to the initial assumption that  $\partial_t \rho$  is small, we approximate  $\rho$  by its steady

state distribution

$$\rho \approx \rho(v_{\min}) \exp [-[U(v) - U(v_{\min})]/D]. \quad (2.13)$$

Thus, the probability for the system to be near  $v_{\min}$  is

$$p = \int_{v_1}^{v_2} \rho dv \approx \rho(v_{\min}) e^{U(v_{\min})/D} \int_{v_1}^{v_2} e^{-U/D} dv. \quad (2.14)$$

The inverse escape rate,  $W$ , is given by the ratio of the probability to be near the bottom of the well to the probability current out of the well.

$$\frac{1}{W} \equiv \frac{p}{S} \approx \frac{1}{D} \int_{v_1}^{v_2} e^{-U/D} dv \int_{v_{\min}}^a e^{U/D} dv. \quad (2.15)$$

The integrals can be approximated by the method of steepest decent. In this method  $U$  is expanded to second order about the point that maximizes the integrand and the bounds of the integration are taken to  $\pm\infty$ . For the first integral  $U$  is expanded about  $v_{\min}$ , and for the second integral  $U$  is expanded about  $v_{\max}$ . The resulting escape rate is thus found to be

$$W = \frac{1}{2\pi} \sqrt{U''(v_{\min})|U''(v_{\max})|} \exp [-(U(v_{\max}) - U(v_{\min}))/D]. \quad (2.16)$$

If the potential allows escape in both directions, the total escape rate is the sum of the rates for escape in the two directions.

Now, suppose that the potential is changing slowly in time. We can model the probability to escape the potential well per unit time with equation (2.16). Thus, the probability for the system to remain in the well until time  $t$ ,  $\rho$ , is governed by

$$\dot{\rho}_{\text{ne}} = -W(t)\rho_{\text{ne}}, \quad \rho_{\text{ne}}(t_0) = 1, \quad (2.17)$$

where the subscript “ne” stands for “not escaped.” This equation admits the solution

$$\rho_{\text{ne}} = \exp \left[ \int_{t_0}^t W dt \right]. \quad (2.18)$$

The probability to escape from the well by time  $t$  is  $\rho_{\text{e}} = 1 - \rho_{\text{ne}}$ . The probability density,  $P$ , of escape at time  $t$ , is  $\dot{\rho}_{\text{e}}$ . This gives

$$P = W \exp \left[ \int_{t_0}^t W dt \right]. \quad (2.19)$$

This result is valid in the slow sweeping limit. In this limit noise-activated escape occurs with probability 1 by the time the the sweep has reached the bifurcation value. If the sweep is fast, however, there must be nonzero probability to pass through the bifurcation value before escape occurs. Results analogous to equation (2.19) for the saddle-node and subcritical pitchfork bifurcations in the fast sweeping limit are developed in the following sections.

Before proceeding to discuss escape in the non-adiabatic, or fast, sweeping condition, a few words must be said about what it means to “escape” in this context. In the slow sweeping limit, discussed above, the duration of the escape event is small compared to the time scale of the sweep. On the long time scale of the sweep it appears that escape happens instantaneously. Accordingly, the escape rate is independent of the point  $a$  at which escape is defined to occur. However, when the sweep is fast, the transient escape process may occur over a duration in which the bifurcation parameter changes significantly. Escape, therefore, does not appear instantaneous and the probability density to escape per unit time depends on the threshold at which “escape” is said to occur. To deal with this complication, we observe that both normal form models considered herein exhibit escape to  $\infty$  in finite time. Accordingly, the escape trajectories become extremely steep at (locally) large values of  $v$ . We thus

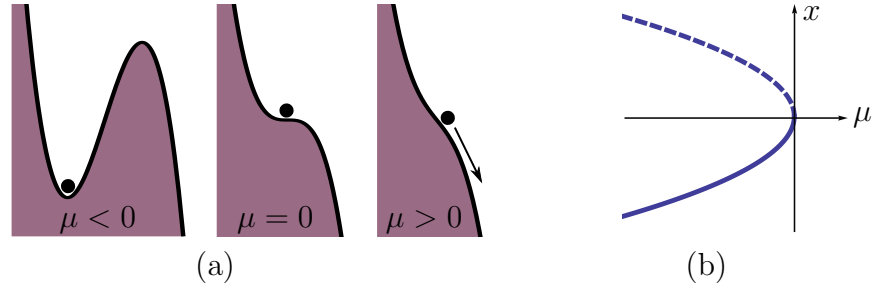


Figure 2.2: Illustration of the evolution of the potential (a), and the standard bifurcation diagram (b), for a saddle-node bifurcation.

define escape to occur when  $v \rightarrow \pm\infty$  and note that the arrival time at some large value of  $v$ , taken to be the limit of the domain of validity of the normal form model, is well approximated by the arrival time at  $\pm\infty$ .

## 2.3 Escape Near a Saddle-Node Bifurcation

When sweeping a parameter near a saddle-node bifurcation, the dynamics along the slow manifold are described by a one-dimensional Langevin equation representing the stochastic normal form. Switching notation from the previous section, the saddle-node normal form is given by [9],

$$\dot{x} = \mu(t) + x^2 + \epsilon\xi(t), \quad (2.20)$$

where  $\mu(t)$  is the bifurcation parameter and  $\xi(t)$  is zero mean, delta-correlated white noise with autocorrelation  $\langle \xi(t)\xi(t') \rangle = 2\delta(t - t')$ . For simplicity, we assume that  $\mu$  is non-decreasing. In this case, the sweep trajectory can be classified by the charac-

teristic sweep rate,  $r$ .

$$r = \frac{\mu_c - \mu_0}{t_c - t_0}, \quad (2.21)$$

where  $\mu_c$  is the bifurcation value (for equation (2.20)  $\mu_c = 0$ ),  $t_c$  is defined by  $\mu(t_c) = \mu_c$ ,  $\mu_0$  is the initial value of the bifurcation parameter, and  $t_0$  is the time at which the sweep is initiated. The dynamics of equation (2.20) are conveniently visualized by an overdamped particle moving in a time-varying potential, as illustrated in figure 2.2a. The bifurcation diagram is shown in figure 2.2b. Our goal is to determine the distribution of escape times  $T$ , i.e., those values of  $T$  for which  $x \rightarrow \infty$  as  $t \rightarrow T$ . A numerical solution for this problem can be obtained by solving the FP equation associated with equation (2.20),

$$\frac{\partial \rho}{\partial t} = -\frac{\partial}{\partial x}[(\mu + x^2)\rho] + \epsilon^2 \frac{\partial^2 \rho}{\partial x^2}, \quad (2.22)$$

with appropriate initial and boundary conditions at large, but finite,  $x$ , the results of which are used to illustrate the connection between the fast and slow sweeping limits. It can be shown by the following simple scaling argument that these limits are given by  $\epsilon^2 \ll r$  and  $\epsilon^2 \gg r$ , respectively: Scaling time by  $r^{-1/3}$  and the coordinate by  $r^{1/3}$  gives rise to a renormalized characteristic sweep rate of unity and a renormalized noise strength of  $\epsilon^2/r$ .

Now, suppose that the system is initially near the local minimum of the potential that exists for  $\mu < 0$  and the sweep is slow (or the noise is large). If  $\mu$  is increased slowly (for the given level of noise intensity), one can approximate the rate of escape by the well-known adiabatic approximation due to Kramers [64, 54] as discussed in



the previous section. For the saddle-node, this rate is

$$W(t) = \frac{\sqrt{-\mu(t)}}{\pi} \exp \left[ -\frac{4(-\mu(t))^{3/2}}{3\epsilon^2} \right]. \quad (2.23)$$

The probability to remain in the well diminishes according to the product of this rate and the probability to remain in the well. Accordingly, the probability density function for escape at time  $T$  in the limit of adiabatic sweeping is given by [67, 54],

$$P(T) = W(T) \exp \left[ -\int_{t_0}^T W(t) dt \right]. \quad (2.24)$$

Of particular interest to us is the case where the noise strength is small compared to the characteristic rate of change of the bifurcation parameter, that is,  $0 \leq \epsilon^2 \ll r$ . In this case, the potential well will disappear before noise activated escape is likely to occur, and the system thus exhibits a delayed bifurcation, escaping to  $x \rightarrow \infty$  at a finite time  $T$ , for which  $\mu(T) > 0$ . To approximate the distribution of escape times for equation (2.20) in this situation, we employ a direct perturbation method. To this end it is convenient to transform the equation using a variation of parameters approach, in which the  $\epsilon = 0$  solution,  $x_0$ , plays the role of the homogeneous solution. The transformation  $x_0 = -\dot{u}/u$  in equation (2.20) with  $\epsilon = 0$  yields,

$$\ddot{u} + \mu(t)u = 0, \quad (2.25)$$

which has linearly independent solutions  $u_1$  and  $u_2$ , so that  $x_0$  can be written as,

$$x_0 = -\frac{\dot{u}_1 + c\dot{u}_2}{u_1 + cu_2}, \quad (2.26)$$

where  $c$  is a constant of integration. To account for the presence of noise, we let  $c$  vary in time. Utilizing expression (2.26) with  $c(t)$  in equation (2.20) gives the equation for

$c(t)$  as,

$$\dot{c} = -\epsilon a(u_1 + cu_2)^2 \xi, \quad (2.27)$$

where  $a^{-1} = u_1 \dot{u}_2 - \dot{u}_1 u_2$  is the Wronskian. The variable  $c$  is a means of parameterizing the solutions of the noise-free problem, and noise causes the system to diffuse among the noise-free trajectories according to equation (2.27).

The escape time,  $T$ , is given by the time at which  $x_0$  becomes unbounded, which, according to equation (2.26), corresponds to  $c(t)$  reaching the condition,

$$c(t) = c_\infty(t) = -\frac{u_1(t)}{u_2(t)}. \quad (2.28)$$

Here the first passage time problem reduces to a transformation of the stochastic variable  $c(t)$  to the times  $T$  for which  $c(T) = c_\infty(T)$ , for some initial distribution of initial conditions. To determine the distribution of  $T$ , it is useful to consider the features of  $c_\infty(t)$ . The function  $c_\infty(t)$  has branches, separated by vertical asymptotes at the zeros of  $u_2(t)$ , and  $c(t)$  evolves between these branches, as depicted in figure 2.3. Also, note that since

$$\frac{dc_\infty}{dt} = \frac{1}{au_2^2} \quad (2.29)$$

does not change sign,  $c_\infty(t)$  is monotonic between branches. In addition, by considering equations (2.27) and (2.28), it is seen that  $\dot{c} = 0$  when  $c = c_\infty$ . Thus, trajectories of  $c(t)$  cross each branch of  $c_\infty(t)$  at a single time. Consequently, in considering the first passage time of  $c(t)$  across a particular branch of  $c_\infty(t)$ , we do not need to account for trajectories that cross the branch multiple times. We can therefore do away with the adsorbing wall boundary condition usually employed in first passage time problems. Without an adsorbing wall boundary condition, a crossing corresponds to

reinjection at  $x = -\infty$ . Hence, subsequent crossings of  $c_\infty$  occur on immediately subsequent branches only. These subsequent crossings occur when the system has once again reached  $x = \infty$ .

The change of coordinates from  $x(t)$  to  $c(t)$ , expressed in equation (2.26), makes the problem amenable to direct perturbation analysis. To develop a first order asymptotic approximation of the escape current, we begin with the expansion,

$$c = c_0 + \epsilon c_1 + \dots \quad (2.30)$$

Substitution of this into equation (2.27) and expanding in powers of  $\epsilon$  yields,

$$\dot{c}_0 = 0, \quad (2.31)$$

$$\dot{c}_1 = -a(u_1 + c_0 u_2)^2 \xi. \quad (2.32)$$

Note that the first order perturbation removes the state-dependent diffusion, and thus Ito and Stratonovich calculus give the same result at this order. Solving equations (2.31-2.32) gives a time-dependent Gaussian probability density function (PDF) for the noisy response of  $c$ , as follows,

$$P_c(c, t) = \left( 4\pi a^2 \epsilon^2 \int_{t_0}^t (u_1 + c_0 u_2)^4 dt' \right)^{-1/2} \times \exp \left[ -\frac{(c - c_0)^2}{4a^2 \epsilon^2 \int_{t_0}^t (u_1 + c_0 u_2)^4 dt'} \right]. \quad (2.33)$$

Using this result, the PDF of escape times can be expressed as,

$$P_\infty(T) = P_c(c_\infty, T) \left| \frac{dc_\infty(T)}{dT} \right|. \quad (2.34)$$

Combining equations (2.29), (2.33), and (2.34), we arrive at an expression for the

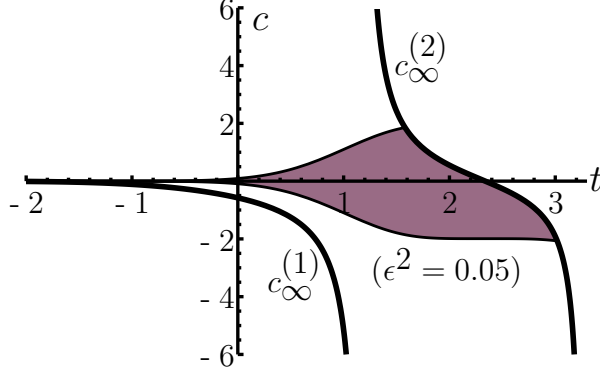


Figure 2.3:  $c_\infty$  boundary for linear sweeping,  $\mu(t) = \mu_0 + rt$ , with  $\mu_0 < 0$ . The first two branches are shown along with the variance (shaded region) of  $c$  for  $\epsilon^2 = 0.05$ .

PDF of escape times,

$$P_\infty(T) = \left( 4\pi a^4 \epsilon^2 u_2^4(T) \int_{t_0}^T (u_1 + c_0 u_2)^4 dt \right)^{-1/2} \quad (2.35)$$

$$\times \exp \left[ -\frac{(u_1(T) + c_0 u_2(T))^2}{4a^2 \epsilon^2 u_2^2(T) \int_{t_0}^T (u_1 + c_0 u_2)^4 dt} \right].$$

Note that this result is quite general, since the details of the parameter sweep  $\mu(t)$ , which dictates  $u_{1,2}(t)$ , are not yet specified. The simplest method for sweeping the bifurcation parameter is linear in time, that is,  $\mu = \mu_0 + rt$ , with  $\mu_0 < 0$  and  $r > 0$ . The affine relationship between the bifurcation parameter and time allows one to identify the bifurcation parameter as a renormalized time variable. Thus, without loss of generality, we take  $\mu = t$ . With this form of sweeping, equation (2.25) becomes Airy's equation in backwards time, that is,  $\ddot{u} + tu = 0$ , with independent solutions,

$$u_1(t) = A_i(-t), \quad (2.36)$$

$$u_2(t) = B_i(-t), \quad (2.37)$$

where  $A_i$  and  $B_i$  are the standard Airy functions, for which the standard parameter  $a = -\pi$  [1]. In principle,  $u_1$  and  $u_2$  can be taken as linear combinations of  $A_i$  and

$B_i$ , however, the present choice is most convenient here. The first two branches of the  $c_\infty$  boundary,  $c_\infty^{(1,2)}$ , are shown in figure 2.3. In the weak noise case, only the second boundary can be crossed, since  $c_\infty^{(1)}$  is bounded above by zero ( $c_\infty^{(1)} < 0$ ) and monotonically decreases ( $\dot{c}_\infty^{(1)} < 0$ ), while  $c_0 > c_\infty^{(1)}$  must hold for initial conditions restricted to be near the minimum of the potential well. Thus, the only way to cross  $c_\infty^{(1)}$  is for  $c(t)$  to diffuse to  $+\infty$  and be reinjected at  $-\infty$ , and this cannot happen under the weak noise assumption. Therefore, computing escape times we consider only those trajectories that reach  $c_\infty^{(2)}$ . Note that  $c_\infty^{(2)}$  spans the time interval between the first and second zeros of  $B_i(-t)$ , so that our approximation of the escape distribution times is necessarily limited to this time interval, which is given below. In principle, this time interval can be adjusted by taking a different linear combination of  $A_i$  and  $B_i$  for  $u_1$  and  $u_2$ , since the time interval is specified by the zeros of  $u_2$ . However, as the perturbation solution requires small noise, the probability of escape outside this time interval is also small.

Equation (2.35) captures the escape distribution with the system initially situated on the noise-free trajectory specified by  $c_0$  at time  $t_0$ . Generally, the dependence on  $c_0$  and  $t_0$  becomes weak as  $|t_0|$  becomes large since

$$c \sim \exp \left[ -\frac{2}{3} |t_0|^{3/2} \right], \quad (2.38)$$

assuming the system begins the sweep near the bottom of the potential well. This weak dependence on this class of initial conditions is a property of the deterministic system and results from the annihilation of the fixed point after the bifurcation. Diffusion only increases this effect as the system settles into a quasi-steady state distribution early in the sweep. Thus, when the sweep is started well before the bifurcation point, the initial conditions are forgotten.

With this understanding, the initial conditions for the linear sweep are taken to

be  $c_0 = 0$  and  $t_0 = -\infty$ . The resulting escape distribution then applies to all initial conditions where  $c_0$  is near zero and  $t_0 \ll -1$ . The corresponding escape current is computed using equations (2.35) and (2.37), resulting in,

$$P_\infty(T) = \left( 4\pi^5 \epsilon^2 B_i^4(-T) \int_{-\infty}^T A_i^4(-t) dt \right)^{-1/2} \times \exp \left[ \frac{-A_i^2(-T)}{4\pi^2 \epsilon^2 B_i^2(-T) \int_{-\infty}^T A_i^4(-t) dt} \right], \quad (2.39)$$

with  $T$  restricted to the range between the first two zeros of  $B_i(-t)$ , that is,  $1.17 < T < 3.27$ .

The first two moments of the escape distribution given by equation (2.39) are illustrated in figure 2.4 along with two sample distributions, one representative of the slow sweeping limit and one representative of the fast sweeping limit. The moments are plotted over a wide range of noise strengths, spanning adiabatic (Kramers) escape and delayed bifurcation. The solid lines represent the solution obtained by numerically solving the FP equation over a finite domain. The equation was solved using the Crank-Nicolson method with Dirichlet boundary conditions at large coordinate values where drift dominates diffusion. The moments for the adiabatic approximation and the approximation developed here are shown as dashed lines. Note that the two limiting cases bracket an intermediate region near  $\epsilon^2 = 1$ , where one must rely on the numerical solution to obtain the distribution. Thus, the present analysis, in addition to providing convenient approximations for the fast sweep rate escape distributions, also offers information about the parameter limitations for the two limiting cases, and a method for determining the distributions when neither approximation holds.

Note that the variance is dramatically larger in the adiabatic case,  $\epsilon^2 \gg 1$ , when compared to the non-adiabatic case,  $\epsilon^2 \ll 1$ . This is the result of the different escape mechanisms in these two limiting cases. In the adiabatic case, escape is a rare event

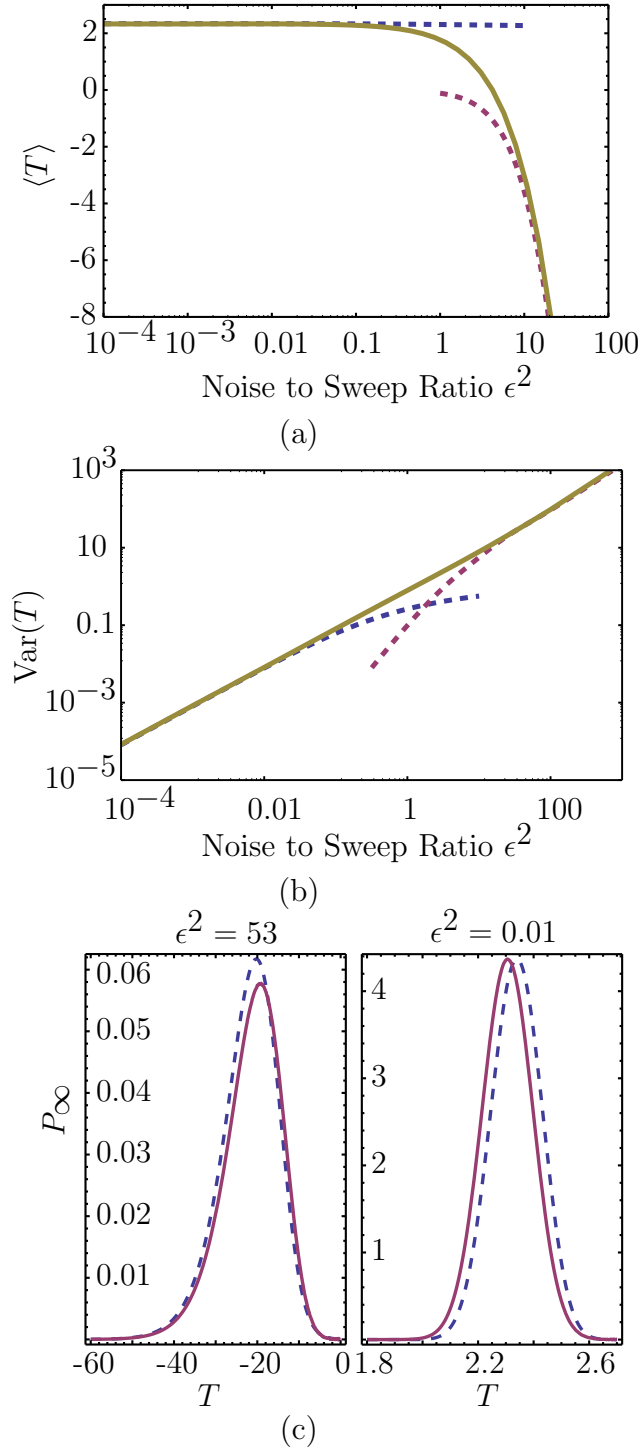


Figure 2.4: Mean (a), variance (b), and sample distributions (c) of the escape time away from a swept saddle-node bifurcation. Numeric solution (solid line) and approximations (dashed) for fast and slow sweeping are shown.

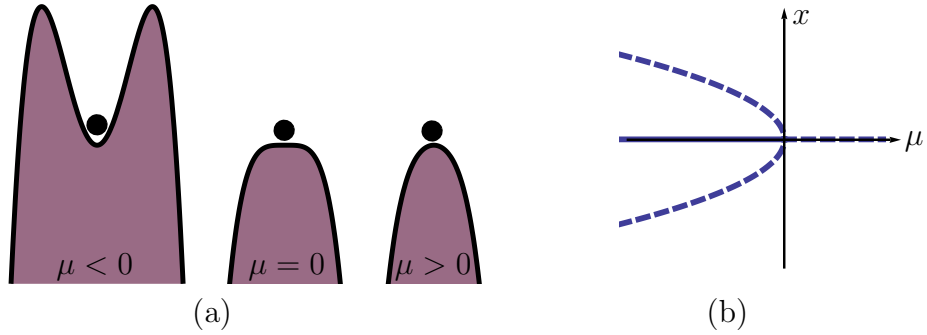


Figure 2.5: Illustration of the evolution of the potential (a), and the standard bifurcation diagram (b), for a subcritical pitchfork bifurcation.

in which the noise overcomes a potential barrier. Thus, the probability of escape over a small time interval is small, but the sweep takes a long time, so escape is virtually inevitable. In this way, the escape events have a wide distribution. In the non-adiabatic case, escape is inevitable, since the potential well disappears, and the solution closely follows the deterministic trajectory that would result from an initial condition at the bottom of the potential well. The escape times are randomly distributed about this trajectory due to diffusion. These observations also indicate why the mean escape time is insensitive to the noise strength for small noise intensity, but highly sensitive to the noise strength for large noise intensity.

## 2.4 Escape Near a Subcritical Pitchfork Bifurcation

Near a subcritical pitchfork bifurcation, the dynamics with noise along the slow manifold are described by the normal form [62],

$$\dot{x} = 2\mu(t)x + 4x^3 + \epsilon\xi(t), \quad (2.40)$$



where, as before,  $\mu$  is the bifurcation parameter,  $\epsilon^2$  is the noise strength, and  $\xi$  is zero mean, delta-correlated white noise with autocorrelation  $\langle \xi(t)\xi(t') \rangle = 2\delta(t - t')$ . It is recognized that the presence of noise shifts the effective bifurcation parameter [85], so  $\mu$  here includes that shift. The illustration of this system as a particle in an evolving potential is shown in figure 2.5a. The bifurcation diagram is shown in figure 2.5b. The FP equation corresponding with equation (2.40) is given by,

$$\frac{\partial \rho}{\partial t} = -\frac{\partial}{\partial x}[(2\mu x + 4x^3)\rho] + \epsilon^2 \frac{\partial^2 \rho}{\partial x^2}, \quad (2.41)$$

where  $\rho = \rho(x, t)$  is the probability distribution for the system state. As in the saddle-node case, we compare approximate results for fast and slow sweeping with numerical solutions of this FP equation.

Suppose the system is initially near the local minimum  $x = 0$  for  $\mu < 0$ . If  $\mu$  is increased slowly, the rate of escape can be approximated by the well-known adiabatic Kramers result [64, 54], given by,

$$W(t) = \frac{\sqrt{8}}{\pi} |\mu(t)| \exp \left[ -\frac{\mu^2(t)}{4\epsilon^2} \right]. \quad (2.42)$$

The probability to remain in the well diminishes according to the product of this rate and the probability to remain in the well. Accordingly, the probability density function for escape at time  $T$  in the limit of adiabatic sweeping is given by [67, 54],

$$P(T) = W(T) \exp \left[ -\int_{-t_0}^T W(t) dt \right]. \quad (2.43)$$

If  $\mu$  is swept quickly, that is  $0 \leq \epsilon^2 \ll \dot{\mu}$ , the system response is dominated by delayed bifurcations. We develop an approximate expression for the escape current in this case using asymptotic expansions.

Note that the method employed for the saddle-node bifurcation is not convenient

for the pitchfork, since the approach is not capable of capturing noise induced independence of initial conditions. This results from the fact that, for the pitchfork, the noise-free system maintains an equilibrium state, albeit unstable, beyond the bifurcation point. For the noise-free system, the initial conditions enter the solution multiplicatively and cannot be neglected. Nevertheless, diffusion removes the dependence on initial conditions when the parameter sweep is started sufficiently far from the bifurcation point, such that the system settles into a quasi-steady-state distribution [122, 14, 104]. To capture this effect we must employ an alternative method.

In this case the solution of the corresponding FP equation is approximated by the method of matched asymptotic expansions. Following Suzuki [107], we separate the sweeping time into a first interval, over which nonlinear drift is ignored, and a second interval, over which diffusion is ignored. We show that, under some assumptions, there exists a time interval over which both approximations are valid, allowing one to match the solutions. A change of coordinates in equation (2.41) makes clear the two phases of response. Let

$$y = \frac{x}{\sigma} \quad \text{where} \quad (2.44)$$

$$\sigma^2 = \epsilon^2 e^{4 \int_{t_0}^t \mu dt'} \left( \sigma_0^2 + 2 \int_{t_0}^t e^{-4 \int_{t_0}^{t'} \mu dt''} dt' \right). \quad (2.45)$$

and where  $\mu$  is assumed to grow monotonically with  $t$ . This particular  $\sigma^2$  is the variance of the solution to the linearized problem in which the nonlinear drift term is neglected. By changing coordinates into one in which the linearized problem has a constant solution, we more explicitly expose the roles of nonlinear drift and its relationship to diffusion.  $\sigma$  has the following properties: it is positive, takes on the value  $\epsilon\sigma_0 \geq 0$  at time  $t = t_0$ , it decreases until the time at which  $2\mu\sigma^2/\epsilon^2 = -1$ , which must occur before the bifurcation point is reached, and it increases monotonically for

$\sigma_0 < \epsilon/\sqrt{-2\mu_0}$ . Taking  $y$  as the new coordinate, equation (2.41) becomes,

$$\frac{\partial \rho}{\partial t} - \frac{\epsilon^2}{\sigma^2} y \frac{\partial \rho}{\partial y} = -2\mu\rho - 4\sigma^2 \frac{\partial}{\partial y} [y^3 \rho] + \frac{\epsilon^2}{\sigma^2} \frac{\partial^2 \rho}{\partial y^2}. \quad (2.46)$$

The second term on the LHS of equation (2.46) arises since  $y$  changes with time,  $t$ . The three terms on the RHS correspond to, in order, linear drift, nonlinear drift, and diffusion. In equation (2.46), the two regions of time become apparent by comparing the coefficients of the nonlinear drift and diffusion terms, namely  $4\sigma^2$  and  $\epsilon^2/\sigma^2$ . The ratio of the two coefficients is,

$$\frac{4\sigma^4}{\epsilon^2}. \quad (2.47)$$

In the initial phase of the response, this ratio is  $\mathcal{O}(\epsilon^2)$  (assuming  $\sigma_0$  is  $\mathcal{O}(1)$ ), implying that diffusion dominates the nonlinear drift. At later times, the ratio is  $\mathcal{O}(\epsilon^{-2})$ , owing to the exponential growth of  $\sigma$ , and the nonlinear drift dominates diffusion. In the intermediate region, the ratio is  $\mathcal{O}(1)$ , and thus  $\sigma^2 \sim \mathcal{O}(\epsilon)$ . Delayed bifurcation dominates the system response when this overlap region occurs beyond the bifurcation point. Now, an upper bound for  $\sigma^2$  at the bifurcation point, i.e., when  $\mu = 0$ , is  $2\pi\epsilon^2/\min \dot{\mu}$ . Thus, the condition  $\epsilon^2 \ll \dot{\mu}$  ensures that the overlap region occurs after the bifurcation point and the system will exhibit delayed bifurcation.

In the initial time region we ignore the nonlinear drift with respect to diffusion and obtain an approximate solution,  $\rho_l$ , of equation (2.46) by solving,

$$\frac{\partial \rho_l}{\partial \tau} = -2\mu\rho_l + \frac{\epsilon^2}{\sigma^2} \left( y \frac{\partial \rho_l}{\partial y} + \frac{\partial^2 \rho_l}{\partial y^2} \right). \quad (2.48)$$

Taking a Gaussian initial condition with zero mean and variance  $\sigma_0^2$ ,  $\rho_l$  is given by

$$\rho_l(y, \tau) = \frac{1}{\sqrt{2\pi\sigma^2}} \exp \left[ -\frac{y^2}{2} \right]. \quad (2.49)$$

At the other end of the process, in the second time region, which leads to escape, diffusion can be ignored with respect to drift. An approximate solution,  $\rho_{nl}$ , of equation (2.46) for this case is obtained by solving,

$$\frac{\partial \rho_{nl}}{\partial \tau} = -2\mu\rho_{nl} - 12\sigma^2 y^2 \rho_{nl} - 4\sigma^2 y^3 \frac{\partial \rho_{nl}}{\partial y}. \quad (2.50)$$

This equation is solved using the method of characteristics, which yields,

$$\rho_{nl}(y, t) = \rho_{nl}^{(1)}(y_1, t_1) \left( \frac{y_1}{y} \right)^3 \exp \left[ -2 \int_{t_1}^t \mu dt' \right], \quad (2.51)$$

$$y_1(y, t|t_1) = y \left[ 1 + y^2 \int_{t_1}^t 8\sigma^2 dt' \right]^{-1/2}, \quad (2.52)$$

where  $\rho_{nl}^{(1)}(y_1, t_1)$  captures the constant of integration along each characteristic. This corresponds to the initial conditions for equation (2.50). Now, time  $t_1$  need not be the starting time of the sweep, but can be taken to be any time before escape. To match the linear and nonlinear solutions, we take  $t_1$  to be some time in the common region where the quantity in equation (2.47) is  $\mathcal{O}(1)$ . To do the matching, we choose  $\rho_{nl}^{(1)}$  such that  $\rho_{nl}$  and  $\rho_l$  are identical to leading order in the common region.

We begin by rewriting equation (2.49) as,

$$\rho_l = \frac{1}{\sqrt{2\pi\sigma(t_1)^2}} \exp \left[ -\frac{y^2}{2} - 2 \int_{t_1}^t \mu dt' - \int_{t_1}^t \frac{\epsilon^2}{\sigma^2} dt' \right]. \quad (2.53)$$

In the common region, the last integral is  $\mathcal{O}(\epsilon)$ , and it can be ignored, resulting in,

$$\rho_l \approx \frac{1}{\sqrt{2\pi}\sigma(t_1)} \exp \left[ -\frac{y^2}{2} - 2 \int_{t_1}^t \mu dt' \right]. \quad (2.54)$$

Note that this is valid because  $t$  is not too far from  $t_1$  as both are in the common region. By the same argument, we drop the integral in equation (2.52). Thus,  $y_1 \approx y$  and the nonlinear solution is approximated by,

$$\rho_{nl} \approx \rho_{nl}^{(1)}(y, \tau_1) \exp \left[ -2 \int_{t_1}^t \mu dt' \right]. \quad (2.55)$$

The two distributions are matched by taking,

$$\rho_{nl}^{(1)}(y_1, t_1) = \frac{1}{\sqrt{2\pi}\sigma(t_1)} \exp \left[ -\frac{y_1^2}{2} \right]. \quad (2.56)$$

It only remains to calculate the probability current at  $\pm\infty$ , the escape current. The escape current comes entirely from the nonlinear drift which is responsible for escape to  $\infty$  in finite time. Thus, the current is given by  $P_\infty(T) = \lim_{x \rightarrow \infty} 8x^3 \rho$ . This gives

$$P_\infty = \frac{8\sigma^2(T)}{\sqrt{2\pi}} \left( 8 \int_{t_1}^T \sigma^2 dt \right)^{-3/2} \exp \left[ \int_{t_1}^T \frac{\epsilon^2}{\sigma^2} dt - \left( 16 \int_{t_1}^T \sigma^2 dt \right)^{-1} \right]. \quad (2.57)$$

Equation (2.57) depends weakly on the choice of  $t_1$ , and to leading order, this dependence can be removed, as follows. First, since  $\epsilon^2/\sigma^2$  is small for times after  $t_1$ , we drop the first integral in the exponent. Second, since  $\sigma^2$  is small for times before  $t_1$ , we extend the lower bound of integration for the remaining integrals back to the bifurcation point, which is a well-defined time and makes a convenient choice. The

resulting approximation is given by,

$$P_{\infty}(T) \approx \frac{8\sigma^2(T)}{\sqrt{2\pi}} \left( 8 \int_{t_b}^T \sigma^2 dt \right)^{-3/2} \exp \left[ - \left( 16 \int_{t_b}^T \sigma^2 dt \right)^{-1} \right], \quad (2.58)$$

where  $t_b$  is the time at which the bifurcation point is reached.

To solve a specific example, we again consider the linear sweep, for which  $\mu = t$ .

In this case,

$$\sigma^2 = \epsilon^2 \sqrt{\frac{\pi}{2}} e^{2t^2} \left( \sqrt{\frac{2\sigma_0^4}{\pi}} e^{-2t_0^2} + \operatorname{erf}(\sqrt{2}t) - \operatorname{erf}(\sqrt{2}t_0) \right). \quad (2.59)$$

For large  $|t_0|$ , that is, starting far from the bifurcation point,  $\sigma$  becomes approximately independent of  $\sigma_0$  and  $t_0$ . Under this assumption, we take the approximation,

$$\sigma^2 \approx \epsilon^2 \sqrt{\frac{\pi}{2}} e^{2t^2} \left( 1 + \operatorname{erf}(\sqrt{2}t) \right). \quad (2.60)$$

For  $\mu = t$ , the bifurcation point is reached when  $t = t_b = 0$ . Thus, the integration of  $\sigma^2$  gives,

$$8 \int_0^T \sigma^2 dt = 2\pi\epsilon^2 \left( \operatorname{erfi}(\sqrt{2}T) + \frac{4T^2}{\pi} {}_2F_2(2T^2) \right), \quad (2.61)$$

where  $\operatorname{erfi}$  is the imaginary error function, and  ${}_2F_2$  is the hypergeometric function  ${}_2F_2(1, 1; 3/2, 2; 2T^2)$  [1]. Thus, the escape distribution for a linear sweep is approximated by,

$$P_{\infty}(T) \approx \frac{2(1 + \operatorname{erf}(\sqrt{2}T))}{\sqrt{2\pi}\epsilon(\pi \operatorname{erfi}(\sqrt{2}T) + 4T^2 {}_2F_2(2T^2))^{3/2}} \times \exp \left[ - \frac{1}{4\epsilon^2(\pi \operatorname{erfi}(\sqrt{2}T) + 4T^2 {}_2F_2(2T^2))} \right]. \quad (2.62)$$

Figure 2.6 illustrates the first three moments and two example distributions of

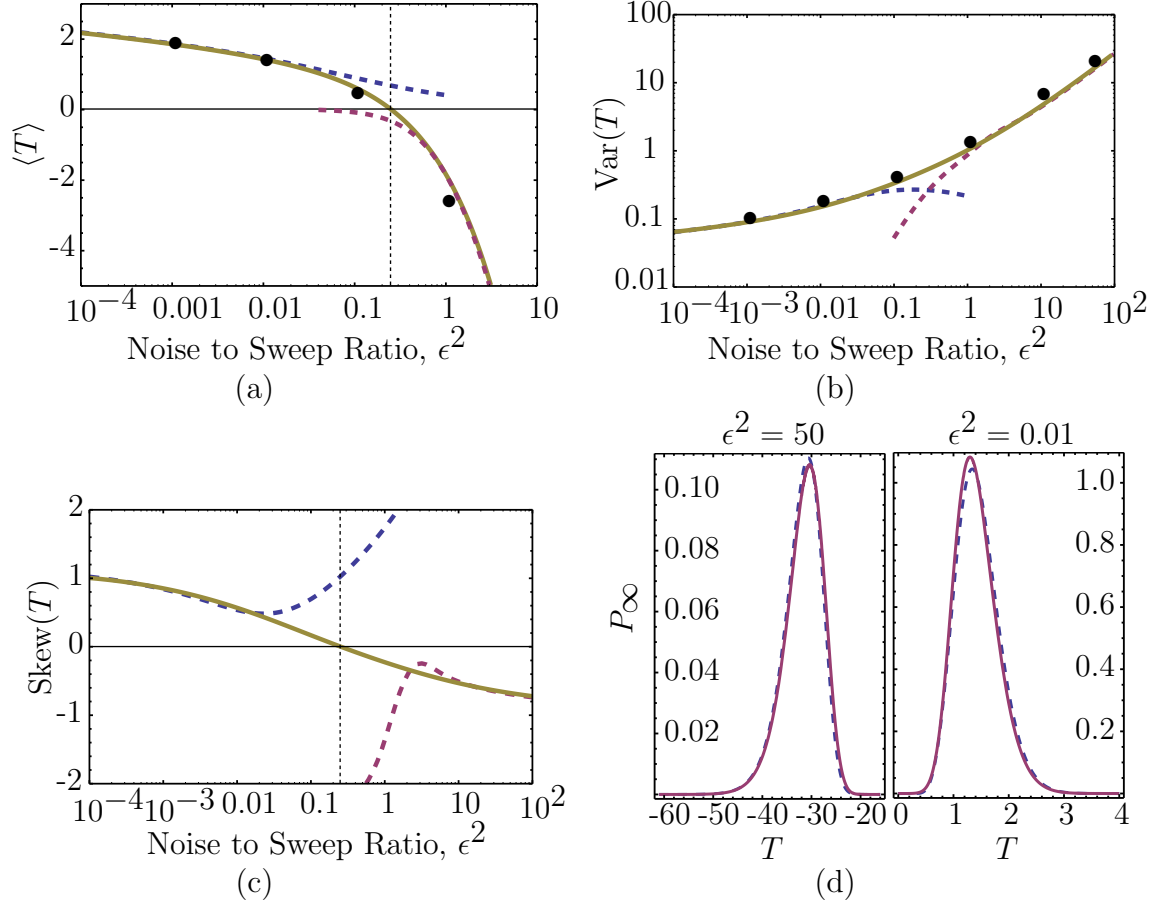


Figure 2.6: Mean (a), variance (b), skewness (c), and example distributions (d) of the distribution of escape times away from a swept subcritical pitchfork bifurcation. Numeric solution (solid lines) and approximations (dashed) for fast and slow sweeping are shown. Dots represent data points from Monte-Carlo simulations of the nonlinear Mathieu equation, equations (C.17) and (C.17), swept through the subcritical pitchfork bifurcation.

the escape current for a linearly swept subcritical pitchfork bifurcation over a wide range of noise intensities computed using numerical and approximate solutions of the FP equation. Solid lines indicate the solution obtained by numerically solving the FP equation over a finite domain. The moments for the adiabatic approximation (large noise) and the delayed bifurcation (small noise) approximation developed in this paper, given in equation (2.62), are shown as dashed lines. The dots represent data points obtained by Monte-Carlo simulation of a nonlinear Mathieu equation near the subcritical pitchfork bifurcation point. In appendix C we illustrate how this system reduces to the one-dimensional model employed in this analysis. An interesting feature of the distributions is that the skewness is positive for delayed bifurcations and negative for activated escape, indicating that the sign of the skewness is an indicator of the sweep rate relative to the noise strength.

## 2.5 Subcritical Pitchfork Bifurcation in a MEMS Resonator

In an experimental setting, it is common to interrogate a nonlinear resonator by slowly sweeping its drive frequency through resonance. This practice captures a portion of the frequency response curve from which device parameters can be fit. Given the discussion in the previous sections of this chapter, we must acknowledge that the branch end points, i.e., the bifurcation points, are not faithfully captured by this experimental technique. To examine this further and compare equation (2.62) with experimental data, in this section we consider a set of sweeping experiments carried out by Chris Burgner at the University of California, Santa Barbara, under the supervision of Prof. Kimberly Turner [16]. These experiments were done on a MEMS gyroscope which exhibits parametric resonance. A scanning electron microscope image of the device is shown in figure 2.7 (a). Figure 2.7 (b) shows the amplitude and



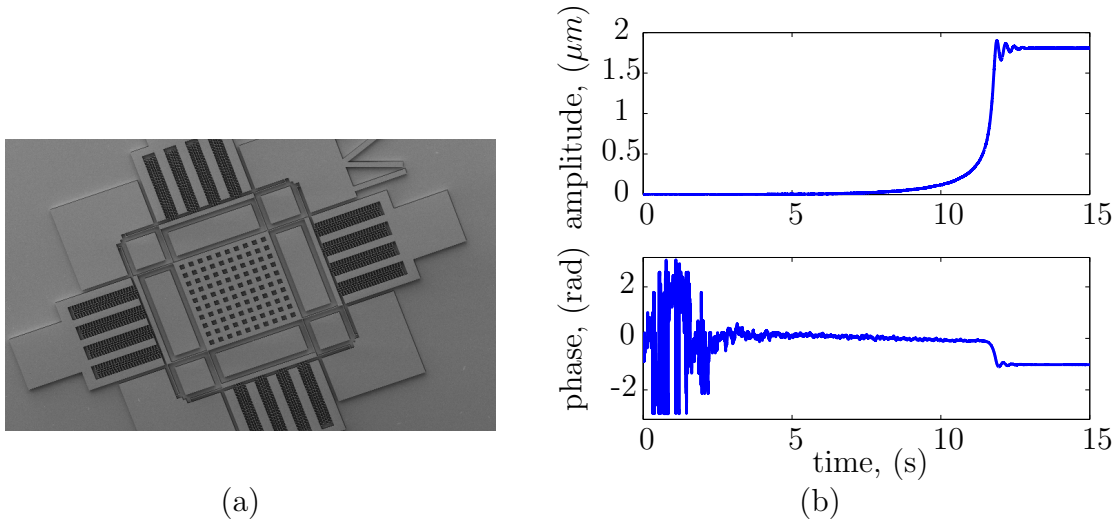


Figure 2.7: (a) SEM of MEMS gyroscope [89]. (b) Amplitude and phase of drive axis vibration during an example escape event under parameter sweep. For interpretation of the references to color in this and all other figures, the reader is referred to the electronic version of this dissertation.

phase of the drive mode of the device during an escape event while the forcing frequency is swept. The device, described in more detail in [89], was employed for this work because it was conveniently available and exhibits a subcritical pitchfork bifurcation in its subharmonic resonant response. The gyroscope possesses two nominally orthogonal vibration modes, the drive mode and the sense mode. The wide frequency range of the resonant response of this nonlinear gyro allows these modes to be significantly mistuned and so in our experiment, which focuses on the drive mode, the sense mode can be ignored. We model the drive mode by

$$\ddot{z} + 2\Gamma\dot{z} + \omega_0^2(1 + \delta_1 + \delta_1 \cos 2\omega t)z + \gamma(1 + \delta_3 + \delta_3 \cos 2\omega t)z^3 = \xi(t) \quad (2.63)$$

$$\langle \xi(t) \rangle = 0 \quad \langle \xi(t)\xi(t') \rangle = \frac{4\Gamma k_B T}{m} \delta(t - t') \quad (2.64)$$

where  $\Gamma$  is the damping rate,  $\omega_0$  is the natural frequency,  $\omega$  is the drive frequency,  $\delta_1$  is the normalized variation of the linear stiffness due to parametric forcing,  $\gamma$  is the nonlinear stiffness coefficient,  $\delta_3$  is the normalized variation of the nonlinear

stiffness due to parametric forcing,  $m$  is the effective mass of the resonator,  $T$  is the temperature, and  $\xi$  is a white Gaussian thermal noise. The reduction of this model near the subcritical pitchfork is carried out in appendix C following the method presented in [62]. The reduced model is

$$\begin{aligned}\frac{dq}{d\tau} &= 2\mu q + 4q^3 + \sqrt{D}\xi(\tau), \\ \langle \xi \rangle &= 0, \quad \langle \xi(\tau)\xi(\tau') \rangle = 2\delta(\tau - \tau'),\end{aligned}\tag{2.65}$$

where

$$\tau = \Gamma t \tag{2.66}$$

$$\mu = \frac{1}{2}(-1 + \sqrt{\beta^2 - \alpha^2}), \tag{2.67}$$

$$r = \frac{1}{\Gamma} \frac{d\mu}{dt} = \frac{1}{8\Gamma^2} \left( (2\alpha + \beta)\omega_0 \frac{d\delta_1}{dt} - 4\alpha \frac{d\omega}{dt} \right), \tag{2.68}$$

$$D = \frac{k_B T \gamma}{32\omega^3 \Gamma} \frac{\alpha\beta^2(3 + 2\delta_3) + \delta_3\beta(\beta + \alpha)^2}{(\beta^2 - \alpha^2)^{3/2}}, \tag{2.69}$$

$$\alpha = \frac{\omega^2 - \omega_0^2(1 + \delta_1)}{2\omega\Gamma} \approx -\frac{\omega_0\delta_1}{2\Gamma} + \frac{\sigma}{\Gamma}, \tag{2.70}$$

$$\beta = \frac{\delta_1\omega_0^2}{4\omega\Gamma} \approx \frac{\omega_0\delta_1}{4\Gamma}. \tag{2.71}$$

In the reduced model, the dynamic variable  $q$  is a linear combination of averaged quadrature components of  $z$  and  $\dot{z}$ . The details of the transformation are left to appendix C.  $\tau$  is a scaled time variable,  $\mu$  is the bifurcation parameter which depends on the device parameters,  $r$  is the non-dimensional sweep rate of the bifurcation parameter assuming that the swept parameters are  $\delta_1$  and/or  $\omega$ ,  $D$  is the non-dimensional effective strength of the noise on the slow manifold,  $\alpha$  is the effective detuning between the drive and natural frequencies, and  $\beta$  is the effective parametric forcing strength. Note that the effective noise strength is also a function of the detuning and forcing strength. To capture the leading order term, these parameters should be evaluated at the bifurcation point where  $\beta_b^2 = \alpha_b^2 + 1$ . The non-dimensional noise to sweep ratio

is given by

$$\epsilon^2 = \frac{D}{r} = \frac{3\Gamma k_B T \gamma}{4\omega_0^3} \frac{\alpha_b \beta_b^2}{(2\alpha_b + \beta_b)\omega_0 \dot{\delta}_1 - 4\alpha_b \dot{\omega}}. \quad (2.72)$$

In this expression we have dropped terms proportional to  $\delta_3$  for convenience since  $\delta_3 \ll 1$  these terms don't contribute much to the value of  $\epsilon^2$ . Note the overdots in equation (2.72) denote derivative with respect to the lab frame time, not the non-dimensionalized scaled time. The non-dimensional parameters  $\alpha_b$  and  $\beta_b$  appear up in equation (2.72) because the dynamics near the bifurcation point depend on the system parameters. These values have been given the subscript  $b$  to denote that they should be evaluated at the bifurcation point encountered during the parameter sweep. Again, this is the point along the parameter sweep trajectory where  $\beta_b^2 = \alpha_b^2 + 1$ . When the frequency is swept along, i.e.  $\dot{\delta}_1 = 0$ , equation (2.72) simplifies to

$$\epsilon^2 = \frac{D}{r} = \frac{3k_B T |\gamma| \delta_1^2}{256\omega_0 \Gamma |\dot{\omega}|}, \quad (2.73)$$

which indicates how  $\epsilon^2$  depends on physical parameters.

A frequency response for the device is shown in figure 2.8. The device was placed in a vacuum chamber at 1mTorr and monitored via a laser vibrometer. At this vacuum level the quality factor of the resonator is  $Q \approx 3000$  and the natural frequency is near 8.485kHz. An electrostatic potential of 15V was placed across the non-interdigitated combs seen in figure 2.7 (a) and the frequency of the drive voltage was swept downward from well above the subcritical pitchfork bifurcation point, which is seen in figure 2.8 to be near 8485Hz. Sweep rates between 0.005 and 0.3 Hz/sec were used and 1000 escape measurements were performed for each sweep rate to generate the family of escape distributions shown in figure 2.9. A single example escape event is shown in figure 2.7 (b). This set of escape distributions was taken with ambient noise.

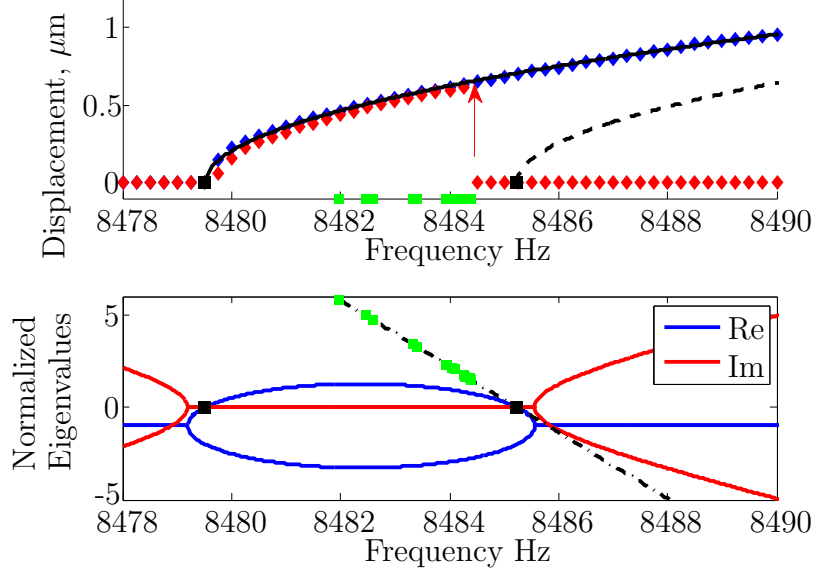


Figure 2.8: (Top) Frequency response for the MEMS resonator. Blue data points track the sweep up and red data points track the sweep down. The green data points represent the mean jump frequency for various sweep rates. Black lines represent fitted stable (solid) and unstable (dashed) frequency response branches. (Bottom) Real and imaginary parts of the eigenvalues belonging to the fixed point at zero. Dashed line represents the linear sweep approximation.

Additional noise was added with base excitation using a piezo element, in order to reach smaller values of the sweep rate to noise ratio. Recall that the normalized mean and variance of escape are functions of this ratio when the sweep is linear in time. The inset of figure 2.9 shows three different distributions that share the same value of  $r/D$  in order to illustrate that, while the normalized statistics depend only on the ratio, the true statistics depend on both values. The experimental distribution shown in the inset has had its mean shifted for comparison. The reason this was required will be discussed presently. The primary attribute we notice about the measured escape distributions is that they all appear to be described by delayed bifurcations. Despite sweeping so slowly that a single escape data point took several minutes to acquire, activated escape over the barrier was not observed. The skew of the distributions was expected to confirm this, but the data was inconclusive. This may be because the data may have been somewhat contaminated by the drifting parameter values of the

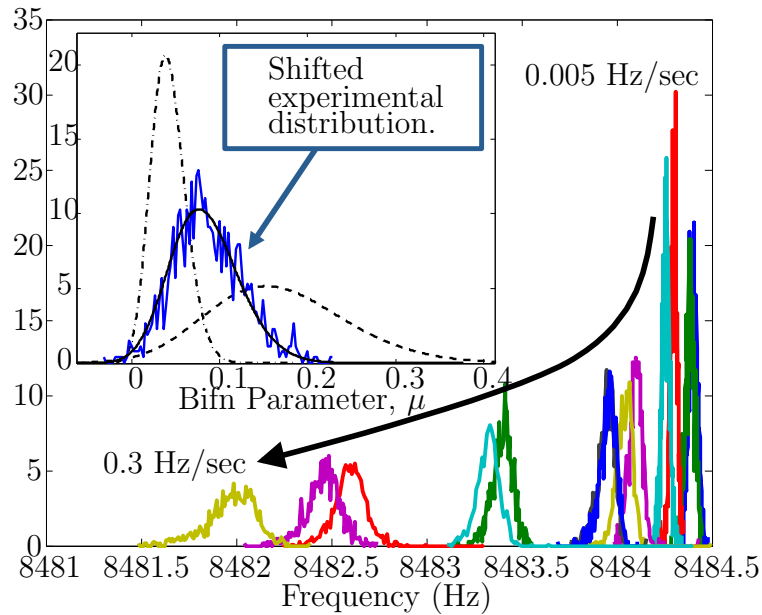


Figure 2.9: Experimentally measured distributions of escape events for ambient noise and sweep rates ranging from 0.005 to 0.3 Hz/sec. The inset shows one such distribution, artificially shifted, and compared against the theoretical distribution. The purpose of the shift is discussed in the text. The three distributions in the inset correspond each to different sweep rate and noise intensities yet all three with the same ratio. This illustrates that, while the normalized statistics depend only on the ratio, the true statistics depend on both values.

resonator. The drift observed was noted to be periodic and correlated to the HVAC cycles of the lab environment. In the data presented here the drift was compensated for by measuring the natural frequency prior to each sweeping experiment.

Figure 2.10 shows the normalized mean and variance of the escape distributions plotted against the sweep rate to noise ratio. The results show qualitative agreement with the result in equation (2.62). We believe the reason for the difference is a deviation from the assumptions employed in the development of equation (2.62). The assumption of a linear sweep requires that the eigenvalue of the bifurcating fixed point change linearly in time. Figure 2.8 shows the quasistatic values of the eigenvalues of the fixed point at zero amplitude during the sweep. The green dots show the mean frequency of escape. It is clear that the linear approximation, shown as the dashed line, is a poor representation of the actual eigenvalue. The eigenvalue is smaller than anticipated and so the response does not grow as fast as expected. Hence the mean occurs later than expected, as seen in figure 2.10(a). This is the reason the example curve in the inset of figure 2.9 was shifted for comparison with the theoretical distribution. The variance is also larger than predicted for most data points. This may also arise from the failure of the linear sweep assumption, since the eigenvalue was smaller than expected it took more time for the system to escape. During this added time the system continued to diffuse, resulting in a larger spread of escape times. In addition, over this wide range of parameter variation the effective noise strength on the center manifold will depend on the bifurcation parameter. Thus, while equation (2.58) could be employed to capture the nonlinear relationship between the eigenvalue and the forcing frequency, it does not account for the change in effective noise intensity.

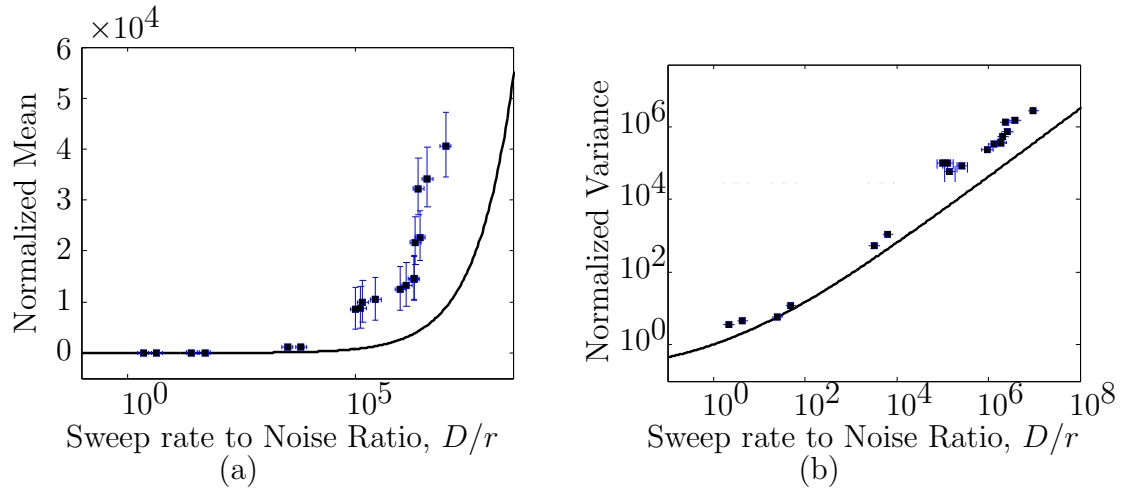


Figure 2.10: Normalized mean (a) and variance (b) of the bifurcation parameter at escape. The solid line represents the mean of the distribution for a linear sweep predicted from the normal form, as given in equation (2.62). The data points were calculated from the measured distributions shown in figure 2.9.

## 2.6 Outlook

As mentioned at the beginning of this chapter, this work was motivated by applications to sensing, parameter fitting, and system identification. Escape experiments, used for these applications, employ highly visible transients which can be useful in very small systems that are difficult to measure [58]. However, when compared to more conventional methods, measurement by collecting escape event data is quite slow [17]. The reason is that there are three time scales acting in the system and activated escape near a bifurcation point operates on the slowest time scale. Moreover, many escape events must be observed (with the exception of single-shot qubit readout [78]) to obtain an estimate of the escape moments. This brings the added complication of parameter drift over such long time scales. If bifurcation location or tracking is to be used for sensing or system identification in a device that can be monitored with reasonable precision, then feedback control [17] or experimental continuation [99] may be more appropriate techniques.

# Chapter 3

## The Dynamical Bridge

In this chapter we discuss the use of noise activated escape in a parametric sensor. The past decade has seen significant advances in the employment of micro- and nano-electromechanical (M/NEMS) resonators as parametric sensors. The small size and high quality factors of these devices enables very sensitive coupling to and/or detection of adsorbed masses on the resonator surface [40, 42, 121, 33, 92, 43, 66], superconducting qubit states [23, 68, 112], and electron transport statistics [6, 5], to cite a few examples. Many of the implementations of NEMS resonators for parametric sensing mirror those of Josephson junction circuits for the same applications [55, 76, 88, 114, 70, 105, 78, 116, 96]. Accordingly, the sensing paradigms are very similar to the methods developed in the 1970s to measure the Josephson junction critical current [67, 58, 47].

The current biased Josephson junction is analogous to the simple pendulum where the critical current is likened to the coefficient of the restoring torque ( $mgl$  in a pendulum) and the phase difference,  $\delta$ , between the superconductor order parameters across the junction is likened to the pendulum angle. For small  $\delta$  the junction is modeled, like many NEMS resonators, by Duffing's equation. Accordingly, it is not surprising to find many common experimental methods associated with both systems.



The measurement paradigm we highlight here is, roughly speaking, the use of such a Duffing resonator as a threshold detector. While there are several variations on this concept, the basic principle is as follows. The system is placed in the bistable regime and brought close to a bifurcation (the threshold). Noise in the system blurs the threshold and so the system is placed sufficiently far from the threshold so that noise only occasionally pushes the system over the edge. This occurs when a rare large outburst of noise pushes the system out of the domain of attraction belonging to the occupied attractor. When this happens the system is said to have escaped. The probability per unit time, or rate, of escape is exponentially sensitive to the distance from the operating point to the threshold and, by extension, to the system parameters. Accordingly, monitoring the time until escape, and performing many such escape experiments, allows one to calculate the mean escape rate and thus determine parameter variation in the resonator with high precision. The threshold position can be thought of as being detected through the measurement of the escape rate. The escape events monitored in this method are often highly visible transient dynamics of the resonator. This can enable a very precise measurement to be made even when the detailed motion of the resonator is difficult to resolve, c.f. [58].

A single-shot variation of this method is employed in qubit readout, relevant for quantum computing [116, 78]. If the state of the qubit, which is coupled to the resonator, displaces the bifurcation sufficiently, then an escape event can be strongly correlated with the qubit state. The qubit state can then be inferred from the occurrence, or lack thereof, of an escape event. This detection scheme has become known as the Josephson bifurcation amplifier [116].

The phenomenon of noise activated escape, on which these measurement methodologies are based, has been studied in great detail. The escape rate has been calculated for Gaussian noise [64], Poisson noise [31] and non-Gaussian perturbations superimposed on Gaussian noise [105, 11, 10, 12]. These and similar results have application

in the measurement of electron transport statistics [7, 55, 53, 88, 114]. It is also known that the escape events occur along trajectories forming narrow tubes in phase space [21, 20]. This gives experimental credence to the method of calculating the escape rate by considering the most probable path.

In this chapter we discuss a variant on the detection schemes described above, called the balanced dynamical bridge [30]. In the dynamical bridge paradigm a bistable system subject to weak noise is arranged such that the probability to be in either state is equal. A perturbing parameter variation or change in the noise statistics can then be measured by the resulting shift in relative state populations, or by the force required to rebalance the system. The balanced dynamical bridge is so named because it is analogous to a bridge circuit in which the voltage across the bridge connection is tuned to zero in order to measure, for example, a resistance. However, here we consider a dynamical system driven by noise, hence the “dynamical” designation.

Our discussion of the balanced dynamical bridge is organized in the following way. In section 3.1 we review the theory of noise activated escape, treating both Gaussian noise and a non-Gaussian perturbing process. In section 3.2 we discuss the dynamical bridge as a general use detector, formulating expressions for the sensitivity and measurement time of the device. In section 3.3 we discuss the dynamical bridge as a detector of non-Gaussian noise. In section 3.4 we discuss the Duffing resonator as an example of a prototypical bistable system. We present the locus of operating points in a two-dimensional parameter space at which the bridge is balanced. In section 3.5 we give an example of measuring non-Gaussian noise by considering a one-dimensional dynamic bridge subject to weak shot noise. Concluding remarks and a discussion of future work are given in section 3.6.

### 3.1 Activated Escape

In section 2.2 we reviewed activated escape by white Gaussian noise in one dimension. In this section we review the general theory of noise activate escape due to additive Gaussian noise perturbed by weak non-Gaussian noise; see [11]. This theory lays the groundwork for our subsequent discussions of bridge sensitivity and detection of non-Gaussian noise.

We begin with a general nonlinear system

$$\dot{\mathbf{q}} = \mathbf{K}(\mathbf{q}) + \sqrt{D}\mathbf{f}(t) + G(\mathbf{q})\boldsymbol{\xi}(t), \quad (3.1)$$

where  $\mathbf{q} \in \mathbb{R}^n$  is the system state vector,  $\mathbf{K}$  is the nonlinear vector field,  $\mathbf{f}$  is a stationary Gaussian noise vector with characteristic strength  $D$ ,  $G \in \mathbb{R}^{n \times m}$  is the non-Gaussian noise matrix coefficient, and  $\boldsymbol{\xi} \in \mathbb{R}^m$  is the non-Gaussian noise vector, assumed to be independent of  $\mathbf{f}$ . Suppose that the noise free system possesses two stable fixed points,  $\mathbf{q}_a$  and  $\mathbf{q}_b$ , and a saddle point,  $\mathbf{q}_s$ , on the boundary between the basins of attraction for  $\mathbf{q}_a$  and  $\mathbf{q}_b$ . If the noise is weak, then the system will likely settle down to the vicinity of one stable fixed point, say  $\mathbf{q}_a$ . It may happen subsequently that a large rare burst of noise pushes the system out of this basin and into that belonging to  $\mathbf{q}_b$ . Suppose we know the path by which the system exits the basin and the accompanying realization of  $\boldsymbol{\xi}$ , then the Gaussian noise realization required to make this transition follows from equation (3.1),

$$\mathbf{f}(t) = D^{-1/2}(\dot{\mathbf{q}} - \mathbf{K}(\mathbf{q}) - G(\mathbf{q})\boldsymbol{\xi}(t)). \quad (3.2)$$

The probability for such a noise outburst to occur is [46]

$$P[\mathbf{f}(t)] \propto \exp \left[ -\frac{1}{2} \int \int \mathbf{f}^T(t') \hat{\mathcal{F}}(t' - t) \mathbf{f}(t) dt dt' \right], \quad (3.3)$$

$$\int \langle \mathbf{f}(t) \mathbf{f}^T(s) \rangle \hat{\mathcal{F}}(s) ds = I \delta(t), \quad (3.4)$$

where  $\mathcal{F}$  is the inverse pair correlator of  $\xi(t)$ . We assume that  $\mathbf{f}$  possesses time reversal symmetry so that  $\hat{\mathcal{F}}(t) = \hat{\mathcal{F}}(-t) = \hat{\mathcal{F}}^T(t)$ . From equation (3.2) we see that the integrand of (3.3) is inversely proportional to the characteristic noise strength. Thus, for weak noise, the probability for a transition to occur is sharply peaked about the most probable switching path, i.e., the path that minimizes  $P[\mathbf{f}(t)]$  in equation (3.3) where  $\mathbf{f}$  is given by (3.2). The mean switching rate is approximately proportional to the probability for the realization of the most probable switching path. If  $\boldsymbol{\xi} = 0$ , the rate is

$$r_0 \propto \exp[-S_0/D] \quad (3.5)$$

$$S_0 = \min \left\{ \frac{1}{2} \int \int (\dot{\mathbf{q}} - \mathbf{K})_{t'}^T \hat{\mathcal{F}}(t' - t) (\dot{\mathbf{q}} - \mathbf{K})_t dt dt' \right\} \quad (3.6)$$

where  $(\dot{\mathbf{q}} - \mathbf{K})_t$  denotes  $\dot{\mathbf{q}}(t) - \mathbf{K}(\mathbf{q}(t))$  and the minimum is taken over all paths that take the system from  $\mathbf{q}_a$  to  $\mathbf{q}_b$ .

When  $\langle \mathbf{f}(t) \mathbf{f}^T(s) \rangle = I \delta(t - s)$ , then  $\hat{\mathcal{F}}(t) = I \delta(t)$  and  $S_0$  simplifies to

$$S_0 = \min \left\{ \frac{1}{2} \int |\dot{\mathbf{q}} - \mathbf{K}|^2 dt \right\}, \quad (3.7)$$

which is the action belonging to an auxiliary Hamiltonian system

$$\mathcal{H} = \frac{1}{2} |\mathbf{p}|^2 + \mathbf{p}^T \mathbf{K}(\mathbf{q}), \quad \mathbf{p} \equiv \dot{\mathbf{q}} - \mathbf{K}(\mathbf{q}). \quad (3.8)$$

The costate,  $\mathbf{p}$ , in this case, is proportional to the optimal noise realization, and the

constant of proportionality is  $\sqrt{D}$ . The path minimizing  $S_0$  in equation (3.7) is the made up of two parts. The first part is the heteroclinic trajectory going from  $\mathbf{q}_a$  to  $\mathbf{q}_s$  along which  $\mathbf{p} \neq 0$ , since this transition requires noise. The second part is the heteroclinic trajectory going from  $\mathbf{q}_s$  to  $\mathbf{q}_b$  along which  $\mathbf{p} = 0$ , since this response is noise free. This second part of the switching trajectory does not contribute to the calculation of the switching probability and so our focus is on the first (noisy) part.

If  $\mathbf{f}$  and  $\boldsymbol{\xi}$  are independent noise processes and  $\boldsymbol{\xi}$  is small compared to  $\mathbf{f}$ , then the mean switching rate can be expressed as [11].

$$r \propto \langle \exp [-S[\boldsymbol{\xi}]/D] \rangle_{\boldsymbol{\xi}} \quad (3.9)$$

where, to leading order,  $S[\boldsymbol{\xi}]$  is

$$S[\boldsymbol{\xi}] = S_0 + \int \boldsymbol{\chi}(t)^T \boldsymbol{\xi}(t) dt, \quad (3.10)$$

$$\boldsymbol{\chi}^T(t) = - \int [\dot{\mathbf{q}}(t') - \mathbf{K}(\mathbf{q}(t'))]^T \hat{\mathcal{F}}(t' - t) G(\mathbf{q}(t)) dt'. \quad (3.11)$$

The quantity  $\boldsymbol{\chi}$  can be thought of as the susceptibility of the activation energy to a perturbing force. The switching rate in the presence of this perturbing noise is

$$r \propto A r_0, \quad (3.12)$$

$$A = \left\langle \exp \left[ -\frac{1}{D} \int \boldsymbol{\chi}^T \boldsymbol{\xi} dt \right] \right\rangle = \Phi_{\boldsymbol{\xi}}[i\boldsymbol{\chi}/D], \quad (3.13)$$

where  $\Phi_{\boldsymbol{\xi}}$  is the characteristic functional of  $\boldsymbol{\xi}$ .

## 3.2 Dynamical Bridge Sensitivity

We now turn to the dynamical bridge. In this section we set  $\boldsymbol{\xi} = 0$  and discuss the bridge as a general use detector. We calculate the sensitivity and measurement time

assuming the rates developed in the previous section are known.

Equation (3.1) serves as the microscopic model for the dynamic bridge. The bridge itself functions on a much longer time scale. For times scales exceeding that of the switching dynamics and correlations of  $\mathbf{f}$ , the coarsened dynamics may be modeled by the master equation

$$\begin{aligned}\dot{P}_1 &= -r_1 P_1 + r_2 P_2, \\ \dot{P}_2 &= r_1 P_1 - r_2 P_2,\end{aligned}\tag{3.14}$$

where  $P_1$  and  $P_2$  are the probabilities to find the system in the first or the second states respectively, and  $r_i$  is the switching rate out of the  $i^{\text{th}}$  state,  $i = 1, 2$ . Normalization of the probability distribution requires  $P_2 = 1 - P_1$  and so we will work with  $P_1$  only for this analysis. The solution to equations (3.14) is

$$P_1(t) = \frac{r_2}{r_1 + r_2} \left(1 - e^{-(r_1 + r_2)t}\right) + P_1(0)e^{-(r_1 + r_2)t},\tag{3.15}$$

from which we see that the characteristic relaxation time of the system is  $t_r \sim (r_1 + r_2)^{-1}$ .

To make a measurement with the dynamic bridge we must measure the probability  $P_1$ . This may be done by measuring some quantity  $x$  that takes on the value  $X_1$  when the system is in state 1 and  $X_2$  when the system is in state 2. The probability to be in state 1 can be estimated from  $N$  measurements of  $x$ , where the system is given time to relax between each measurement. Thus, the total measurement time is on the order  $Nt_r$  and gives the probability estimate

$$\hat{P}_1 = \frac{1}{N(X_1 - X_2)} \sum_{i=1}^N (x_i - X_2).\tag{3.16}$$

The mean and variance of the estimator  $\hat{P}_1$  are

$$\langle \hat{P}_1 \rangle = \bar{P}_1, \quad (3.17)$$

$$\langle (\hat{P}_1 - \bar{P}_1)^2 \rangle = \frac{\bar{P}_1 - \bar{P}_1^2}{N}, \quad (3.18)$$

where  $\bar{P}_1 = r_2/(r_1 + r_2)$  is the steady state value of  $P_1$ . Equations (3.17) and (3.18) show that  $\hat{P}_1$  is an unbiased estimator of  $\bar{P}_1$  with uncertainty proportional to  $N^{-1/2}$ .

Now, suppose that some parameter of the bridge system,  $\lambda$ , changes by an amount  $\Delta\lambda$ . The sensitivity of the dynamic bridge is given by  $\partial_\lambda \bar{P}_1$ . In calculating this quantity, we ignore the dependence of the rate prefactor on  $\lambda$  under the assumption that  $D$  is small. Thus the dominant change in the transition rates comes from the change in activation energy with respect to  $\lambda$ . Under this assumption, the bridge sensitivity is given by

$$\frac{\partial \bar{P}_1}{\partial \lambda} = \frac{r_1 r_2}{D(r_1 + r_2)^2} \left( \frac{\partial(S_1 - S_2)}{\partial \lambda} + \frac{S_1 - S_2}{D} \frac{\partial D}{\partial \lambda} \right), \quad (3.19)$$

where  $S_i$  is the activation energy (equation (3.6)) to escape from the  $i^{\text{th}}$  state,  $i = 1, 2$ . Equation (3.19) applies for any  $r_1$  and  $r_2$ . The most sensitive operating point is at the balance point where  $r_1 = r_2$  and  $S_1 \approx S_2$ . In this case equation (3.19) simplifies to  $\partial_\lambda \bar{P}_1 \approx D^{-1} \partial_\lambda (S_1 - S_2)$ , which quantifies how the dynamical bridge becomes increasingly sensitive with decreasing noise.

In order to detect a change  $\Delta\lambda$ , we must measure  $\bar{P}_1$  to sufficient accuracy. In order to see a shift in the occupation probability, the shift in  $\bar{P}_1$  should be on the order of the error in our estimate. Thus, we require

$$\sqrt{\langle (\hat{P}_1 - \bar{P}_1)^2 \rangle} \sim \frac{\partial \bar{P}_1}{\partial \lambda} \Delta\lambda \quad (3.20)$$

The variance of  $\hat{P}_1$ , equation (3.18), is bounded by  $1/4N$ , so we use this value to obtain an upper bound for the number of measurements that must be made on the bridge. Solving for  $N$  and multiplying by the relaxation time gives the measurement time

$$Nt_r = \frac{(r_1 + r_2)^3}{4r_1^2 r_2^2} \frac{D^2}{\Delta\lambda^2} \left( \frac{\partial(S_1 - S_2)}{\partial\lambda} + \frac{S_1 - S_2}{D} \frac{\partial D}{\partial\lambda} \right)^{-2}, \quad (3.21)$$

$$\approx r \left( \frac{D}{\Delta\lambda \partial_\lambda(S_1 - S_2)} \right)^2, \quad \text{at the balance point.} \quad (3.22)$$

From expressions (3.21) and (3.22), we find that the measurement time increases exponentially with decreasing noise, owing to the exponential dependence of  $r_{1,2}$  on  $D$ .

We conclude this section by again considering the case where  $\langle \mathbf{f}(t) \mathbf{f}^T(s) \rangle = I\delta(t-s)$ . This gives  $\hat{\mathcal{F}}(t) = I\delta(t)$  and  $\partial_\lambda S_i$  can be written as a simple integral along the most probable switching path.

$$\frac{\partial S_{1,2}}{\partial\lambda} = \int (\dot{\mathbf{q}} - \mathbf{K}(\mathbf{q}))^T \frac{\partial \mathbf{K}(\mathbf{q})}{\partial\lambda} dt, \quad (3.23)$$

where  $\mathbf{q}$ , for  $S_{1,2}$ , is evaluated along the heteroclinic trajectory taking the system from  $\mathbf{q}_{a,b}$  to  $\mathbf{q}_S$ .

### 3.3 Detection of Non-Gaussian Noise

The dynamical bridge can also be used as a sensitive detector of non-Gaussian noise. Suppose we have the system (3.1) and we have the ability to turn  $\boldsymbol{\xi}$  on and off. Then we can use the the system as a dynamical bridge to determine a degree of non-Gaussian character in the noise  $\boldsymbol{\xi}$ . The ability to turn  $\boldsymbol{\xi}$  on and off allows us to remove the mean by examining the mean fluctuation of the coordinate  $\mathbf{q}$  about the



fixed points  $\mathbf{q}_a$  or  $\mathbf{q}_b$ . A bias can then be applied to compensate for the mean of  $\boldsymbol{\xi}$ , which is convenient for the development, as described below.

In general, the addition of the perturbing noise  $\boldsymbol{\xi}$  will change the transition rates, see section 3.1, and this will shift the relative occupancy ratio in the bridge. The ratio of probabilities to be in state 1 and 2 is

$$\frac{P_1}{P_2} = \frac{r_2}{r_1} = \frac{A_2}{A_1} \frac{r_2^{(0)}}{r_1^{(0)}}, \quad (3.24)$$

where  $r_i^{(0)}$  is the switching rate out of the  $i^{\text{th}}$  state when  $\boldsymbol{\xi} = 0$ . Balancing the bridge before exposure to the perturbation sets  $r_1^{(0)} = r_2^{(0)}$ . We now introduce the random variable

$$z_i = \int dt \boldsymbol{\chi}_i^T(t) \boldsymbol{\xi}(t), \quad (3.25)$$

where  $\boldsymbol{\chi}_i(t)$  is given in equation (3.11) and the subscript denotes escape from the  $i^{\text{th}}$  state. Let  $\kappa_n^{(i)}$  be the  $n^{\text{th}}$  cumulant of  $z_i$ . From equation (3.13), the pre factors,  $A_i$ , are the moment generating functions for  $z_i$  and the logarithm,  $\ln A_i$ , is the cumulant generating function. Thus,

$$\ln A_i = \sum_{n=1}^{\infty} \frac{\kappa_n^{(i)}}{n!(-D)^n}. \quad (3.26)$$

Note, if  $\boldsymbol{\xi}$  is Gaussian, then  $z_i$  is also Gaussian and  $\kappa_n = 0$  for  $n > 2$ . Of course, here we assume  $\boldsymbol{\xi}$  is non-Gaussian, so we keep all cumulants. From equation (3.26), the probability ratio becomes

$$\frac{P_1}{P_2} = \exp \left[ \sum_{n=1}^{\infty} \frac{\kappa_n^{(2)} - \kappa_n^{(1)}}{n!(-D)^n} \right]. \quad (3.27)$$

We have mentioned above how the mean of  $\boldsymbol{\xi}$  can be removed by an applied bias. If

the second cumulants  $\kappa_2^{(1)}$  and  $\kappa_2^{(2)}$  can be balanced, they too can be removed from equation (3.27). In this case, the population ratio will depend only on higher order cumulants, i.e., on the non-Gaussian character of  $\boldsymbol{\xi}$ . The second cumulant of  $z_i$  can be expressed as follows

$$\kappa_2^{(i)} = \int dt dt' \boldsymbol{\chi}_i^T(t) \langle \boldsymbol{\xi}(t) \boldsymbol{\xi}^T(t') \rangle \boldsymbol{\chi}_i(t'). \quad (3.28)$$

From equations (3.11) and (3.28) it can be shown that  $\kappa_2^{(1)}$  and  $\kappa_2^{(2)}$  will be equal if

$$\int ds ds' \hat{F}(s-t) G(\mathbf{q}_i(s)) \langle \boldsymbol{\xi}(s) \boldsymbol{\xi}^T(s') \rangle G^T(\mathbf{q}_i(s')) \hat{F}(s'-t') = c \hat{F}(t-t'), \quad (3.29)$$

where  $\mathbf{q}_i$  is evaluated along the heteroclinic escape trajectory out of state  $i$  and  $c$  is some constant, equal for  $i = 1, 2$ . This condition is satisfied if, for example,  $\mathbf{f}$  is a vector of uncorrelated Gaussian white noise processes,  $\boldsymbol{\xi}$  is a vector of uncorrelated Poisson noise processes, and  $G \propto I$ . If the mean has been removed, and if the second cumulants cancel, then the population ratio of the bridge will reflect a measure of the non-Gaussian character of  $\boldsymbol{\xi}$ , which is captured in the series of cumulants of  $z_{1,2}$ , that is, by the projection of the noise realizations onto the switching susceptibility. This will be illustrated by an example in section 3.5. Note that while the second cumulants drops out of equation (3.27), they remain in equation (3.26) and thus change the switching rate. In this case, the second cumulant can be lumped together with that of the Gaussian noise,  $f$ , and be understood as a renormalization of the Gaussian noise strength.

### 3.4 The Duffing Resonator Bridge

In this section we discuss the lightly damped Duffing resonator and its use as a dynamic bridge. We map out the bistable region of parameter space and numerically determine the locus of points in this space where the bridge is balanced, i.e.,  $r_1 = r_2$ . The resonator, subject to a periodic driving force and additive noise, is described by

$$\ddot{y} + 2\Gamma\dot{y} + \omega_0^2 y + \gamma y^3 = h \cos \omega t + \hat{f}(t), \quad (3.30)$$

where,  $y$  is the oscillator coordinate,  $\omega_0$  is its natural frequency,  $\Gamma$  is the friction coefficient, ( $\Gamma \ll \omega_0$ ),  $\gamma$  is the nonlinearity parameter, and  $\hat{f}(t)$  is Gaussian white noise with  $\langle \hat{f}(t) \rangle = 0$  and  $\langle \hat{f}(t)\hat{f}(t') \rangle = 2\hat{D}\delta(t-t')$ . We assume near resonant forcing of amplitude  $h$  and frequency  $\omega$  with  $\omega^2 - \omega_0^2 \ll \omega^2$ . It is convenient to switch from  $y$  to a slowly-varying complex amplitude,  $u$ , using the well-known Van der Pol transformation

$$y(t) = \sqrt{\frac{2\omega\Gamma}{3|\gamma|}} u e^{i\omega t} + c.c., \quad (3.31a)$$

$$\dot{u} e^{i\omega t} + c.c. = 0. \quad (3.31b)$$

We apply this transformation to equation (3.30), neglect fast oscillating terms, and move to a nondimensional time scale,  $\tau$ , to obtain

$$\dot{u} = -(1 + i\Omega)u + i \operatorname{sgn}(\gamma)|u|^2 u - i\sqrt{\beta} - if(\tau), \quad (3.32)$$

where the dot,  $(\dot{\phantom{x}})$ , is now interpreted as the derivative with respect to  $\tau$  and the following nondimensional parameters have been defined, along with the nondimensional

noise  $f(\tau)$ ,

$$\tau = \Gamma t, \quad (3.33)$$

$$\Omega = \frac{\omega^2 - \omega_0^2}{2\omega\Gamma}, \quad (3.34)$$

$$\beta = \frac{3|\gamma|h^2}{32\omega^3\Gamma^3}, \quad (3.35)$$

$$f(\tau) = \sqrt{\frac{3|\gamma|}{8\omega^3\Gamma^3}} e^{-i\omega\tau/\Gamma} \hat{f}(\tau/\Gamma), \quad (3.36)$$

where  $f(\tau)$  refers to  $f(t)$  in (3.1). By neglecting the fast oscillating moments, we approximate the real ( $f_{\text{r}}$ ) and imaginary ( $f_{\text{i}}$ ) parts of  $f$  as two independent white Gaussian noise processes with [35]

$$\langle f_{\text{r}}(\tau) \rangle = \langle f_{\text{i}}(\tau) \rangle = \langle f_{\text{r}}(\tau) f_{\text{i}}^*(\tau') \rangle = 0, \quad (3.37\text{a})$$

$$\langle f_{\text{r}}(\tau) f_{\text{r}}^*(\tau') \rangle = \langle f_{\text{i}}(\tau) f_{\text{i}}^*(\tau') \rangle = D\delta(t - t'). \quad (3.37\text{b})$$

where  $D$  is the nondimensional noise strength

$$D = \frac{3|\gamma|\hat{D}}{8\omega^3\Gamma^2}. \quad (3.38)$$

In the absence of noise ( $f(\tau) = 0$ ), the fixed point are found by setting equation (3.32) to zero. Thus, the fixed points must satisfy

$$u = \frac{\sqrt{\beta}}{\text{sgn}(\gamma)|u|^2 - \Omega + i}. \quad (3.39)$$

Taking the norm of (3.39) gives a cubic equation in  $|u|^2$ ,

$$|u|^6 - 2\text{sgn}(\gamma)\Omega|u|^4 + (\Omega^2 + 1)|u|^2 - \beta = 0. \quad (3.40)$$

The fixed points are associated with the the positive real roots of this equation. The bistable region is bounded by two saddle-node bifurcations. The amplitudes of  $u$  at which these bifurcations occur can be found by taking the derivative of (3.40) with respect to  $|u|^2$  and solving for the bifurcation value of  $|u|^2$

$$|u|_B^2 = \frac{2}{3} \operatorname{sgn}(\gamma) \Omega \pm \sqrt{\Omega^2 - 3}, \quad (3.41)$$

where the subscript  $B$  denotes a saddle-node bifurcation value. This solution is substituted back into (3.40) to determine the boundaries of the bistable region in parameter space, which can be expressed as

$$\beta_B = \frac{2}{27} (\operatorname{sgn}(\gamma) \Omega (\Omega^2 + 9) \pm (\Omega^2 - 3)^{3/2}), \quad \Omega^2 \geq 3. \quad (3.42)$$

This bistable region is illustrated in figure 3.3 as the region between the solid lines. Plotting with axes  $\Omega^{-2}$  and  $\beta\Omega^{-3}$  allows us to visualize the bistable region as a closed region of parameter space. Inside the bistable region the system posses two stable fixed points and one saddle point. Returning to the notation of section 3.1, we set the real and imaginary components of  $u$  to be the elements of the two component vector  $\mathbf{q} \in \mathbb{R}^2$ . The costate,  $\mathbf{p} \in \mathbb{R}^2$ , is proportional to the optimal realization of the noise quadratures; the real and imaginary components of  $f(\tau)$ . The most probable or optimal switching trajectories, as described in section 3.1, are heteroclinic solutions of the Hamiltonian system, given here by

$$\mathcal{H} = \frac{|\mathbf{p}|^2}{2} + (|\mathbf{q}|^2 - \Omega)(\mathbf{q} \wedge \mathbf{p}) - \mathbf{q}^T \mathbf{p} - p_2 \sqrt{\beta}, \quad (3.43)$$

where  $\wedge$  is the wedge product defined as  $\mathbf{q} \wedge \mathbf{p} = q_1 p_2 - q_2 p_1$ , and  $p_2$  is understood to be the second component of the two dimensional vector  $\mathbf{p}$ . The pair of heteroclinics for a sample set of parameters is depicted in figures 3.1 and 3.2. In figure 3.1 the

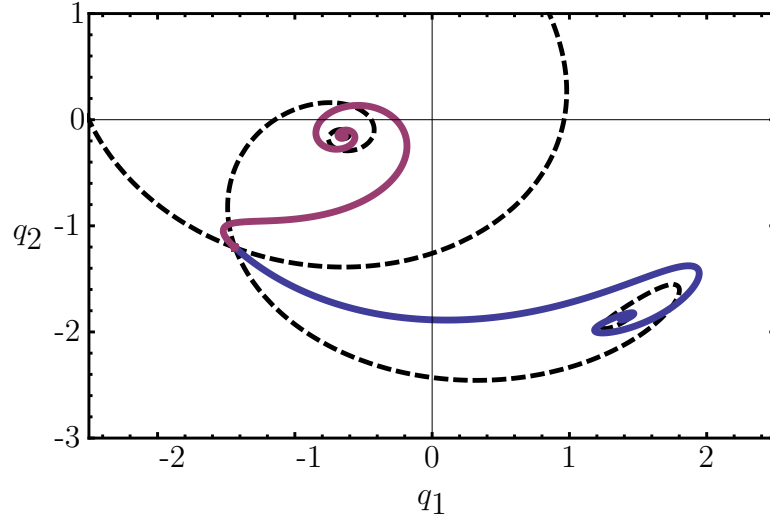


Figure 3.1: The blue and magenta lines depict heteroclinic solutions connecting the operation points to the saddle point for system (3.43), as projected onto the  $(q_1, q_2)$  plane. Solid lines represent the  $p \neq 0$  solutions and the dashed lines are the noise-free ( $p = 0$ ) stable and unstable manifolds of the saddle point. Parameter values:  $\Omega = 4.706182$  and  $\beta = 8.501802$

heteroclinic is projected onto the  $(q_1, q_2)$  plane. The dashed lines are noise-free stable and unstable manifolds of the saddle point. The solid lines show the most probable path by which noise will drive the system from the stable fixed points to the saddle point. Upon reaching the saddle point, the system will relax to one of the stable fixed points, most likely following quite closely the corresponding noise-free unstable manifold. Figure 3.2 shows the heteroclinic projected onto the  $(p_1, p_2)$  plane. The trajectories represent the most probable realization of the noise quadratures that gives rise to a switching event. These trajectories begin and end at the noise-free equilibria, hence at  $\mathbf{p} = \mathbf{0}$ .

The heteroclinics shown in figures 3.1 and 3.2 were obtained by the method of shooting. The parameter values were chosen because the action along these two heteroclinics is equal. Thus, these heteroclinics represent a balanced bridge configuration (at least up to the difference in prefactors). The locus of points in parameter space for which the action is equal for both switching directions is plotted as the dashed line

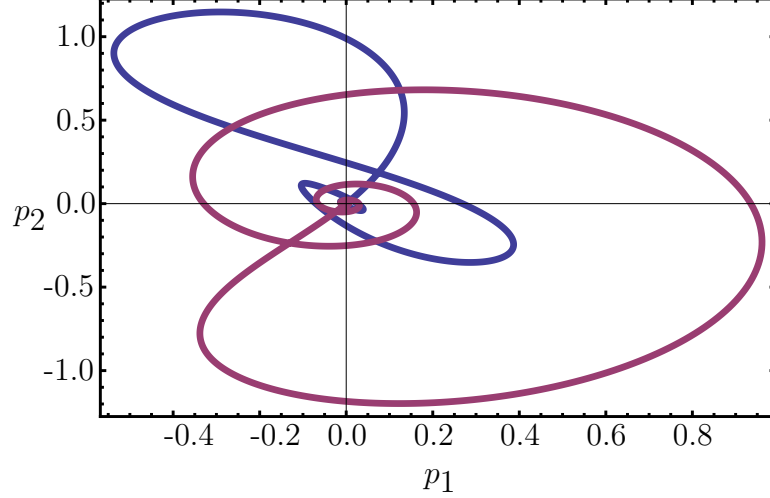


Figure 3.2: Heteroclinic solutions for system (3.43) projected onto the  $(p_1, p_2)$  plane. For the solution with  $\Omega = 4.706182$  and  $\beta = 8.501802$ . Note that these heteroclinics start and end at noise-free points where  $p_1 = p_2 = 0$ .

in figure 3.3. The balance curve in figure 3.3 was determined numerically. However, the end points were obtained from results given in [36], where it was shown that (for  $\gamma > 0$ ) on this locus  $\lim_{\Omega^{-2} \rightarrow 0} \beta \Omega^{-3} = 0.13$  and near the cusp at  $\Omega^{-2} = 1/3$  the balance curve lies approximately halfway between the two saddle-node branches, and is given by  $\beta_{bl} \Omega^{-3} = 2(1 + 9\Omega^{-2})/27$ . These results set the stage for using the Duffing system with additive Gaussian noise as a balanced bridge.

### 3.5 Shot Noise Measurement

Near the cusp ( $\Omega^{-2} = 1/3$ ) the system discussed above collapses onto a one-dimensional slow manifold. On the balance curve, the system reduces to the classic overdamped symmetric quartic double well potential. In this section we discuss the measurement of shot noise statistics by such a system.

Shot noise is characterized by the pulse area,  $g$ , and pulse rate,  $\nu$ . Thus, we

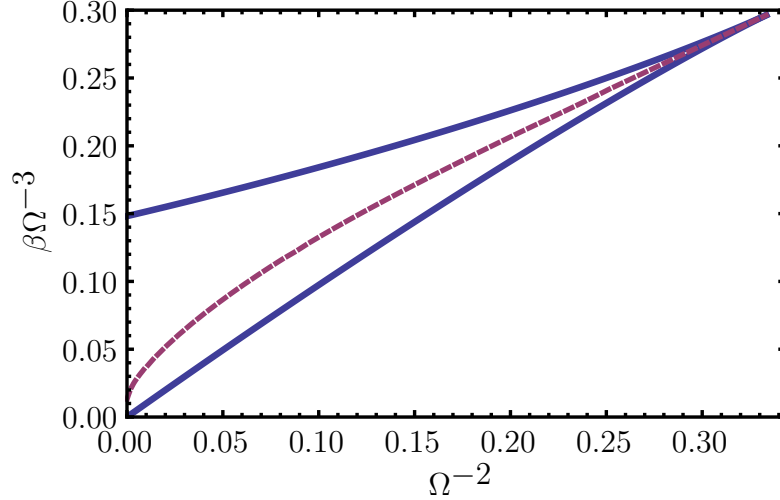


Figure 3.3: Two dimensional parameter space for the Duffing resonator. Solid lines are saddle-node branches which enclose the bistable region. The dashed line is the balance curve on which the escape actions for two stable states are equal,  $S_1 = S_2$ . In the weak noise limit this line is very close to the line where the escape rates are equal.

suppose our system is described by the equation

$$\dot{q} = -U'(q) + \sqrt{D}f(t) + \xi(t) - \nu g, \quad (3.44)$$

where  $q$  is a scalar,  $f(t)$  is a white Gaussian noise with  $\langle f(t)f(t') \rangle = \delta(t - t')$ , and  $\xi(t)$  is a Poisson process. We assume that the shot noise acting on the resonator is modulated by the resonator driving signal so that it appears as a simple Poisson process on the slow manifold. Our system is assumed to move in a overdamped double-well potential, as shown in Fig. 3.4, that can be described by

$$U(q) = -\frac{1}{2}q^2 + \frac{1}{4}q^4. \quad (3.45)$$

The mean  $\langle \xi \rangle = \nu g$  has been explicitly removed in order that the bridge, as discussed in section 3.3, will be sensitive to only the higher moments. It is assumed that this mean can be measured and compensated for. This measurement also amounts



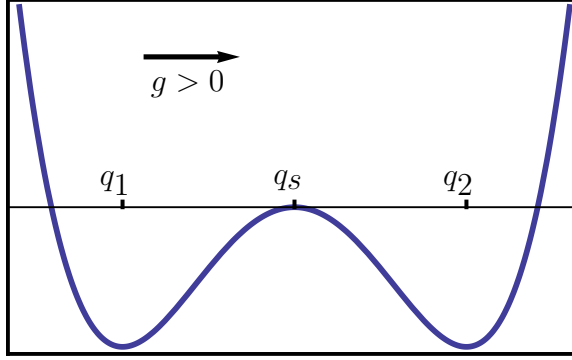


Figure 3.4: Double-well potential of equation (3.45);  $q_1$  and  $q_2$  denote positions of stable fixed points, while  $q_s$  refers to the unstable fixed point. Poisson pulses with positive area  $g$  change the switching rates such that  $r_1 > r_2$ , resulting in a shift of the occupation probability from  $q_1$  towards  $q_2$ .

to the first of the two data points required to calculate  $\nu$  and  $g$ .

The cumulant generating function is known for the Poisson process. For the zero mean Poisson process under consideration,  $\xi - \nu g$ , it is given by

$$\ln A_i = \nu \int dt \left\{ e^{-g\chi_i(t)/D} + g\chi_i(t)/D - 1 \right\}. \quad (3.46)$$

Equating this term by term to equation (3.26), (repeated here)

$$\ln A_i = \sum_{n=1}^{\infty} \frac{\kappa_n^{(i)}}{n!(-D)^n},$$

gives

$$\kappa_1^{(i)} = 0, \quad (3.47)$$

$$\kappa_n^{(i)} = \nu g^n \int dt \chi_i^n(t), \quad n > 1. \quad (3.48)$$

As discussed in section 3.1, the susceptibility,  $\chi_i$ , is a heteroclinic solution of the

auxiliary Hamiltonian system. For this system, the Hamiltonian is

$$\mathcal{H} = \frac{p^2}{2} - pU'(q), \quad p = \dot{q} + U'(q). \quad (3.49)$$

The heteroclinic trajectories of interest connect the fixed points  $(q, p) = (\pm 1, 0)$  with the saddle point  $(q, p) = (0, 0)$ . By inspection, we see that  $\mathcal{H} = 0$  along these trajectories. Accordingly, the heteroclinics are solutions to

$$\dot{q} = U'(q), \quad (3.50)$$

that is, the reversed-time deterministic trajectories. For the potential given in equation (3.45), the solutions are

$$q_{\pm}^{(h)}(t) = \pm \left[1 + e^{2t}\right]^{-1/2}, \quad (3.51)$$

and the attendant susceptibilities are given by

$$\chi_{1,2} = -2\dot{q}_{\pm}^{(h)}(t) = \pm 2e^{2t}(1 + e^{2t})^{-3/2}. \quad (3.52)$$

Using equation (3.50), the integrals in equation (3.48) can be evaluated explicitly. Applying the result to equation (3.27) gives

$$\frac{P_1}{P_2} = \exp \left[ -\nu \sum_{n=1} \left( \frac{2g}{D} \right)^{2n+1} \frac{\Gamma(n+1/2)}{(2n+1)\Gamma(3n+3/2)} \right], \quad (3.53)$$

where  $\Gamma(n)$  is the Euler Gamma function. Figure 3.5 shows  $\log(P_2/P_1)/\nu$  as a function of  $g/D$  along with Monte-Carlo simulation results. The inset in the figure shows the same quantities as the primary axes over a larger range. The Monte-Carlo simulations were carried out with parameter values  $D = 0.04$  and  $\nu = 0.5$ . The weak noise

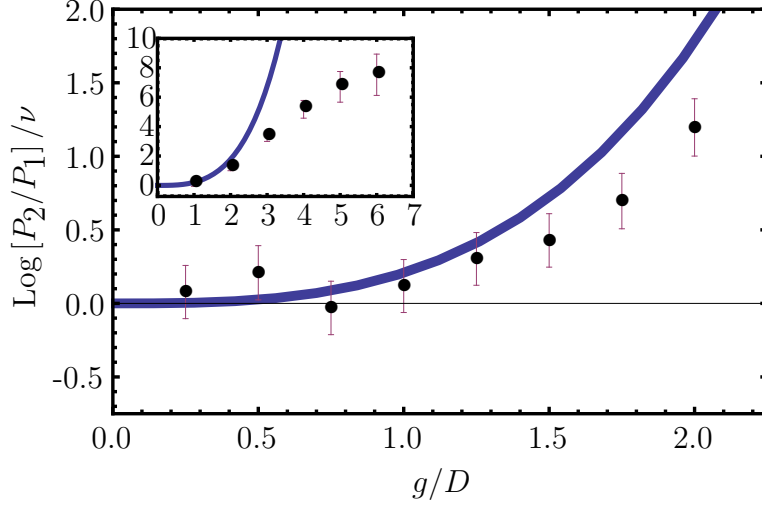


Figure 3.5: Change in probability ratio due to the addition of zero mean shot noise, equations (3.53). Data are results from Monte-Carlo simulations with  $D = 0.04$  and  $\nu = 0.5$ . The inset shows the same quantities over a larger range.

limit assumed by the analysis requires  $D/2\Delta U \ll 1$ , where  $\Delta U$  is the barrier height. We also assumed that the non-Gaussian noise was weak compared to the Gaussian noise; this condition is  $\nu g^2 \ll D$ . The parameters used give  $D/2\Delta U = 0.08$  and require  $g/D \ll 7$ . Figure 3.5 shows reasonable agreement in this region.

For  $g/D$  not too large, the series can be truncated at  $n = 2$ . This accounts for up to the fifth order moments of  $\xi$ . The error due to this truncation grows monotonically with  $g/D$ , reaching approximately 2% error for  $g/D = 6$ . The truncation, and use of the relation  $\langle \xi \rangle = \nu g$ , give a quadratic equation for  $g^2$ . Solving for  $g^2$  and taking the positive root gives

$$g^2 = -\frac{715}{32}D^2 + \sqrt{\left(\frac{715}{32}D^2\right)^2 - \frac{225225D^5}{256\langle \xi \rangle} \ln \frac{P_1}{P_2}}, \quad (3.54)$$

where the label “1” applies to the stable fixed point at  $q = -1$  and the label “2” applies to the stable fixed point at  $q = 1$ . By considering the two cases of positive and negative  $g$  we now show that equation (3.54) gives a positive real result for  $g^2$ . For positive  $g$ ,  $\langle \xi \rangle$  is also positive. Moreover, since the system is overdamped, pulses

pushing in the positive direction can only decrease  $P_1$  while increasing  $P_2$ . Thus, for positive pulses,  $g > 0$ ,  $\ln P_1/P_2 < 0$  and  $\langle \xi \rangle > 0$ , and so equation (3.54) gives a positive real result for  $g^2$  from which we take the positive root for  $g$ . On the other hand, when  $g < 0$ , we have  $\ln P_1/P_2 > 0$  and  $\langle \xi \rangle < 0$ , and equation (3.54) still gives a positive real result for  $g^2$  from which we take the negative root for  $g$ . Generally, the sign of  $g$  is found from the sign of  $\ln(P_1/P_2)$ .

Equation (3.54) is our final result, from which  $g$  is found. Use of this equation requires measurement of the quantities  $D$ ,  $\langle \xi \rangle$ , and  $P_1/P_2$ . The Gaussian noise strength,  $D$ , and the non-Gaussian noise mean,  $\langle \xi \rangle$ , can be measured from the quasi steady state distribution around a fixed point of the drift vector. Specifically, the Gaussian noise strength can be found from the width of the distribution about the fixed point, and the mean can be found from the force required to rebalance the distribution, as described above, and reiterated here: With  $\xi$  turned off, the mean of this quasi steady state distribution is measured. With  $\xi$  turned on, this mean may shift. A bias force is applied until the mean has been restored to the value found with  $\xi$  turned off. The force to rebalance gives  $\langle \xi \rangle$ . The final quantity required to estimate  $g$  is the population ratio  $P_1/P_2$ . This is found by observing the system for a period of time over which many escape events occur. The system can be sampled with sufficiently long sampling period and the probabilities can be estimated by use of equation (3.16). From these three measurements, the full counting statistics are found.

## 3.6 Outlook

In this chapter we discussed a parametric sensing strategy based on noise-induced escape. Parametric sensing is applicable to a wide range of problems. It only requires that one can couple a quantity of interest to the parameters, or effective parameters,

of the device while preventing disturbances from doing the same. While this may not be a trivial task, parametric sensors have found success in force and mass [121, 40, 42, 33, 43, 66] spectroscopy, and measurement of electron transport [6, 5], among other applications. Likewise, the dynamic bridge may be employed for force or mass spectroscopy, as it can be made extremely sensitive to changes in the natural frequency of the resonator. However, this comes at the cost of long measurement times.

Alternatively, the bridge can be used for measurements of counting statistics, as demonstrated in sections 3.3 and 3.5. The processes that may be counted with a NEMS bridge depend on the mean rate and how it compares to the relaxation time of the resonator. Pulse rates much faster than the relaxation time of the resonator will appear approximately Gaussian, and therefore the higher moments will be difficult to measure. Intriguing possible applications include measuring the transport of electrons through a single electron transistor, or the transport of cells through a micro-channel, both of which can be viewed as shot noise processes that can affect the dynamics of a NEMS resonator.

# Chapter 4

## Phase Noise in Nonlinear Oscillators

An oscillator is a device which produces a periodic signal. Such devices are central to many areas of science and technology including timing, spectroscopy, communications, radar, GPS, etc. An oscillator is constructed from a frequency selective device, which is inevitably lossy, and a feedback loop designed to compensate for this energy loss in order to maintain a constant amplitude periodic signal. See, for example, Figure 4.1(b). The frequency selective element may be, for example, a mechanical pendulum as in a grandfather clock, a quartz crystal as in many electronic oscillator circuits, or a microwave cavity as in a hydrogen MASER. In all cases there are random perturbations acting on the elements of the oscillator system stemming from the environment. Each perturbation may knock the oscillator phase a little forward or backward. Over time many small perturbations accumulate and the oscillator phase diffuses. Figure 4.1(a) illustrates the different routes by which fluctuations affect the oscillator phase. Fundamentally, this diffusion problem cannot be completely eliminated because an oscillator must be autonomous and thus have time-translational symmetry. In other words, if we build an oscillator and set it up in a given initial

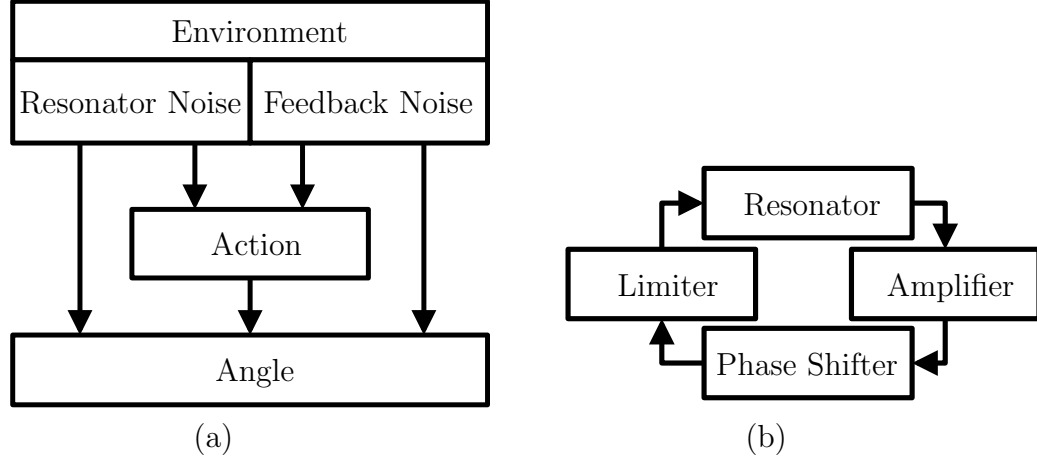


Figure 4.1: Noise roadmap (a) illustrating the different routes by which fluctuations may affect the angle. Prototypical oscillator block diagram (b).

configuration, then we can observe its behavior. If we and set the oscillator in the same initial configuration at a different time, we expect it to behave the same. This property implies that the oscillator cannot know about a fixed reference point in time. Likewise, it has no way to know if its perception of time has slipped a little bit from “true” time. Thus, the only thing we can do to make a better oscillator is to reduce the action of perturbations on the phase. There are two approaches one can take to address this problem. The first approach, which is hardware specific, is to combat the disturbances at their source. For example, we can put the oscillator in a temperature controlled environment to diminish perturbations due to temperature fluctuations. The second approach is to tune the oscillator parameters so that it operates optimally given the perturbations that are present. Returning to the noise roadmap in figure 4.1(a), the first approach is analogous to reducing the quantity of noise descending along the four lines from the environment block. The second approach may be used to, for example, cut the noise route connecting the action to the angle or reduce the noise strength relative to the oscillator’s inertia. In general both approaches must be employed. In this chapter, however, we focus on some fundamental issues related to the second approach.

Our goal is to analyze oscillators constructed with nano-electro-mechanical systems (NEMS) as frequency selective elements. During the past decade NEMS have demonstrated operation at high frequencies with high quality factors and low power consumption [94]. These qualities put NEMS in a position to be a key component in the development of compact, robust, low phase-noise frequency sources [45]. However, due to their size, NEMS exhibit strong nonlinearity and relatively large noise levels, which limit the linear dynamic range [90]. The realization of NEMS microwave sources therefore requires engineering beyond the linear dynamic range of the frequency selective element. Thus, a fully nonlinear treatment of the problem is required. We approach the problem by examining the slow dynamics in the action-angle coordinate representation of an oscillator. For alternative analyses of phase noise, see [27, 22, 80].

Our treatment of this problem is arranged as follows. Our fundamental assumptions include neglecting the dynamics of the feedback loop and treating the resonator as nearly conservative. We therefore model the oscillator with the resonator's equations of motion. The most appropriate coordinate system in which to perform the analysis is in terms of the action-angle coordinates of the resonator. Accordingly, we review action-angle coordinates in section 4.1. We then discuss a microscopic model for the resonator in section 4.2. This section provides insight into the noise forces acting on an open-loop resonator. In section 4.3, we consider the closed loop dynamics of a general nonlinear oscillator. Our primary result is an expression for the spectrum of fractional frequency fluctuations in the oscillator. This expression is useful for oscillator tuning and optimization. We illustrate this by example in section 4.4, in which we examine an oscillator employing a biased Duffing resonator. Using noise and damping effects developed from the microscopic model presented in section 4.2, and a simple feedback model, we discuss oscillator tuning over a reduced two-dimensional parameter space. The region of parameter space we consider is restricted to reasonable values. In this restricted region, the minimum phase diffusion rate is



found when the resonator is maximally biased and operated at a particular amplitude where the frequency of the resonator is locally independent of the amplitude. Following this example, we conclude the chapter with section 4.5 in which we discuss possible directions for future research.

## 4.1 Action-Angle Coordinates

In the treatment of weakly nonlinear resonators we often employ the van der Pol transformation in order to write the equations as a set of coupled first order differential equations with small perturbations (see section 2.1). The van der Pol transformation represents the solution to the linear unperturbed problem, and the effects of the perturbations are incorporated by allowing the constants of motion (e.g., amplitude and phase) to vary in time. These variations are slow when the perturbations are small. To handle a strongly nonlinear resonator we can also perform a change of coordinates based upon the solution of the unperturbed system, which is nonlinear in this case. For perturbations of strongly nonlinear conservative systems the appropriate transformation is to action-angle coordinates, as described in this section. This review of action-angle coordinates follows from [50, 69]. The coordinate transformation leads to equations for the action and angle of the resonator, which are analogous to the amplitude and phase coordinates employed in the weakly nonlinear case. For the complete solution it is necessary to know the solution of the unperturbed nonlinear problem. In this section, however, we perform the transformation using general functions which contain the solution, and appeal only to properties that these functions can be shown to possess. Thus, while we demonstrate the method, its application is case specific. We provide an example with explicit calculations in section 4.4.

We begin by considering a nearly conservative nonlinear resonator described by

the equations of motion

$$\begin{aligned}\dot{q} &= p, \\ \dot{p} &= -U'(q) + F(q, p, t),\end{aligned}\tag{4.1}$$

where  $U(q)$  is the potential describing the nonlinear stiffness of the resonator and  $F$  is a perturbation. As discussed above, we wish make a change of coordinates reflecting the solution of the conservative subsystem described by the Hamiltonian

$$H = \frac{p^2}{2} + U(q).\tag{4.2}$$

We assume that the potential,  $U$ , is confining so that the system exhibits periodic behavior. The conservative subsystem can also appropriately be called an oscillator since it exhibits periodic motion. For a given energy,  $E = H$ , the system will oscillate between two turning points,  $q_a$  and  $q_b$ , which are solutions of the equation  $E = U(q_a) = U(q_b)$ . In phase space, the trajectory of the system belongs to a family of closed orbits parameterized by  $E$ . To achieve action-angle coordinates we want to transform the coordinate and momentum of the system such that this family of orbits becomes a family of circles, each of which is traversed at a constant, but energy dependent, angular rate,  $\Omega(E)$ . This transformation must preserve the area of the orbits so that the parameterized family remains ordered by the energy; such a transformation is a canonical transformation. By virtue of this transformation, an orbit will be transformed into a circle with a radius given by its area normalized by  $2\pi$ . This radius is the action,  $I$ , defined by

$$I(E) = \frac{1}{2\pi} \oint p dq.,\tag{4.3}$$

which is a monotonic function of  $E$ . We can therefore use  $I$  in place of  $E$  to param-

eterize the family of periodic orbits. To show that  $I$  is monotonic, we consider the derivative,

$$\frac{\partial I}{\partial E} = \frac{1}{\pi} \int_{q_a}^{q_b} \frac{\partial p}{\partial E} dq = \frac{1}{\pi} \int_{q_a}^{q_b} \frac{1}{p} dq = \frac{1}{\pi} \int_{t_a}^{t_b} dt = \frac{T}{2\pi} \geq 0, \quad (4.4)$$

where  $T$  is the period of the orbit. To obtain this result we have used  $\partial_p E = \partial_p H = p$  and  $dq = p dt$ . Thus, for any orbit of finite non-zero period,  $I$  is monotonic and we find that the resonator frequency is given by

$$\omega(I) = \left( \frac{\partial I}{\partial E} \right)^{-1}. \quad (4.5)$$

In order to ensure that the phase space transformation preserves area, we used a generating function for the transformation [50]. For the action-angle coordinate transformation, the generating function is

$$S_0(q, I) = \int p(q, I) dq. \quad (4.6)$$

The function  $p(q, I)$  is obtained from equations (4.2) and (4.3) with  $E(I) = H$ . The canonical coordinate transformation defined by a generating function of this type is given by [50]

$$p = \frac{\partial S_0(q, I)}{\partial q}, \quad (4.7)$$

$$\Theta = \frac{\partial S_0(q, I)}{\partial I}, \quad (4.8)$$

where  $q$  and  $p$  are the old coordinate and conjugate momentum and  $\Theta$  and  $I$  are the new coordinate and conjugate momentum. In principle, to perform this coordinate change, it is necessary to evaluate and invert equations (4.3) and (4.8). However, here we are looking at the general case, and so we do not need to do this, only note

that it is possible. In order to apply this transformation to equations (4.1), we make use of the following identities,

$$\left(\frac{\partial q}{\partial \Theta}\right)_I^{-1} = \frac{\partial \Theta}{\partial q}\bigg|_I = \frac{\partial^2 S_0(q, I)}{\partial I \partial q} = \frac{\partial p}{\partial I}\bigg|_q = \frac{\partial p}{\partial E}\bigg|_q \frac{\partial E}{\partial I} = \frac{\omega}{p}, \quad (4.9)$$

$$\frac{\partial p}{\partial \Theta}\bigg|_I = -\frac{1}{p}U'(q)\frac{\partial q}{\partial \Theta}\bigg|_I = -\frac{1}{\omega}U'(q), \quad (4.10)$$

$$\frac{\partial p}{\partial I}\bigg|_{\Theta} = \frac{\omega}{p} - \frac{1}{p}U'(q)\frac{\partial q}{\partial I}\bigg|_{\Theta}. \quad (4.11)$$

Now, we can rewrite equation (4.1) in terms of the new coordinates,  $\Theta$  and  $I$ , by using the functions  $p(\Theta, I)$  and  $q(\Theta, I)$ , as follows

$$\dot{q} = \frac{\partial q}{\partial \Theta}\dot{\Theta} + \frac{\partial q}{\partial I}\dot{I} = \frac{p}{\omega}\dot{\Theta} + \frac{\partial q}{\partial I}\dot{I} = p, \quad (4.12)$$

$$\dot{p} = \frac{\partial p}{\partial \Theta}\dot{\Theta} + \frac{\partial p}{\partial I}\dot{I} = -\frac{1}{\omega}U'(q)\dot{\Theta} + \left(\frac{\omega}{p} - \frac{U'(q)}{p}\frac{\partial q}{\partial I}\right)\dot{I} = -U'(q) + F. \quad (4.13)$$

Solving for  $\dot{I}$  and  $\dot{\Theta}$  gives the resonator equation in action-angle coordinates

$$\begin{aligned} \dot{I} &= (\partial_{\Theta} q)F, \\ \dot{\Theta} &= \omega(I) - (\partial_I q)F. \end{aligned} \quad (4.14)$$

Note that when  $F = 0$  this provides the desired form in which the phase space consists of circles on which  $I$  remains constant and which are traversed at constant angular rate  $\omega(I)$ . When  $F$  is small, we use this convenient solution as a basis for perturbation calculations.

## 4.2 Microscopic Resonator Model

Before proceeding to treat equations (4.14), we pause to discuss what kind of terms we might expect to find in the perturbation,  $F$ , for an oscillator. Generally, we

can split  $F$  up into two parts, one arising from the resonator's interaction with the environment and another arising from the feedback loop. In this section we consider the first part. In section 4.3 we consider the complete closed loop dynamics.

In order to examine components of  $F$  that arise from the resonator's interaction with the environment, we must model the resonator and environment as a complete system. We therefore review the theory of an oscillator coupled to a medium, following Dykman and Krivoglaz [36]. The interested reader is directed to this reference and its cited works for a more complete discussion.

Our microscopic resonator model is a nonlinear conservative oscillator coupled to a bath modeled by a large number of harmonic oscillators. This model is appropriate for a NEMS resonator where the nonlinear resonator of interest is a particular mode of the complete device and substrate system. The thermal bath consists of the myriad of other vibrational modes of this system. We assume the nonlinear oscillator is driven by an external force and therefore its coordinate and momenta are not necessarily small. On the other hand, the bath oscillators are assumed to have small amplitude so that we can drop cubic and higher order terms in the Hamiltonian. A change of coordinates among the bath variables is always possible that will decouple the linear bath subsystem, and so we also drop coupling between modes of the bath. Finally, we assume that the coupling between the oscillator of interest and the bath is weak, and so we keep only the linear terms in the bath coordinates. The Hamiltonian for this combined system is given by

$$H = \frac{p_0^2}{2} + U(q_0) + \sum_k \left( \frac{p_k^2}{2} + \frac{1}{2} \omega_k^2 q_k^2 + \epsilon_k q_k H_I(p_0, q_0) \right) - q_0 f_0 \cos \omega t, \quad (4.15)$$

where the singled-out nonlinear oscillator is described by coordinate  $q_0$ , momentum  $p_0$ , and potential  $U(q_0)$ , and the bath oscillators are described by coordinates  $q_k$  and momenta  $p_k$ . The function  $H_I$  captures the dependence of the interaction energy on

the nonlinear oscillator's coordinate and momentum. For now, we leave this function unspecified. The equations of motion for this system can be written as

$$\dot{q}_0 = p_0 + \frac{\partial H_I}{\partial p_0} \sum_k \epsilon_k q_k, \quad (4.16)$$

$$\dot{p}_0 = -U'(q_0) - \frac{\partial H_I}{\partial q_0} \sum_k \epsilon_k q_k + f_0 \cos \omega t, \quad (4.17)$$

$$\ddot{q}_k + \omega_k q_k = -\epsilon_k H_I(p_0, q_0), \quad (4.18)$$

where we have removed the bath momenta variables by the substitution  $p_k = \dot{q}_k$ . We can remove the bath variables from equations (4.16) and (4.17) by formally solving equation (4.18). The solution is

$$q_k(t) = A_k \cos(\omega_k t + \phi_k) - \int_0^t \frac{\epsilon_k}{\omega_k} \sin(\omega_k(t - \tau)) H_I(p_0(\tau), q_0(\tau)) d\tau, \quad (4.19)$$

where  $A_k$  and  $\phi_k$  capture the initial conditions of the  $k^{\text{th}}$  environmental oscillator. These are unknown and so we model them as random variables distributed according to the laws of equilibrium thermodynamics. Since the bath oscillators are uncoupled, their initial conditions are independent random variables. The probability for the  $k^{\text{th}}$  bath oscillator to have amplitude  $A_k \in [A, A + dA]$  and phase  $\phi_k \in [\phi, \phi + d\phi]$  is given by the Boltzmann distribution

$$P\{A_k \in [A, A + dA], \phi_k \in [\phi, \phi + d\phi]\} = \frac{\omega_k^2}{2\pi k_b T} \exp\left[-\frac{\omega_k^2 A^2}{2k_b T}\right] A dA d\phi, \quad (4.20)$$

where  $A_k \geq 0$ ,  $\phi_k \in [0, 2\pi]$ ,  $k_b$  is Boltzmann's constant, and  $T$  is the bath temperature. The phase,  $\phi_k$ , is uniformly distributed, so equation (4.20) is independent of  $\phi$ . To apply equation (4.19) to equations (4.16) and (4.17) we must consider the sum

over  $k$  on  $\epsilon_k q_k$ . We partition this term into two pieces. The first piece is the sum over the homogeneous solutions, which gives a random process,  $\xi(t)$ , parameterized by the random variables  $A_k$  and  $\phi_k$ . The second piece is the sum over the particular solutions which gives a functional,  $L[p_0, q_0]$ , describing the retarded reaction of the environment on the nonlinear oscillator. These effects are expressed as

$$\xi(t) \equiv \sum_k \epsilon_k A_k \cos(\omega_k t + \phi_k), \quad (4.21)$$

$$L[p_0, q_0] \equiv \sum_k \int_0^t \frac{\epsilon_k^2}{\omega_k} \sin(\omega_k(\tau - t)) H_I(p_0(\tau), q_0(\tau)) d\tau. \quad (4.22)$$

The environment is assumed to contain a large number of harmonic oscillators. Accordingly, we approximate the sum over  $k$  as an integral. Toward this end, we define the spectral density of the bath,  $g(\omega)$ , as

$$\sum_{\omega < \omega_k < \omega + d\omega} \frac{\epsilon_k^2}{\omega_k} = \omega g(\omega) d\omega. \quad (4.23)$$

As mentioned above, the sum over the homogeneous solutions of the bath oscillators,  $\xi(t)$ , represents a stochastic process. This process has zero mean, since the phases are uniformly distributed over  $[0, 2\pi]$ , and the autocorrelation function for this process is given by

$$\langle \xi(t) \xi(t') \rangle = k_b T \int_0^\infty g(\omega) \cos(\omega(t - t')) d\omega. \quad (4.24)$$

In the simple case where  $g$  is a constant, we have  $\langle \xi(t) \xi(t') \rangle = \pi g k_b T \delta(t - t')$ . The power spectral density for  $\xi$  is then given by

$$S_\xi(\omega) = \int_{-\infty}^\infty e^{-i\omega t} \langle \xi(t) \xi(0) \rangle dt = \pi k_b T g(\omega). \quad (4.25)$$

The sum over the particular solutions of the bath oscillators, equation (4.22), requires more detailed treatment. First, we write the interaction term,  $H_I$ , as

$$H_I(p_0(\tau), q_0(\tau)) = \sum_n A_n(\tau) e^{i\Omega_n \tau}, \quad (4.26)$$

where  $\Omega_n = n\Omega$  are the harmonics of the expansion frequency. Next we note that when  $t - \tau$  becomes sufficiently large the summation of sinusoids in equation (4.22) becomes approximately zero. The time beyond which this occurs is the correlation time of the bath,  $t_c$ . This correlation time is of the order  $\omega_c^{-1}$  where  $\omega_c$  is the cutoff frequency, i.e., the largest frequency of the bath oscillators. We now assume that the coefficients  $A_n$  change very little over the bath correlation time,  $t_c$ . Accordingly, we expand  $A_n$  in a Taylor series about  $\tau = t$  and keep only the first term,

$$H_I(p_0(\tau), q_0(\tau)) = \sum_n e^{i\Omega_n \tau} (A_n(t) + \dot{A}_n(t)(\tau - t) + \dots), \quad (4.27)$$

$$\approx \sum_n A_n(t) e^{i\Omega_n \tau}. \quad (4.28)$$

This assumption requires that the resonator relaxes slowly with respect to the bath correlation time. After making this approximation in equation (4.22) we can evaluate the integral over the time variable,  $\tau$ . This gives

$$\begin{aligned} L &\approx \sum_{n,k} \frac{\epsilon_k^2}{\omega_k} A_n(t) e^{i\Omega_n t} \int_{-t}^0 dt_1 e^{i\Omega_n t_1} \sin(\omega_k t_1) \\ &= \sum_{n,k} \frac{\epsilon_k^2}{2\omega_k} A_n(t) e^{i\Omega_n t} \left[ \frac{1 - e^{-i(\Omega_n - \omega_k)t}}{\Omega_n - \omega_k} - \frac{1 - e^{-i(\Omega_n + \omega_k)t}}{\Omega_n + \omega_k} \right]. \end{aligned} \quad (4.29)$$

In order to further simplify the expression for the functional  $L$ , we consider only times much larger than the correlation time of the bath,  $t \gg t_c$ . This allows us to ignore the initial transient of the bath and arrive at a “steady-state” resonator model. For



large  $t$ , we make the approximation (for  $t > 0$ )

$$\frac{1 - e^{-i(\Omega_n \pm \omega)t}}{\Omega_n \pm \omega} \approx i\pi\delta(\Omega_n \pm \omega) + \text{v.p.} \frac{1}{\Omega_n \pm \omega}, \quad (4.30)$$

where v. p. stands for the principal value. Approximating the sum as an integral in equation (4.29) and applying equation (4.30) gives

$$L \approx \sum_n A_n(t) e^{i\Omega_n t} [2i\Gamma_n \Omega_n - P_n], \quad (4.31)$$

where  $\Gamma_n$  and  $P_n$  are

$$\Gamma_n \equiv \frac{1}{4}\pi g(\Omega_n), \quad (4.32)$$

$$P_n \equiv \text{v.p.} \int_0^\infty \frac{\omega^2 g(\omega)}{\Omega_n^2 - \omega^2} d\omega. \quad (4.33)$$

This completes the development of the microscopic resonator model. We now rewrite the resonator equations so that they can be viewed collectively. We also drop the subscript '0' on the coordinate and momentum, since all other similar coordinates have been removed. The resulting resonator equations are

$$\dot{q} = p + \frac{\partial H_I}{\partial p} \left( \xi(t) + L[p, q] \right), \quad (4.34)$$

$$\dot{p} = -U'(q) - \frac{\partial H_I}{\partial q} \left( \xi(t) + L[p, q] \right) + f_0 \cos \omega t, \quad (4.35)$$

$$A_n = \frac{\Omega}{2\pi} \int_{-\pi/\Omega}^{\pi/\Omega} H_I e^{-in\Omega t} dt, \quad (4.36)$$

$$L[p, q] \approx \sum_n e^{in\Omega t} A_n \left[ 2in\Omega \Gamma_n - P_n \right]. \quad (4.37)$$

As a simple example, suppose that  $U = \frac{1}{2}\omega_0^2 q^2$  and  $H_I = q$ , which is the simplest example that yields a nontrivial result. We suppose that  $q = ue^{i\omega t} + c.c.$  and

$p = i\omega u e^{i\omega t} + c.c.$  where *c.c.* stands for complex conjugate. For this example, the expansion frequency for  $H_I$  is  $\Omega = \omega$  and we have  $A_1 = u$ ,  $A_{-1} = u^*$  and  $A_n = 0$  for all other  $n$ . Applying this example to equations (4.34)-(4.37) yields a differential equation  $u(t)$ . Assuming that  $u$  changes slowly in time, we apply the method of averaging. The resulting slow flow equation for  $u$  is

$$\dot{u} = \left( -\Gamma - i(\omega - \hat{\omega}_0) \right) u - \frac{if_0}{4\omega} + \frac{ie^{-i\omega t}}{2\omega} \xi(t), \quad (4.38)$$

where  $\hat{\omega}_0$  is the renormalized resonator frequency  $\hat{\omega}_0^2 = \omega_0^2 - P$  and we have dropped the subscripts on  $\Gamma$  and  $P$  since there is only one value for each, namely  $\Gamma_1$  and  $P_1$ . This result is self consistent with our assumptions so long as the damping rate,  $\Gamma$ , the detuning,  $\omega - \hat{\omega}_0$ , the external excitation amplitude,  $f_0$ , and the noise  $\xi$  are sufficiently small. This is consistent with a high quality resonator forced near its resonant frequency. The noise force  $ie^{-i\omega t}\xi(t)/2\omega$  can be approximated by a complex white Gaussian noise with uncorrelated real and imaginary parts, each with strength  $\Gamma k_b T / \omega^2$ , so smallness of  $\Gamma$  implies smallness of  $\xi$ . This is the same slow flow equation one would obtain from the phenomenological resonator model

$$\ddot{q} + 2\Gamma\dot{q} + \hat{\omega}_0^2 q = f_0 \cos \omega t - \xi(t). \quad (4.39)$$

Thus we see that the coupling to the bath has the net effect of producing a frequency shift, a damping force, and a noise force for the resonator.

As another example, suppose that  $U = \frac{1}{2}\omega_0^2 q^2 + \frac{1}{4}\gamma q^4$  and  $H_I = q + \alpha q^2$ . Then we employ the conventional van der pol transformation  $q = x \cos \omega t + y \sin \omega t$ ,  $p = -\omega x \sin \omega t + \omega y \cos \omega t$ . Applying this transformation to equations (4.34)-(4.37) gives the equations for the quadrature coordinates  $x$  and  $y$ . These coordinates vary slowly in time if the detuning  $\omega - \hat{\omega}_0$ , the renormalized nonlinear coefficient,  $\hat{\gamma} = \gamma - \frac{2}{3}\alpha^2(2P_0 +$

$P_2$ ), the damping coefficients,  $\Gamma_n$ , and the noise,  $\xi(t)$ , are small. As in the previous example,  $\hat{\omega}_0$  is the renormalized linear oscillator frequency,  $\hat{\omega}_0^2 = \omega_0^2 - P_1$ . Assuming that these terms are small, we apply the method of averaging and obtain

$$\begin{aligned} \dot{x} = & -\Gamma_1 x - \alpha^2 \Gamma_2 (x^2 + y^2) x - (\omega - \hat{\omega}_0) y - \frac{3\hat{\gamma}}{8\omega} (x^2 + y^2) y \\ & + \frac{\xi(t)}{\omega} \sin \omega t (1 + 2\alpha x \cos \omega t + 2\alpha y \sin \omega t), \end{aligned} \quad (4.40)$$

$$\begin{aligned} \dot{y} = & -\Gamma_1 y - \alpha^2 \Gamma_2 (x^2 + y^2) y + (\omega - \hat{\omega}_0) x + \frac{3\hat{\gamma}}{8\omega} (x^2 + y^2) x + \frac{f_0}{4\omega} \\ & - \frac{\xi(t)}{\omega} \cos \omega t (1 + 2\alpha x \cos \omega t + 2\alpha y \sin \omega t). \end{aligned} \quad (4.41)$$

These slow flow equations are consistent with those resulting from the phenomenological model

$$\ddot{q} + 2\Gamma_1 \dot{q} + 8\alpha^2 \Gamma_2 q^2 \dot{q} + \hat{\omega}_0^2 q + \hat{\gamma} q^3 + (1 + 2\alpha q) \xi(t) = f_0 \cos \omega t. \quad (4.42)$$

This model exhibits additive and multiplicative noise. It is known that the diffusion rate of the phase of a self excited oscillator resulting from additive noise decreases with increasing oscillator amplitude [72]. This motivates strong driving of the oscillator's frequency selective element, eliciting nonlinear behavior. The above example illustrates that how larger resonator amplitudes can bring multiplicative noise from the coupling to the environment. The multiplicative noise can be thought of as a fluctuation in the frequency of the resonator. We show below, equation (4.84), that the multiplicative noise produces phase diffusion in an oscillator that does not decrease with oscillator amplitude while the oscillator is operated in the linear range.

In the analysis above we have neglected quadratic terms in the bath coordinates,  $q_k$ , in the interaction energy which couples the oscillator to the environment, see equation (4.15). This was done to simplify the discussion in this dissertation. These terms, however, can contribute to phase noise in self excited oscillators. Analysis

of a resonator model including these terms can be found in references [34, 36]. Our analysis in the following section begins with a general phenomenological model, so the simplified microscopic model employed in this section does not diminish the generality of the subsequent results.

### 4.3 Oscillator Frequency Fluctuations

In this section, we consider general closed loop equations for a self-sustained nonlinear oscillator. We neglect the dynamics of the feedback loop, modeling the feedback forces on the resonator as instantaneous functions of the resonator state. As in the previous section, the resonator is assumed to be lightly damped as a result of weak coupling to a thermal bath. In the previous section we demonstrated that coupling to the bath produces three types of forces acting on the resonator: conservative forces that renormalize the resonator potential, damping forces which account for the loss of energy into the bath, and stochastic forces which result from the summed motion of the many degrees of freedom present in the bath. From this insight, we model our self-excited oscillator phenomenologically as follows. The resonator is assumed to be nearly conservative with a potential  $U(q)$ . This contains the conservative forces due to coupling to the bath. In addition, we add the friction forces  $L(p, q)$  which capture the energy loss into the bath, the driving, or gain, forces  $G(p, q)$  which arise from the feedback loop, and the fluctuating forces  $f(p, q, t)$  which arise from the thermal motion of the bath and the noise processes produced by the feedback electronics. Thus, the resonator equation of motion is

$$\dot{q} = p, \tag{4.43}$$

$$\dot{p} = -\partial_q U + G(p, q) - L(p, q) + f(p, q, t). \tag{4.44}$$

Note that we found that coupling to the bath can produce additional terms in the  $\dot{q}$  equation when the coupling is a function of  $p$ . For this model, we assume that should any such coupling be present, we can redefine  $p$  to be identically  $\dot{q}$  and lump the resulting perturbations into  $f$ . We assume that  $L$  and  $G$  are small compared to the characteristic value of the conservative force,  $|\partial_q U|$ , which implies small dissipation and small gains required to maintain oscillation. The various effects lumped into  $f$  are also assumed to be similarly small, and the stochastic processes found in  $f(p, q, t)$  are taken to be stationary with zero mean. Stationarity is required for the oscillator to have time-translational symmetry, and any nonzero mean may be moved from  $f$  to the other terms in the equation.

Important for our analysis is the separation of time scales into the “fast” time on the order of the vibration period, and slow times on the order of the vibration decay rate. It is this slow scale on which small random perturbations accumulate. As discussed in section 4.1, action-angle coordinates are the natural variables for the treatment of this nearly conservative system, for which the action and angle will vary on the slow time scale. Thus, we use a canonical coordinate transformation from  $(p, q)$  to action-angle coordinates,  $(I, \phi)$ , expressed by functions  $p(\phi, I), q(\phi, I)$  that are  $2\pi$  periodic in  $\phi$ . Without loss of generality, we set  $\phi = 0, \pi$  at the turning points at which  $p = 0$ . Accordingly,  $q$  is an even function in  $\phi$  and  $p$  is odd in  $\phi$ . To describe the oscillator in action-angle coordinates, we use equation (4.14) with the perturbation,  $F$ , from equations (4.43) and (4.44). This gives

$$\dot{I} = (\partial_\phi q)(G - L + f), \quad (4.45)$$

$$\dot{\phi} = \omega(I) - (\partial_I q)(G - L + f). \quad (4.46)$$

The assertion that  $G$ ,  $L$ , and  $f$  are weak perturbations on the resonator imply that all terms in equations (4.45) and (4.46) are small compared to  $\omega(I)$  during steady-state

operation. The oscillator action and frequency fluctuate about their mean values,  $I_0 = \langle I \rangle$  and  $\Omega = \langle \dot{\phi} \rangle$  respectively. It is assumed that these fluctuations are small and that  $\omega(I)$  remains close to  $\Omega$ , i.e. any shift in the resonator frequency due to the perturbative terms is also small. Equations (4.45) and (4.46) exhibit a separation of time scales, since the angle,  $\phi$ , varies rapidly while the action,  $I$ , and the time deviation,  $x(t)$ , defined by [3],

$$x(t) = \frac{\phi - \Omega t}{\Omega}, \quad (4.47)$$

vary slowly. The time deviation  $x(t)$  is a quantity of primary interest for the applications of a resonator as a time standard, as it describes the deviation of time as measured by the oscillator from the desired (true) time. A related quantity is the time derivative of  $x(t)$ , known as the fractional frequency fluctuation [3],

$$y(t) = \dot{x}(t) = \frac{\dot{\phi} - \Omega}{\Omega}, \quad (4.48)$$

which is an instantaneous measure of the oscillator frequency deviation. Among the common measures of oscillator stability [3] is the spectrum of fractional frequency fluctuations,  $S_y(\nu)$ , which we presently use to quantify the frequency noise in our oscillator model.

We begin by defining the phase deviation  $\varphi = \phi - \Omega t$ . Changing phase variables from  $\phi$  to  $\varphi$  in equations (4.45) and (4.46) gives

$$\dot{I} = (\partial_{\varphi} q)(G - L + f), \quad (4.49)$$

$$\dot{\varphi} = \sigma(I) - (\partial_I q)(G - L + f), \quad (4.50)$$

where  $\sigma(I) = \omega(I) - \Omega$  is the oscillator detuning, which is assumed to be small. With the change to the phase deviation, the right hand sides of equations (4.49) and (4.50)

have become small, and are also periodic in time. Thus, the oscillator equations are now in a form amenable to the method of averaging.

In appendix B we discuss how a near-identity coordinate transformation can be used to push the time-periodic aspects of the system out to higher order. Subsequent truncation of the series yields a simplified model that asymptotically describes the system behavior. This method can be used to treat non-white noises, and therefore can handle  $1/f$  type noise (here  $f$  is frequency) so long as the perturbations remain small. This requires that either a finite time interval be considered, or a low frequency cut-off be imposed on  $1/f$  type noises, which amounts to the same thing. We now treat equations (4.49) and (4.50) with this method. First, we expand the stochastic terms in a Fourier series in  $\phi$ . We assume that the Fourier coefficients can be separated into functions of action,  $I$ , and time,  $t$ ,

$$(\partial_\mu q)f = \sum_{n,k} A_{n,k}^{(\mu)}(I) e^{ik(\varphi + \Omega t)} \zeta_n(t), \quad \mu = I, \varphi. \quad (4.51)$$

The near identity coordinate transformation operates on the use of a fictitious narrow band filter with impulse response  $h(t)$  and frequency response  $H(\omega)$  centered at  $\omega = 0$  with  $H(0) = 1$ . Moreover, we assume that the cutoff frequency for this filtering function is less than  $\Omega/2$ . By use of this filtering function, we construct the transformed stochastic processes,  $\xi_\varphi$  and  $\xi_I$ , by the integral

$$\xi_\mu \equiv \sum_{n,k} A_{n,k}^{(\mu)} e^{ik\varphi} \int_{-\infty}^{\infty} h(t - t') \zeta_n(t') e^{ik\Omega t'} dt'. \quad (4.52)$$

The processes  $\xi_\mu$  have zero mean by our original assumption on  $f$ . The spectra of  $\xi_\mu$  can be calculated from the spectra of  $\zeta_n(t)$ . Let

$$\langle \zeta_n(t) \zeta_m(t') \rangle = \frac{1}{2\pi} \int_{-\infty}^{\infty} R_{n,m}(\omega) e^{i\omega(t-t')} d\omega. \quad (4.53)$$

Since we assumed the filtering function has a cutoff frequency less than  $\Omega/2$ , the transformed noise processes are wide-sense stationary. Letting  $S_{\mu,\nu}$  be the cross-spectrum of  $\xi_\mu$  and  $\xi_\nu$ , we find

$$\begin{aligned} S_{\mu,\nu}(I, \omega) &= \int_{-\infty}^{\infty} \langle \xi_\mu(I, t) \xi_\nu(I, 0) \rangle e^{-i\omega t} dt \\ &= \sum_{n,m,k} A_{n,k}^{(\mu)}(I) A_{m,-k}^{(\nu)}(I) R_{n,m}(\omega - k\Omega) |H(\omega)|^2. \end{aligned} \quad (4.54)$$

From equation (4.54) we can see how the nearly periodic motion of the oscillator selects the noise spectra near the harmonics of its fundamental frequency. The noise in these narrow bands is modulated down to baseband by the oscillator motion and accumulates over long times, resulting in diffusion of the phase. A diagram illustrating this phenomenon is shown in figure 4.2. In this figure a hypothetical noise spectrum is plotted along with several narrow-band filtering functions. These functions are given different heights illustrating that the magnitudes of the harmonics modulating the noise typically decrease as the order of the harmonic increases. This effect is described in the functions  $A_{n,k}^{(\mu)} A_{m,-k}^{(\nu)}$ , which we expect to show a general trend of decreasing with increasing  $k$ .

The formulation in appendix B illustrates how the noise terms  $(\partial_\mu q)f$  also give rise to a deterministic drift term. The noise-induced drift can likewise be written in terms of the Fourier expansion coefficients, as follows

$$\begin{aligned} d_\mu &= \sum_{n,m,k} \left[ A_{n,k}^{(\varphi)} \frac{\partial A_{m,-k}^{(\mu)}}{\partial I} + ik A_{n,k}^{(I)} A_{m,-k}^{(\mu)} \right] \\ &\quad \times \int_{-\infty}^{\infty} R_{n,m}(\omega - k\Omega) \frac{1 - |H(\omega)|^2}{2\pi i \omega} d\omega. \end{aligned} \quad (4.55)$$

From equation (4.55) we can see that the noise-induced drift is a mean effect arising from the noise at frequencies away from the oscillator harmonics. If the noise is taken



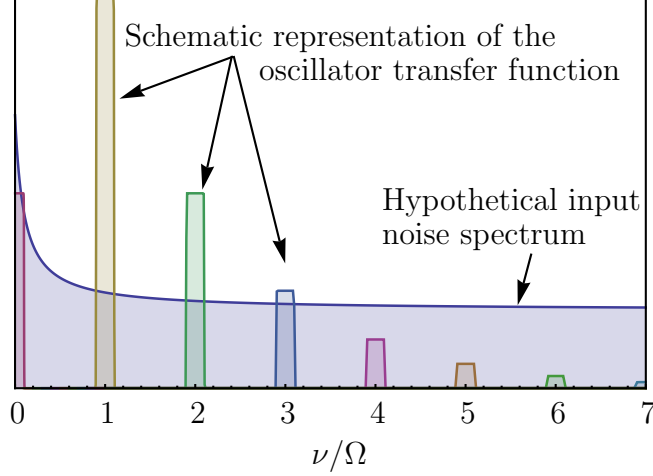


Figure 4.2: Illustration depicting how noise is filtered and down-converted. The noise is selected near the oscillator harmonics, that is, in the shaded regions, weighted by the Fourier coefficients in equation (4.51), and modulated down to baseband by the oscillator motion.

to be white, then  $R_{n,m}$  is a constant and the integrand is odd. Thus, the integration gives zero and this drift is zero.

The final term in the transformed equations comes from the deterministic part of the oscillator equation. This is simply the average of the deterministic terms over one period. The final form of equations (4.49) and (4.50) after the transformation is

$$\dot{I} \approx \overline{(\partial_\varphi q)(G - L)} + d_\varphi(I) + \xi_\varphi(I, t), \quad (4.56)$$

$$\dot{\varphi} \approx \sigma(I) - \overline{(\partial_I q)(G - L)} - d_I(I) - \xi_I(I, t), \quad (4.57)$$

where the overline means averaging over  $\varphi$ . We note that the right hand sides of equations (4.56) and (4.57) are independent of  $\varphi$ . This is a consequence of the time-translational symmetry of the oscillator. Without knowledge of a reference time, the phase must have a zero eigenvalue and so it does not appear in equations (4.56) and (4.57). We expect the oscillator to reach a steady state where the action fluctuates about a mean value, denoted  $I_0$ . Assuming these fluctuations are small, we expand

equations (4.56) and (4.57) in  $I$  about  $I_0$ . Let

$$0 = [(\partial_\varphi q)(G - L) + d_\varphi(I)]_{I=I_0}, \quad (4.58)$$

$$\Omega = [\omega(I) - (\partial_I q)(G - L) - d_I(I)]_{I=I_0}, \quad (4.59)$$

$$\alpha = \frac{\partial}{\partial I} [(\partial_\varphi q)(G - L) + d_\varphi(I)]_{I=I_0}, \quad (4.60)$$

$$\beta = \frac{\partial}{\partial I} [\sigma(I) - (\partial_I q)(G - L) - d_I(I)]_{I=I_0}. \quad (4.61)$$

Keeping only leading order terms in the expansion, we approximate equations (4.56) and (4.57) as

$$\dot{I} = -\alpha(I - I_0) + \xi_\varphi(I_0, t), \quad (4.62)$$

$$\dot{\varphi} = \beta(I - I_0) - \xi_I(I_0, t). \quad (4.63)$$

The fractional frequency fluctuation, defined in equation (4.48), can be expressed as  $y = \dot{\varphi}/\Omega$ . To find its first two moments, we solve equation (4.62) and substitute the solution into equation (4.63). Naturally  $y$  has zero mean since we defined  $\Omega$  to be the mean frequency. We characterize the second moment of  $y$  by its power spectral density. The spectrum of frequency fluctuations can be written as a function of the spectra of the noises acting on the action and angle coordinates,  $\xi_\varphi$  and  $\xi_I$ , and is given by

$$S_y(\omega) = \frac{\beta^2}{\Omega^2} \frac{S_{\varphi, \varphi}(\omega)}{\alpha^2 + \omega^2} - \frac{2\alpha\beta}{\Omega^2} \frac{S_{\varphi, I}(\omega)}{\alpha^2 + \omega^2} + \frac{1}{\Omega^2} S_{I, I}(\omega), \quad (4.64)$$

where the spectra  $S_{\mu, \nu}$  are given in equation (4.54). From equation (4.64) we see that the fluctuations that cause phase diffusion can be sorted into two groups. The first group are noise sources that cause fluctuations in the resonator action, which then couples to the phase, resulting in phase diffusion. The second group are noise

sources that directly affect the phase. The first group can be removed by setting  $\beta = 0$  such that the oscillator action and phase coordinates are decoupled. For an oscillator employing a linear resonator as the frequency selective element, we have  $\sigma'(I) = 0$ . In addition, we note that  $\partial_I q$  is an even function of  $\phi$ . Therefore, the action and phase coordinates will be uncoupled if  $G - L$  is an odd function of  $\phi$  and  $d_I = 0$ . This is often the case, and even if it is not, the coupling will generally be small since  $\sigma'(I) = \omega'(I)$  is the dominant term in (4.61). This is one reason why it is often favorable to use linear resonators in oscillator designs. However, nonlinear resonators may also exhibit decoupling of the action and phase coordinates [38]. In the next section we discuss an example and examine the phase noise characteristics of a hypothetical oscillator constructed with such a resonator.

Before discussing the example, however, we will provide a summary of the necessary steps required to calculate the spectrum of frequency fluctuations. The necessary tasks are as follows.

1. Obtain an ODE model for the oscillator.
2. Separate the model into i) a conservative subsystem with potential  $U$ , ii) a deterministic perturbation,  $G - L$ , and iii) a zero mean stochastic perturbation,  $f$ .
3. Calculate the action-angle transformation for the conservative subsystem to obtain the orbit function  $q(\Theta, I)$  and the frequency dispersion  $\omega(I)$ .
4. Calculate the Fourier coefficients of the noise terms  $(\partial_\mu q)f$  for  $\mu = \Theta, I$ , implicitly defined in equation (4.51).
5. Choose a filtering function,  $H(\omega)$ , e.g. a rectangular window of width  $\min[\omega(I)/2]$ .
6. Calculate the noise induced drift using equation (4.55).
7. Average the deterministic perturbation over one cycle of the angle.
8. Calculate  $\Omega$ ,  $\alpha$ , and  $\beta$  using equations (4.59-4.61).
9. Calculate the slow noise spectra using equation (4.54).
10. Calculate the spectrum of frequency fluctuations using equation (4.64).

## 4.4 The Biased Duffing Oscillator

In this section, we examine the phase noise in an oscillator employing a prototypical nonlinear resonator modeled by Duffing's equation with constant bias force. The exercise is an illustration of the results obtained in the previous section and demonstrates how phase noise can be reduced by tuning the oscillator's operating point. We begin by considering the conservative subsystem that generates the periodic orbits along which the perturbations are calculated. The potential of the conservative subsystem is given by

$$U(q) = \frac{1}{4}q^4 + \frac{1}{2}q^2 + \lambda q, \quad (4.65)$$

where  $\lambda$  is the bias force. Equation (4.65) is a one-parameter family of resonator potentials which brings another parameter to our optimization problem in addition to those describing the feedback force. In order to do this, we must first calculate the action-angle coordinate transformation. This requires the four roots of the equation  $U(q) - E = 0$ , which are difficult to find in closed form for arbitrary  $\lambda$ . Thus, we let  $a$ ,  $b$ ,  $c$ , and  $c^*$  represent the four roots, to be found numerically, and proceed with the analysis. Note that these roots are functions of the bias parameter,  $\lambda$ , and the operating action,  $I$ . We let  $a$  and  $b$  be the real roots with  $b > a$ ,  $q(0, I) = b$ , and  $q(\pi, I) = a$ . The complex root are not of interest for the present analysis.

The conservative subsystem of our oscillator model is described by the differential equation  $\ddot{q} + U'(q) = 0$ . The solution to this equation is

$$q(t) = \frac{(aB + bA) + (bA - aB) \operatorname{cn}(u|m)}{(A + B) + (A - B) \operatorname{cn}(u|m)}, \quad (4.66)$$

$$u = \sqrt{\frac{AB}{2}} t, \quad (4.67)$$

where  $\operatorname{cn}(u|m)$  is a Jacobi elliptic function with argument  $u$  and parameter  $m$ , and

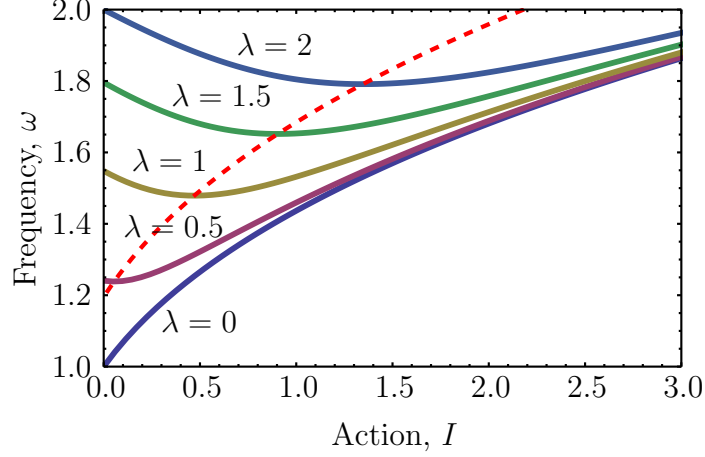


Figure 4.3: Frequency dispersion for the biased Duffing resonator for several values of the bias. Red dashed line is the locus of critical (zero dispersion) points.

$A$ ,  $B$ , and  $m$  are

$$A = |a - c|, \quad (4.68)$$

$$B = |b - c|, \quad (4.69)$$

$$m = \frac{(a - b)^2 - (A - B)^2}{4AB}. \quad (4.70)$$

The fundamental frequency of  $q(t)$  given in equation (4.66) is

$$\omega(I) = \frac{\pi\sqrt{2AB}}{4K(m)}, \quad (4.71)$$

where  $K(m)$  is the complete elliptic integral of the first kind with parameter  $m$  [1, 18]. The frequency as a function of action is shown in figure 4.3 for various values of  $\lambda$ . The key feature of the frequency dispersion curves is the extrema, called zero dispersion points, which exist for sufficiently large  $\lambda$ . The red dashed line in figure 4.3 traces the locus of these extrema. While this resonator exhibits points of zero dispersion, it is just one example of a broad class of nonlinear resonators with this feature; for other examples see [101]. The complete action-angle coordinate transformation can be constructed from the solution (4.66) by assigning each point on the orbit an angle

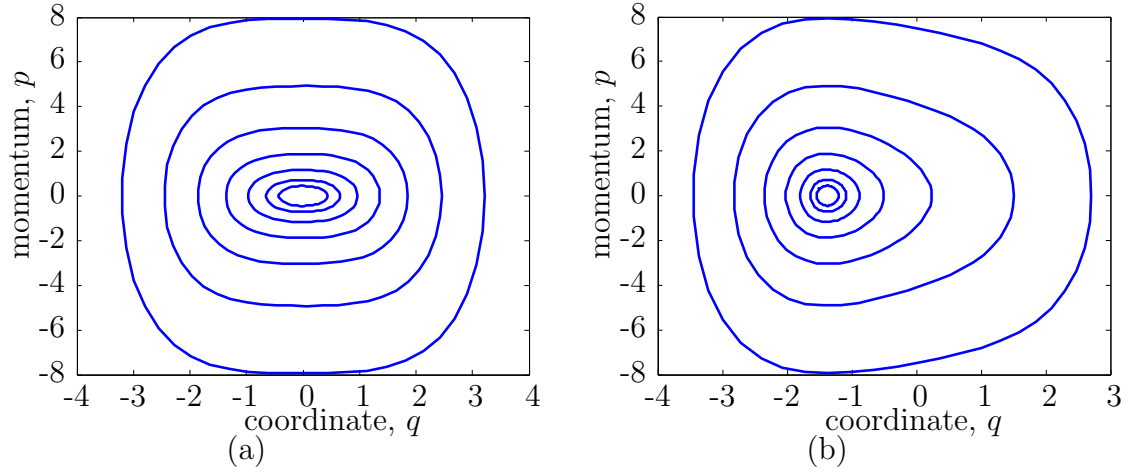


Figure 4.4: Several closed orbits belonging to the potential (4.65) with (a)  $\lambda = 0$  and (b)  $\lambda = 4$ .

from 0 to  $2\pi$ . We do this by relating the angle to time,

$$t = \frac{2K(m)}{\pi} \sqrt{\frac{2}{AB}} \phi. \quad (4.72)$$

This gives the coordinate transformation

$$q(\phi, I) = \frac{(aB + bA) + (bA - aB) \operatorname{cn}(u|m)}{(A + B) + (A - B) \operatorname{cn}(u|m)}, \quad (4.73)$$

$$p(\phi, I) = \omega(I) \frac{\partial q(\phi, I)}{\partial \phi}, \quad (4.74)$$

$$u = \frac{2K(m)}{\pi} \phi. \quad (4.75)$$

Several example orbits are shown in figure 4.4, for  $\lambda = 0$  and  $\lambda = 4$ . These figures show that the one parameter family of potentials considered in this problem includes orbits with a variety of shapes.

Before proceeding to discuss the other aspects of our oscillator model, we will examine the function  $q(\phi, I)$  in the limits of large and small action. For small action

$U(q)$  can be approximated as a parabola. Thus

$$q(\phi, I) \approx q_0(\lambda) + \sqrt{\frac{2I}{\omega_0(\lambda)}} \cos \phi, \quad (4.76)$$

where  $\omega_0(\lambda)$  is the frequency of the resonator in the limit  $I \rightarrow 0$ . For small action the frequency is independent of the action and so we have  $q \propto I^{1/2}$  and  $p \propto I^{1/2}$ . For large action, the potential can be approximated by  $U \approx q^4/4$ , giving

$$q(\phi, I) \approx \left( \frac{3\pi}{2K(0.5)} I \right)^{1/3} \text{cn} \left( \frac{2K(0.5)}{\pi} \phi \right). \quad (4.77)$$

In this approximation we have  $q \propto I^{1/3}$  and  $\omega \propto I^{1/3}$ , so  $p \propto I^{2/3}$ . From these limiting cases for  $q(\phi, I)$ , we can develop scaling laws for noise sources that may provide insight useful for locating an optimal operating point. For example, suppose that  $f$  includes the term  $(q - q_0)^a p^b \zeta_i(t)$ . Such noise terms may arise from nonlinear coupling, through the coordinate, to the environment or noise in the feedback loop. By considering time symmetries of the response and the small and large action limits of  $p$  and  $q$ , we can obtain some useful information about the noise processes  $\xi_\varphi$  and  $\xi_I$  that are ultimately responsible for diffusion of the oscillator phase. First, we recall that  $q$  is even in  $\phi$  and  $p$  is odd in  $\phi$ . It follows that

$$A_{i,-k}^{(I)} = (-1)^b A_{i,k}^{(I)}, \quad (4.78)$$

$$A_{i,-k}^{(\varphi)} = (-1)^{b+1} A_{i,k}^{(\varphi)}. \quad (4.79)$$

Next, by applying the scaling limits for  $p$  and  $q$  noted above we determine the following

scaling of the harmonic coefficients,

$$A_{i,k}^{(I)} \propto \begin{cases} I^{(a+b-1)/2} & \text{for small } I \\ I^{(a+2b-2)/3} & \text{for large } I \end{cases}, \quad (4.80)$$

$$A_{i,k}^{(\varphi)} \propto \begin{cases} I^{(a+b+1)/2} & \text{for small } I \\ I^{(a+2b+1)/3} & \text{for large } I \end{cases}. \quad (4.81)$$

Using the symmetry arguments, equations (4.78) and (4.79), the sum over  $k$  with  $n = m$  in equation (4.55) gives zero. Therefore, a noise such as the one considered here cannot directly induce a frequency shift, though such a shift may be possible through correlations with other noises. Next we examine the scaling of the spectral components,  $S_{\mu,\nu}$ , arising from the noise term considered. Applying the scaling laws in equations (4.80) and (4.81) to equation (4.54) we find

$$S_{\varphi,\varphi} \propto \begin{cases} I^{a+b+1} & \text{for small } I \\ I^{(2a+4b+2)/3} & \text{for large } I \end{cases}, \quad (4.82)$$

$$S_{\varphi,I} \propto \begin{cases} I^{a+b} & \text{for small } I \\ I^{(2a+4b-1)/3} & \text{for large } I \end{cases}, \quad (4.83)$$

$$S_{I,I} \propto \begin{cases} I^{a+b-1} & \text{for small } I \\ I^{(2a+4b-4)/3} & \text{for large } I \end{cases}. \quad (4.84)$$

It is understood that additive noise in an oscillator employing a linear resonator produces phase noise that decreases as the inverse of the oscillator amplitude squared [72]. This result is captured here as well. For small action the resonator is approximately linear and the action-angle coupling coefficient is approximately zero. The spectrum  $S_{I,I}$  dominates the spectrum of fractional frequency fluctuations. For an additive noise  $a = b = 0$  and we have  $S_{I,I} \propto I^{-1}$ . For large action multiplicative noise will dominate additive noises. Moreover,  $S_{\varphi,\varphi}$  will dominate  $S_{I,I}$  unless the



action linear coefficient  $\alpha$  is very large and/or the action-angle coupling coefficient  $\beta$  is very small. Thus we again see, as we saw in equation (4.64), that is favorable to operate the oscillator where the action and angle become decoupled, that is, where  $\beta = 0$ . Operating in this parameter subspace, the remaining parameters should be chosen to minimize  $S_{I,I}$ . Note that a minimum w.r.t. action should exist if multiplicative noises of sufficiently high order,  $2a + 4b - 4 > 0$ , exist. Otherwise, we should raise the action as high as possible to reduce the phase noise.

To continue with our example, we now construct the remaining terms in our oscillator model. We choose our loss and noise terms by appealing to the microscopic resonator model discussed in section 4.2. Moreover, we will assume the “Ohmic dissipation model” by taking  $g(\omega)$  to be a constant value  $g$  for  $\omega$  up to a cutoff frequency  $\omega_c$ . This model is valid when the bath can respond quickly compare to the motion of the resonator. The consequence of this assumption is that we take  $P_n = P$  and  $\Gamma_n = \Gamma$  for all  $n$ . Next, we take

$$H_I = (q - q_0) + \frac{1}{2}(q - q_0)^2, \quad (4.85)$$

and assume those terms proportional to  $P$  have already been incorporated into the potential given in equation (4.65). With this form of the interaction function,  $H_I$ , the loss of energy to the bath is given by the microscopic resonator formulation, equations (4.16) and (4.17),

$$L = 2\Gamma p \left( 1 + 2(q - q_0) + (q - q_0)^2 \right). \quad (4.86)$$

The first term is the usual viscous friction, the averaged effect of which is linear in the action,  $I$ ,

$$\overline{(\partial_\phi q) L_1} = \frac{\Gamma}{\pi} \int_{-\pi}^{\pi} p \frac{\partial q}{\partial \phi} d\phi = \frac{\Gamma}{\pi} \oint p dq = 2\Gamma I. \quad (4.87)$$

The higher order terms, which cannot be averaged in closed form, give nonlinear friction. This loss model does not shift the frequency since  $q - q_0$  and  $\partial_I q$  are even in  $\phi$  and  $p$  is odd, rendering  $\overline{(\partial_I q)L} = 0$  by symmetry. The microscopic resonator model also gives the multiplicative noise acting on the resonator due to the environment

$$f_{\text{env}} = \xi_{\text{env}}(t) \left( 1 + q - q_0 \right). \quad (4.88)$$

For simplicity we assume that  $\xi_{\text{env}}(t)$  is a white noise with strength  $D_{\text{env}}$ . The white noise assumption is the simplest since the noise-induced drift terms  $d_\varphi$  and  $d_I$  in the averaged oscillator model, equations (4.56) and (4.57), are zero.

To compensate for the energy loss, the feedback loop must replenish the resonator's energy. This can be done in a variety of ways from simple positive feedback to parametric forcing. The various methods may differ in the details, but they result in a qualitatively similar average effect. We therefore choose to consider a saturated feedback of the resonator velocity, with specific gain model of

$$G = g_1 \tanh[g_2(q(\phi + \theta, I) - q_0)], \quad (4.89)$$

where  $g_1$  is the feedback saturation level,  $g_2$  is a parameter used to capture the rapid, but finite, rate of change of the saturation device in the feedback circuit, and  $\theta$  is a phase shift. This phase shift is necessary for the force  $G$  to do work on the resonator. The maximum work is done when  $\theta = \pm\pi/2$ . This type of feedback could be constructed by measuring the resonator motion, amplifying it, and then passing it through a hard limiter. The physical implementation of the feedback loop must also bring with it some noise. We therefore add to our noise model a term arising from the feedback loop. A simple model is to assume that the feedback coefficients  $g_1$  and

$\theta$  fluctuate about their nominal values. This leads to the feedback noise model

$$\begin{aligned} f_{\text{fb}} = & \xi_{\text{fb},1}(t) \tanh[g_2(q(\phi + \theta, I) - q_0)] \\ & + \xi_{\text{fb},2}(t) \frac{g_1 g_2}{\omega} \text{sech}^2[g_2(q(\phi + \theta, I) - q_0)] p(\phi + \theta, I), \end{aligned} \quad (4.90)$$

where  $\xi_{\text{fb},1}(t)$  represents the fluctuations of  $g_1$  and  $\xi_{\text{fb},2}(t)$  represents the fluctuations of  $\theta$ . Both noises are assumed to be white and uncorrelated with each other and  $\xi_{\text{env}}$ , and the noise strengths are taken to be  $D_{\text{fb},i}$ ,  $i = 1, 2$ .

This oscillator model possesses three tunable parameters: the feedback parameters,  $g_1$ , and  $\theta$ , and the resonator (bias) parameter  $\lambda$ . All other parameters can be thought of as given once a resonator element is selected. The feedback parameter  $g_1$  is related to the action at the oscillator operating point by requiring  $\langle \dot{I} \rangle = 0$ . Thus, we can replace this parameter with the operating action  $I_0$ . For simplicity, we set  $\theta = \pi/2$  so that the feedback does the maximum work on the resonator. We are thus left with two tunable parameters which we can vary over a reasonable range. The action will be confined to values less than 10, where the nonlinearity becomes extremely strong. The bias will be confined to values less than 2.5 which corresponds with shifting the equilibrium position to  $q_0 = -1.11$ , pushing the system again into the strongly nonlinear region. For our numeric study we will let  $\Gamma = 5 \times 10^{-4}$  which corresponds with a quality factor of  $Q = 1000$  when the resonator is unbiased and undergoing small oscillations. This value of the quality factor is commonly obtainable for N/MEMS devices [81]. For the slew rate parameter we set  $g_2 = 500$ , and for the noise strengths we set  $D_{\text{fb},1} = D_{\text{fb},2} = 10D_{\text{env}}$ .

Figure 4.5 shows the logarithm of the spectrum of fractional frequency fluctuations evaluated at zero frequency,  $S_y(0)$ , normalized by  $D_{\text{env}}$ . This quantity represents the long term phase diffusion coefficient. Figure 4.6 shows the corresponding mean oscillator frequencies. In both plots a dashed white line indicates the locus of zero

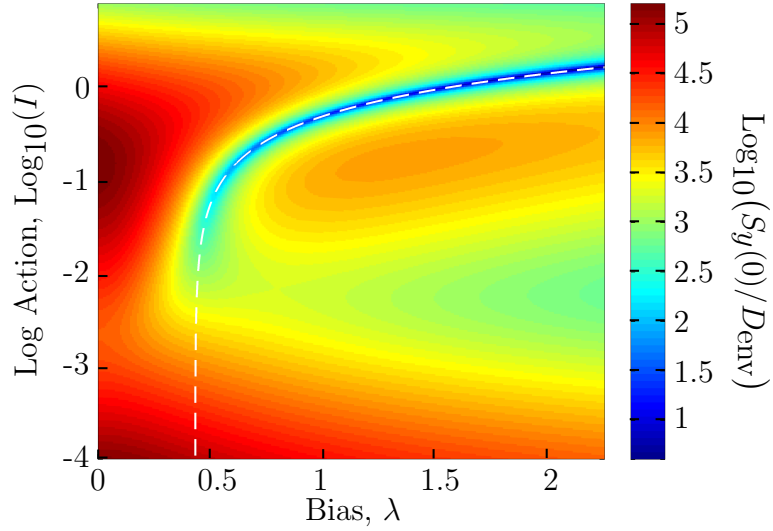


Figure 4.5: The logarithm of the normalized long term phase diffusion coefficient,  $\log_{10}(S_y(0)/D_{\text{env}})$ , as a function of operating action and bias force. Dashed white line is the locus of zero dispersion ( $\partial_I \omega(I) = 0$ ) points. For interpretation of the references to color in this and all other figures, the reader is referred to the electronic version of this dissertation.

dispersion points. Figure 4.5 is remarkable in its complex topography. The key feature is the narrow valley around the zero dispersion line for large action. Recall that we noted, based upon the scaling results found above, that  $S_{I,I}$  dominates in the expression for  $S_y$  for small action. This is why the narrow valley around the zero dispersion curve fades away for small action. Meanwhile, for large action, we observed that  $S_{\varphi,\varphi}$  should dominate. Accordingly, we see a reduction in the phase diffusion coefficient near the zero dispersion line, where the phase is protected from fluctuations in the action. In the parameter range considered the phase diffusion coefficient can be reduced by at most 5dB by these tuning parameters. This is consistent with observations made by Chris Burgner at the University of Santa Barbara (private communication) on a real device. Improvement on the order of 10's of decibels will likely require attacking the noises at their source.

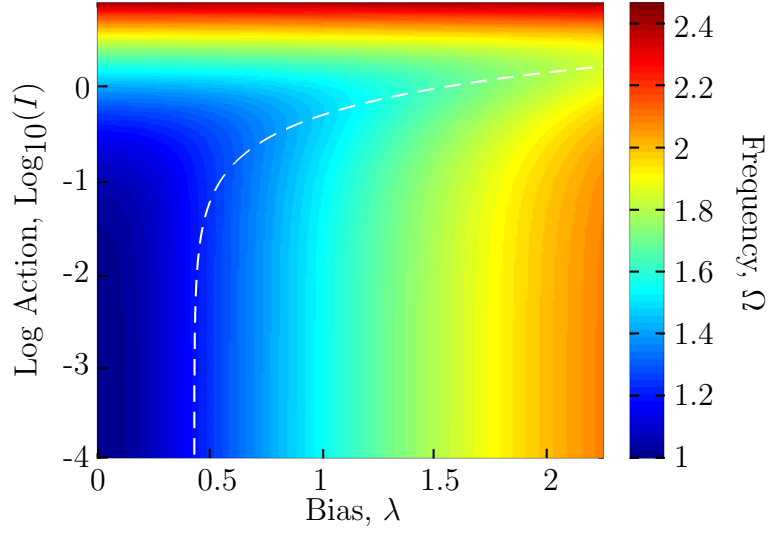


Figure 4.6: Mean oscillator frequency as a function of operating action and bias force. Dashed white line is the locus of zero dispersion ( $\partial_I \omega(I) = 0$ ) points. For interpretation of the references to color in this and all other figures, the reader is referred to the electronic version of this dissertation.

## 4.5 Outlook

Equation (4.64) is the primary result of this chapter. It can be employed as a tool to guide the effort to engineer better N/MEMS oscillators. The equation can serve as a cost function for oscillator optimization or to help target primary noise sources. In this work, we demonstrated the utility of this expression with a hypothetical oscillator model. Building a model matched to experimental observations of a real oscillator may prove more informative. In addition, an interesting problem that could be investigated using this formulation is to determine the optimum potential for an oscillator. Equation (4.64) evaluated at  $\omega = 0$  would provide the cost function for the optimization problem. It is likely that the answer will depend on the noise model and so an appropriate model would need to be generated. Such an effort is beyond the scope of this work, but could be the next step.

# Chapter 5

## Conclusions

In this work we examined several noise-induced phenomena that are to be found in nano- and micro-electromechanical systems. Our aim has been to exploit these phenomena, where possible, for system identification and sensing applications. The exception being our discussion of nonlinear oscillators in chapter 4 where our goal was to remove the effect of noise as much as possible. In general, however, our viewpoint has been one of embracing the noise and nonlinearity that are an inevitable part of miniaturization.

In chapter 2 we examined delayed subcritical pitchfork and saddle-node bifurcations in the presence of noise. This investigation was born out of an attempt to port, to MEMS sensors, the bifurcation detection methods used in the 1970s to locate the critical current in Josephson junctions. During the initial stages of our investigation the issue of sweep rate became important, and it was not clear what it meant to sweep fast or slow. In the present work we determined that “fast” means fast with respect to the noise strength, and that this is indeed the situation in many MEMS devices, leading to delayed bifurcations. The experimental demonstration of our analytic results met with limited success. It turned out that the sweeping experiments took so long that drift in the device parameters became problematic. Despite efforts

to remove this effect by measuring the device frequency before each parameter sweep, this effect may have influenced the data. In addition the sweep rate required for the normal form to remain valid appears to have been so slow that we swept clean through the local region. These issues arose in large part because these experiments were performed before the analysis was complete. A more systematic experiment on a MEMS device has yet to be done, and is left for future work.

In chapter 3 we examined the balanced dynamical bridge as a general use detector and a detector of non-Gaussian noise. This dynamic bridge sensing strategy was inspired by the exponential dependence of the escape rate on device parameters and the success of the Josephson bifurcation amplifier. As a general use detector, we found that the bridge requires a long time to produce a measurement. The problem is that the system encodes the information in the occupation probabilities and measuring these probabilities is time-consuming, requiring the record of many events. The detection of non-Gaussian noise suffers from this same problem. However, using the bridge in this manner can be slightly faster since the non-Gaussian noise can increase the switching rate. Moreover, other methods of detecting the non-Gaussian character of a stochastic process operate on similar principles, and so here the dynamic bridge becomes competitive. We discussed an example where we considered shot noise measured by a one-dimensional bridge. Future work on this project may include a comparison of the dynamical bridge sensitivity to other detection methods. In addition, one may consider a dynamical bridge constructed from a parametric resonator. The inherent symmetry in parametric resonance will automatically balance the occupation probabilities and create a device that is sensitive to symmetry breaking perturbations such as direct forcing at the resonant frequency.

In chapter 4 we examined the spectrum of fractional frequency fluctuations in an oscillator with a nonlinear frequency selective element. We ignored the dynamics of the feedback loop elements, focusing on the resonator equation. We developed an

expression for the spectrum of fractional frequency fluctuations as a function of the oscillator noise model and the nominal resonator orbit. We proposed that such an expression could be useful to tune an oscillator to minimize the rate of phase diffusion. We considered a prototype model based on the biased Duffing resonator with which to demonstrate this oscillator tuning. We showed how the oscillator can be tuned using the resonator zero-dispersion points to decouple the action and angle fluctuations. The minimum phase diffusion constant w.r.t. the oscillator operating action was found to be near the zero-dispersion points for sufficiently large action. The example system showed reduction in the phase diffusion rate of up to 5 decibels by operating at this point. Future work on this subject of oscillator design can be divided into two separate projects. First, a detailed model of an existing oscillator can be constructed in an effort to optimally tune that oscillator. Second, one could attempt to minimize the phase diffusion constant by shaping the limit cycle. The tools we employed would limit the class of limit cycles to those arising from a one degree-of-freedom potential system. However, other perspectives would allow the consideration of more general limit cycles [27, 80]. This problem naturally depends on the noise model employed, and so these two suggested directions for future research are closely related.



## Appendices

# Appendix A

## Stochastic Processes

In this appendix we discuss some of the tools for the analysis of dynamic systems with random terms. This discussion provides some background for the material in the body of this dissertation. The interested reader is directed to references [93, 61, 60] for additional material.

### A.1 The Kinetic Equation for a Stochastic Process

Consider a stochastic process,  $X(t)$ , where  $X \in \mathcal{R}^d$ . We'll use  $X(t)$  to denote the stochastic process itself and  $x$  to denote possible values that  $X(t)$  can take at various times. Now, let  $\rho(x, t)$  be the probability distribution for  $X(t)$  at time  $t$ . Thus,  $\rho(x, t)dx$  is the probability that  $X(t) = x$ . Also, let  $P(x, t + \tau | x', t)$  be the probability that  $X(t + \tau) = x$  given that  $X(t) = x'$ ; this is known as the **transition probability**. It is the probability that the process  $X(t)$  will make a transition from  $x'$  to  $x$  over the time  $[t, t + \tau]$ . A **Markov process** is one whose future value depends only on the present, not the past. We can see that  $P(x, t + \tau | x', t)$  takes only two arguments, the value of  $X$  at the present time  $t$  and the value of  $X$  at the future time  $t + \tau$ . So, if  $X(t)$  is Markovian, then  $P(x, t + \tau | x', t)$  contains the complete description of the

process. Using the transition probability,  $P$ , we can determine the evolution of the probability distribution  $\rho$ . The probability for  $X(t + \tau) = x$  can be understood as the the sum of the probabilities for the process,  $X$ , to transition to  $x$  over the time  $[t, t + \tau]$  from all values  $x'$  at time  $t$ . That is,  $\rho(x, t + \tau)$  is the probability to get to  $x$  in the time interval  $[t, t + \tau]$  from anywhere. Thus, we can write

$$\rho(x, t + \tau) = \int P(x, t + \tau | x', t) \rho(x', t) dx'. \quad (\text{A.1})$$

We can make use of (A.1) to develop a partial differential equation for  $\rho(x, t)$ .

We begin by expanding the integrand for small  $x - x'$ . We will assume that  $x$  is a  $d$ -dimensional real vector,  $x \in \mathbb{R}^d$ . Let  $\Delta = x - x'$ , then we can write the integrand of equation (A.1) as

$$P(x, t + \tau | x', t) \rho(x', t) = P(x' + \Delta, t + \tau | x', t) \rho(x', t), \quad (\text{A.2})$$

$$= \sum_{n_1, \dots, n_d} \frac{(-\Delta_1)^{n_1} \dots (-\Delta_d)^{n_d}}{n_1! \dots n_d!} \frac{\partial^{n_1 + \dots + n_d}}{\partial x_1^{n_1} \dots \partial x_d^{n_d}} \times P(x + \Delta, t + \tau | x, t) \rho(x, t), \quad (\text{A.3})$$

where we have expanded  $x'$  about  $x$  in a Taylor series and the sum for  $n_i$  goes from 0 to  $\infty$ . Substitution of this into equation (A.1) gives

$$\begin{aligned} \rho(x, t + \tau) = & \sum_{n_1, \dots, n_d} (-1)^{n_1 + \dots + n_d} \frac{\partial^{n_1 + \dots + n_d}}{\partial x_1^{n_1} \dots \partial x_d^{n_d}} \rho(x, t) \\ & \times \int \frac{\Delta_1^{n_1} \dots \Delta_d^{n_d}}{n_1! \dots n_d!} P(x + \Delta, t + \tau | x, t) d\Delta. \end{aligned} \quad (\text{A.4})$$

Now, the integral in equation (A.4) can be written as

$$\prod_{i=0}^d \int \frac{\Delta_i^{n_i}}{n_i!} P(x + \Delta, t + \tau | x, t) d\Delta = \left\langle \prod_{i=0}^d \frac{1}{n_i!} [X_i(t + \tau) - x_i]^{n_i} \right\rangle \Big|_{X_i(t)=x_i}, \quad (\text{A.5})$$

which are the moments of the probability distribution of  $X(t + \tau) - X(t)$  given that  $X(t) = x$ , weighted by  $1/(n_1! \cdots n_d!)$ . The collection of these quantities describe the probability distribution of the next step that the stochastic process,  $X(t)$ , takes over the time  $\tau$  if it takes on the value  $x$  at time  $t$ . We now introduce the **Kramers-Moyal coefficients**,  $\mathcal{D}^{(n_1 \cdots n_d)}(x, t)$ .

$$\mathcal{D}^{(n_1 \cdots n_d)}(x, t) = \lim_{\tau \rightarrow 0} \frac{1}{\tau} \left\langle \prod_{i=0}^d \frac{1}{n_i!} [X_i(t + \tau) - x_i]^{n_i} \right\rangle \Big|_{X_i(t)=x_i}. \quad (\text{A.6})$$

These are the coefficients of the first order term in an expansion of equation (A.5) in  $\tau$  about  $\tau = 0$ , so long as at least one  $n_i$  is nonzero. When all  $n_i$  are zero the integral equation (A.5) is equal to 1 by the normalization of  $P$ . Thus, for small  $\tau$ , we have

$$\begin{aligned} \rho(x, t + \tau) = \rho(x, t) + \sum_{\substack{n_1, \dots, n_d \\ m=n_1+\dots+n_d \neq 0}} (-1)^m \frac{\partial^m}{\partial x_1^{n_1} \cdots \partial x_d^{n_d}} \rho(x, t) \mathcal{D}^{(n_1 \cdots n_d)}(x, t) \tau. \end{aligned} \quad (\text{A.7})$$

Next we subtract  $\rho(x, t)$  from both sides of equation (A.7) and divide by  $\tau$ . In the limit of  $\tau \rightarrow 0$  we have the **kinetic equation** of the stochastic process  $X(t)$ , given by

$$\frac{\partial \rho(x, t)}{\partial t} = \sum_{\substack{n_1, \dots, n_d \\ n_1 + \dots + n_d \neq 0}} (-1)^{n_1 + \dots + n_d} \frac{\partial^{n_1 + \dots + n_d}}{\partial x_1^{n_1} \cdots \partial x_d^{n_d}} \mathcal{D}^{(n_1 \cdots n_d)}(x, t) \rho(x, t). \quad (\text{A.8})$$

We now further discuss the meaning of the Kramers-Moyal coefficients. There are  $d$

coefficients for which only one of the integers  $n_i = 1$  and the rest are zero. Changing to a more compact notation, we can write this sub set as  $\mathcal{D}_i^{(1)} \equiv \mathcal{D}(0,0,\dots,1,\dots,0)$  where the 1 occurs in the  $i^{\text{th}}$  place. In  $\mathcal{D}_i^{(1)}$  the superscript denotes the order of the coefficient and the subscript denotes which  $n_i = 1$ . This set of coefficients give the mean step made by the stochastic process  $X(t)$  over a small time normalized by the time. Thus these coefficients are called the **drift vector** or **drift coefficient**. Similarly, we can consider the coefficients of order 2. We can label these as  $\mathcal{D}_{ij}^{(2)} \equiv \mathcal{D}(0,0,\dots,1,0,0,\dots,0,1,\dots,0)$  denoting the second order coefficient where  $n_i = 1$  and  $n_j = 1$  if  $i \neq j$  and  $n_i = 2$  if  $i = j$ . These coefficients describe the variance of the step made by the stochastic process over a small time normalized by this time. Thus  $\mathcal{D}^{(2)}$  is called the **diffusion coefficient**.

Now, equation (A.8) is pretty unwieldy when it represents an infinite series. Calculating the infinite number of coefficients  $\mathcal{D}^{(n_1 \cdots n_d)}$  could be difficult, if not impossible. However, the **Pawula Theorem** says that the series  $\mathcal{D}^{(n_1 \cdots n_d)}$  will terminate at either the first or the second order (i.e.  $n_1 + n_2 + \cdots n_d = 1$  or  $2$ ) or, if it does not, it must have an infinite number of terms in it. Thus, one only has to check the third order term to find out if the series terminates at second order or is infinite. This holds under the condition that  $\rho(x, t)$  is to be always positive, which it must be, since its a probability distribution.

As an example, consider the standard one-dimensional **Brownian motion**, a.k.a. a **Wiener process**, defined by

$$\mathcal{D}^{(1)} = 0 \quad \mathcal{D}^{(2)} = 1 \quad \mathcal{D}^{(n)} = 0, \quad n \geq 3. \quad (\text{A.9})$$

In this case equation (A.8) and its solution are

$$\dot{\rho} = \rho'' \quad \Rightarrow \quad \rho(x, t) = \sqrt{\frac{1}{4\pi t}} \exp \left[ -\frac{(x - x(0))^2}{4t} \right]. \quad (\text{A.10})$$

The case where the Kramers-Moyal coefficients are nonzero only at first and second order is very interesting and useful. Now we know one process that fits in that category, Brownian motion, but what about a stochastic process that represents the response of a dynamic system? As we will see in the next section, when a dynamic system is forced by Gaussian white noise, its Kramers-Moyal expansion is also truncated at second order. So, all that is left to do is to calculate these coefficients for our system of interest. To do this, all we have to do is solve our system equation over a short time interval  $\tau$ , and then take the limit according to (A.6). Solving our system over a small time interval  $\tau$ , however, is where the trouble comes in. It turns out that the answer depends on how we interpret the noise. We will discuss this further in the next two sections. We begin with a “physical” interpretation of the noise, assuming that it is smooth on time scales much shorter than the time scale of the evolution of our system.

## A.2 The Langevin Equation

Suppose we have the system

$$\dot{X}_i = f_i(X, t) + g_{ij}(X, t)\xi_j(t). \quad (\text{A.11})$$

This is our Langevin equation. The time functions  $\xi_j(t)$  are assumed to be zero mean random functions that are smooth on a sufficiently short time scale. This smoothness comes from the ‘physical’ interpretation, arguing that real quantities are smooth. Smoothness implies that the standard rules of calculus apply. Now, we want to integrate our equation over a short time  $\tau$  with initial condition  $X(t) = x$ . So we

integrate (A.11) w.r.t. time

$$X_i(t + \tau) - x_i = \int_t^{t+\tau} \left[ f_i(X(t'), t') + g_{ij}(X(t'), t') \xi_j(t') \right] dt', \quad (\text{A.12})$$

and apply an iterative approach, assuming  $f$  and  $g$  are sufficiently well behaved functions. First we approximate  $f$  and  $g$  as

$$f(X(t'), t') \approx f_i(x, t'), \quad (\text{A.13})$$

$$g_{ij}(X(t'), t') \approx g_{ij}(x, t'). \quad (\text{A.14})$$

Applying these approximations to equation (A.12) gives the zeroth order approximation,

$$X_i^{(0)}(t + \tau) - x_i = \int_t^{t+\tau} \left[ f_i(x, t') + g_{ij}(x, t') \xi_j(t') \right] dt'. \quad (\text{A.15})$$

Going to the next order, we take

$$f_i(X(t'), t') \approx f_i(x, t') + \frac{\partial f_i(x, t')}{\partial x_k} (X_k^{(0)}(t') - x_k), \quad (\text{A.16})$$

$$g_{ij}(X(t'), t') \approx g_{ij}(x, t') + \frac{\partial g_{ij}(x, t')}{\partial x_k} (X_k^{(0)}(t') - x_k), \quad (\text{A.17})$$

to get the first order approximation

$$\begin{aligned} X_i^{(1)}(t + \tau) - x_i &= \int_t^{t+\tau} \left\{ f_i(x, t') + g_{ij}(x, t') \xi_j(t') \right. \\ &+ \int_t^{t'} \left[ \frac{\partial f_i(x, t')}{\partial x_k} f_k(x, t'') + \frac{\partial f_i(x, t')}{\partial x_k} g_{kj}(x, t'') \xi_j(t'') \right. \\ &\left. \left. + \frac{\partial g_{ij}(x, t')}{\partial x_k} f_k(x, t'') \xi_j(t') + \frac{\partial g_{ij}(x, t')}{\partial x_k} g_{kl}(x, t'') \xi_j(t') \xi_l(t'') \right] dt'' \right\} dt'. \end{aligned} \quad (\text{A.18})$$

This is a sufficient order for our purposes. Now, we take the expectation or ensemble average, then we take  $f(x, t') \approx f(x, t)$  and  $g(x, t') \approx g(x, t)$ , and find

$$\begin{aligned} \langle X_i(t + \tau) - x_i \rangle &= \int_t^{t+\tau} f_i(x, t') dt' \\ &+ \int_t^{t+\tau} \int_t^{t'} \frac{\partial g_{ij}(x, t')}{\partial x_k} g_{kl}(x, t'') \langle \xi_j(t') \xi_l(t'') \rangle dt'' dt' + \mathcal{O}(\tau^2). \end{aligned} \quad (\text{A.19})$$

Now, we assume that the noise processes  $\xi_i$  are **wide sense stationary**. This means that  $\langle \xi_i(t) \xi_j(t') \rangle$  depends only on the time difference  $t - t'$ . Moreover, we assume that the processes have short memory compared to the rate of change of  $X$ . Thus,  $\langle \xi_i(t) \xi_j(t') \rangle$  is a narrow function of  $t - t'$  that goes to zero for  $t - t' \ll \tau$ . It is reasonable, therefore, to make the approximation  $\langle \xi_i(t) \xi_j(t') \rangle = 2D_{ij} \delta(t - t')$ . The  $\delta$ -correlation implies that the power spectral density is constant, so the noise is white. Unfortunately, things are not quite that simple. In equation (A.19) we integrate  $\delta(t)$  up to  $t = 0$  from below and thus the result of the integration depends on how we define the  $\delta$  function. For example, we could assume

$$\delta(t) = \lim_{h \rightarrow 0} \frac{\theta(t + h) - \theta(t - h)}{2h}, \quad (\text{A.20})$$

where  $\theta(t)$  is the unit step function. In this case integration over half the  $\delta$ -function gives 1/2. Alternatively, we could assume

$$\delta(t) = \lim_{h \rightarrow 0} \frac{\theta(t) - \theta(t - h)}{h}. \quad (\text{A.21})$$

In this case the integration gives zero. The choice we make for the definition of the  $\delta$ -function must reflect the noise properties. We will continue with our discussion



assuming the former case so the integration gives  $1/2$ . Thus, we obtain

$$\langle X_i(t + \tau) - x_i \rangle = f_i(x, t)\tau + \frac{\partial g_{ij}(x, t)}{\partial x_k} g_{kl}(x, t) D_{jl} \tau + \mathcal{O}(\tau^2). \quad (\text{A.22})$$

Next, we consider the second moments of  $X_i(t + \tau) - x_i$ .

$$\begin{aligned} \langle [X_i(t + \tau) - x_i][X_j(t + \tau) - x_j] \rangle &= \\ &\int_t^{t+\tau} \int_t^{t+\tau} g_{ik}(x, t') g_{jl}(x, t'') \langle \xi_k(t') \xi_l(t'') \rangle dt' dt'' + \dots \\ &= 2\tau g_{ik}(x, t) g_{jl}(x, t) D_{kl} + \mathcal{O}(\tau^2). \end{aligned} \quad (\text{A.23})$$

The third and higher moments are all higher order in  $\tau$ ,

$$\langle [X_i(t + \tau) - x_i][X_j(t + \tau) - x_j][X_k(t + \tau) - x_k] \rangle = \mathcal{O}(\tau^2). \quad (\text{A.24})$$

Thus we find that a dynamic system subject to white Gaussian noise is Markovian with Kramers-Moyal coefficients

$$\mathcal{D}_i^{(1)}(x, t) = f_i(x, t) + \frac{\partial g_{ij}(x, t)}{\partial x_k} g_{kl}(x, t) D_{jl}, \quad (\text{A.25})$$

$$\mathcal{D}_{ij}^{(2)}(x, t) = g_{ik}(x, t) g_{jl}(x, t) D_{kl}, \quad (\text{A.26})$$

$$\mathcal{D}^{(n)}(x, t) = 0, \quad n \geq 3. \quad (\text{A.27})$$

Plugging these coefficients into equation (A.8) gives the **Fokker-Planck equation**.

### A.3 Ito and Stratonovich Integrals

The stochastic process  $\xi(t)$  is not a proper function when it is truly  $\delta$ -correlated because it is discontinuous at every point. Rather than deal with this, mathematicians prefer to deal with the Brownian motion or the Wiener process we saw earlier. And

so, rather than write a Langevin equation like (A.11), they write the **stochastic differential equation** (SDE)

$$dX_i = f_i(X, t)dt + g_{ij}(X, t)d_{jk}dW_k, \quad (\text{A.28})$$

where  $dW_k$  is the increment of a Brownian motion. The noise strength and correlation has been explicitly written in the matrix  $d$ . Note that, to agree with the above,  $dd^T = D$ . Since a Brownian motion is continuous, the increments  $dW_k$  are well defined. Now, if we integrate the SDE (A.28) with initial conditions  $X(t) = x$  we get

$$X_i(t + \tau) - x_i = \int_t^{t+\tau} f_i(X(t'), t')dt' + \int_t^{t+\tau} g_{ij}(X(t'), t')d_{jk}dW_k(t'). \quad (\text{A.29})$$

Applying the same iterative procedure as above, we find

$$X_i^{(0)}(t + \tau) - x_i = \int_t^{t+\tau} f_i(x, t')dt' + \int_t^{t+\tau} g_{ij}(x, t')d_{jk}dW_k(t'), \quad (\text{A.30})$$

and

$$\begin{aligned} X_i^{(1)}(t + \tau) - x_i &= \int_t^{t+\tau} \left\{ f_i(x, t')dt' + g_{ij}(x, t')d_{jk}dW_k(t') \right. \\ &+ \int_t^{t'} \left[ \frac{\partial f_i(x, t')}{\partial x_k} f_k(x, t'')dt''dt' \right. \\ &+ \frac{\partial f_i(x, t')}{\partial x_k} g_{kj}(x, t'')d_{jl}dW_l(t'')dt' \\ &+ \frac{\partial g_{ij}(x, t')}{\partial x_k} f_k(x, t'')d_{jl}dt''dW_l(t') \\ &\left. \left. + \frac{\partial g_{ij}(x, t')}{\partial x_k} g_{kl}(x, t'')d_{jn}d_{lm}dW_m(t'')dW_n(t') \right] dt' \right\}. \end{aligned} \quad (\text{A.31})$$

As in the Langevin approach discussion, we take  $f(x, t') \approx f(x, t)$  and  $g(x, t') \approx g(x, t)$ , and find

$$\begin{aligned} X_i^{(1)}(t + \tau) - x_i &= f_i(x, t)\tau + g_{ij}(x, t)d_{jk} \int_0^\tau dW_k(t') \\ &+ \frac{\partial g_{ij}(x, t)}{\partial x_k} g_{kl}(x, t)d_{jn}d_{lm} \int_0^\tau \int_0^{t'} dW_m(t'')dW_n(t') + \dots \end{aligned} \quad (\text{A.32})$$

We have pushed all terms that won't contribute into the  $\dots$  and shifted the limits on the integrals w.r.t.  $dW$  because the Brownian motion increment  $dW$  is **stationary**, that is its statistics don't depend on the the location of the time origin. The reason why we needed to shift the limits of integration is because the definition of these stochastic integrals is written with these limits. Now, these stochastic integrals can be of either the Ito or Stratonovich type, depending on interpretation. These integrals are defined as follows. Let  $0 = t_0 < t_1 < t_2 \dots < t_{N-1} < t_N = \tau$  and  $\Delta = t_{i+1} - t_i$ . Then an integral of the Ito type of a function  $\Phi(W(t), t)$  with respect to  $dW(t)$  is defined by

$$I_I = \int_0^\tau \Phi(W(t), t)dW(t) = \lim_{\Delta \rightarrow 0} \sum_{i=0}^{N-1} \Phi(W(t_i), t_i)[W(t_{i+1}) - W(t_i)], \quad (\text{A.33})$$

and an integral of the Stratonovich type is defined by

$$\begin{aligned} I_S &= \int_0^\tau \Phi(W(t), t)dW(t) \\ &= \lim_{\Delta \rightarrow 0} \sum_{i=0}^{N-1} \Phi\left(\frac{W(t_{i+1}) + W(t_i)}{2}, \frac{t_{i+1} + t_i}{2}\right) [W(t_{i+1}) - W(t_i)]. \end{aligned} \quad (\text{A.34})$$

In both integrals,  $W(t)$  is a standard Wiener process or Brownian motion defined as

$$W(0) = 0, \quad \langle W(t) \rangle = 0, \quad (\text{A.35})$$

$$\text{Var}(W(t)) = 2t, \quad \text{Var}(W(t) - W(s)) = 2t - 2s. \quad (\text{A.36})$$

Now if we consider the term  $\int_0^\tau dW(t')$  in (A.32), we have  $\Phi = 1$  and so both Ito and Stratonovich give the same answer

$$\int_0^\tau dW(t') = \lim_{\Delta \rightarrow 0} \sum_{i=0}^{N-1} [W(t_{i+1}) - W(t_i)] = W(\tau). \quad (\text{A.37})$$

So, the double integral in (A.32) gives

$$\int_0^\tau \int_0^{t'} dW(t'') dW(t') = \int_0^\tau W(t') dW(t'). \quad (\text{A.38})$$

What we need is the expectation of this integral. The Stratonovich definition gives

$$\begin{aligned} \left\langle \int_0^\tau W(t') dW(t') \right\rangle_S &= \left\langle \lim_{\Delta \rightarrow 0} \frac{1}{2} \sum_{i=0}^{N-1} [W(t_{i+1} + W(t_i))] [W(t_{i+1}) - W(t_i)] \right\rangle \\ &= \lim_{\Delta \rightarrow 0} \frac{1}{2} \sum_{i=0}^{N-1} \langle W^2(t_{i+1}) - W^2(t_i) \rangle = \lim_{\Delta \rightarrow 0} \sum_{i=0}^{N-1} t_{i+1} - t_i = \tau. \end{aligned} \quad (\text{A.39})$$

The Ito definition gives

$$\begin{aligned} \left\langle \int_0^\tau W(t') dW(t') \right\rangle_I &= \left\langle \lim_{\Delta \rightarrow 0} \sum_{i=0}^{N-1} W(t_i) [W(t_{i+1}) - W(t_i)] \right\rangle \\ &= \lim_{\Delta \rightarrow 0} \frac{1}{2} \langle W^2(\tau) \rangle - \frac{1}{2} \sum_{i=0}^{N-1} \langle [W(t_{i+1}) - W(t_i)]^2 \rangle = 0. \end{aligned} \quad (\text{A.40})$$

Applying equations (A.37)-(A.40) to (A.32) we obtain our expression for  $X(t+\tau) - x$ .

$$\langle X_i(t+\tau) - x_i \rangle = f_i(x, t)\tau + \frac{\partial g_{ij}(x, t)}{\partial x_k} g_{kl}(x, t) d_{jn} d_{lm} \left\langle \int_0^\tau W_m(t) dW_n(t) \right\rangle_{I, S}, \quad (\text{A.41})$$

with

$$\left\langle \int_0^\tau W_m(t) dW_n(t) \right\rangle_I = 0, \quad (\text{A.42})$$

$$\left\langle \int_0^\tau W_m(t) dW_n(t) \right\rangle_S = \tau \delta_{nm}. \quad (\text{A.43})$$

Thus, we have

$$\mathcal{D}_{i, \text{Ito}}^{(1)} = f_i(x, t), \quad \mathcal{D}_{i, \text{Strat}}^{(1)} = f_i(x, t) + \frac{\partial g_{ij}(x, t)}{\partial x_k} g_{kl}(x, t) D_{jl}. \quad (\text{A.44})$$

It can also be shown that the diffusion coefficient,  $\mathcal{D}^2$ , is the same for both. The Stratonovich interpretation matches the Langevin approach of the previous section with definition (A.20) and the Ito interpretation matches the Langevin approach with definition (A.21). The choice of stochastic calculus to be used should be made by considering the origin and character of the noise processes. In [61] there is a chapter on this topic. Ito calculus appears better suited for numeric solutions of stochastic differential equations [61] because the equations can be directly integrated. Stratonovich calculus would require an implicit scheme. When performing simulations of Stratonovich stochastic systems it is usually necessary to write an equivalent Ito SDE. To do this one would take the drift and diffusion coefficients from the Stratonovich system and write an Ito SDE that gives rise to these same coefficients using Ito calculus.

# Appendix B

## Stochastic Averaging

In this appendix we discuss the method of averaging applicable to dynamic systems with random terms. This method should apply to systems with non-white and/or non-Gaussian noise. The approach is meant to be as simple as possible, employing only basic understanding of stochastic processes. No proof is given however, just an explanation of the method and the thought processes behind it.

We are interested in equations of the form

$$\dot{x}_i = \epsilon f_i(x, t) + \epsilon^{1/2} g_{ij}(x, t) \xi_j(t), \quad (\text{B.1})$$

where  $\xi$  represents some stochastic process, the functions  $f$  and  $g$  are periodic, or at least have discrete spectrum, and  $\epsilon$  is a small parameter. Note that this scaling is consistent with the microscopic resonator model in section (4.2). The noise  $\xi$  is assumed to be continuous and differentiable so that conventional calculus rules apply. In other words, equation (B.1) is to be interpreted in the Stratonovich sense. The goal is to simplify this system by pushing the non-essential aspects of the system to higher orders in  $\epsilon$  by means of a near-identity coordinate transformation. These non-essential terms are then ignored by virtue of their smallness, recognizing that

the truncated equations will provide a good approximation over a long but generally finite time scale. In addition to the above, we assume that the stochastic process  $\xi$  is wide-sense stationary with zero mean, that is

$$\langle \xi_i(t) \rangle = 0, \quad (\text{B.2})$$

$$\langle \xi_i(t) \xi_j(t + \tau) \rangle = r_{ij}(\tau), \quad (\text{B.3})$$

and, we introduce the power spectrum of  $\xi$ ,

$$R_{ij}(\omega) = \int_{-\infty}^{\infty} r_{ij}(\tau) e^{-i\omega\tau} d\tau. \quad (\text{B.4})$$

For this averaging process only the second order statistics are needed, so we will not specify  $\xi$  any further. As stated above, we assume the time variation of  $f$  and  $g$  is made up of several discrete frequencies. Thus we write

$$f_i(y, t) = \sum_n F_i^{(n)}(y) e^{i\Omega_n t}, \quad (\text{B.5})$$

$$g_{ij}(y, t) = \sum_n G_{ij}^{(n)}(y) e^{i\Omega_n t}, \quad (\text{B.6})$$

with  $F_i^{(-n)} = (F_i^{(n)})^*$ ,  $G_{ij}^{(-n)} = (G_{ij}^{(n)})^*$ , and  $\Omega_{-n} = -\Omega_n$ . Here we must make a point of notation. We make use of the convention of summation over repeated indices written as subscripts, and we often use  $i$  as an index. So, when  $i$  appears as a subscript it is meant as an index. However, when it appears elsewhere it is meant as the imaginary unit. We now proceed with the coordinate transformation.

## B.1 A Near-Identity Coordinate Transformation

In order to simplify equation (B.1), we would like to change to a coordinate system in which the system appears as simple as possible, given the smallness of  $\epsilon$ . To do this, we begin by defining the general near-identity coordinate transformation

$$x_i = y_i + \epsilon^{1/2} U_i(y, t) + \epsilon V_i(y, t). \quad (\text{B.7})$$

The functions  $U$  and  $V$  are left unspecified for the present. The problem of defining these two functions is the subject of the next two sections. In this section, we simply solve for the equation of motion of  $y$  with these general functions. We do this by first taking the time derivative of (B.7) and equating it with (B.1) in which we have replaced  $x$  with  $y$  via a Taylor series expansion

$$\dot{x}_i = \dot{y}_i + \epsilon^{1/2} \frac{\partial U_i(y, t)}{\partial y_j} \dot{y}_j + \epsilon \frac{\partial V_i(y, t)}{\partial y_j} \dot{y}_j + \epsilon^{1/2} \dot{U}_i(y, t) + \epsilon \dot{V}_i(y, t), \quad (\text{B.8})$$

$$= \epsilon f_i(y, t) + \epsilon^{1/2} g_{ij}(y, t) \xi_j(t) + \epsilon \frac{\partial g_{ij}(y, t)}{\partial y_k} U_k(y, t) \xi_j(t) + \dots \quad (\text{B.9})$$

From (B.8) and (B.9) we solve for  $\dot{y}$  up to  $\mathcal{O}(\epsilon)$ .

$$\dot{y}_i = \epsilon^{1/2} \left( g_{ij} \xi_j - \dot{U}_i \right) + \epsilon \left( f_i + \frac{\partial g_{ij}}{\partial y_k} U_k \xi_j - \frac{\partial U_i}{\partial y_j} g_{jk} \xi_k + \frac{\partial U_i}{\partial y_j} \dot{U}_j - \dot{V}_i \right). \quad (\text{B.10})$$

Now, it remains to choose  $U$  and  $V$  such that equation (B.10) becomes as simple as possible. The constraint on the choice is that the coordinate transformation, equation (B.7), must remain well ordered. Thus, we must choose  $U$  and  $V$  such that they remain bounded. It is by this condition that we identify the principle part of equation (B.1) that cannot be reduced.



## B.2 Stochastic Averaging Part I: $\mathcal{O}(\epsilon^{1/2})$

To begin, we consider the function  $U$ . The role of this function is to replace the stochastic process  $g(y, t)\xi(t)$  with something simpler, call it  $\bar{\xi}(y, t)$ . The process  $g\xi$  is wide-sense cyclo-stationary. Thus, the most general form of  $\bar{\xi}$  then is also a wide-sense cyclo-stationary process. We don't go through the exercise here, but it can be shown that the principle part of  $g\xi$ , that is the part that must be contained in  $\bar{\xi}$ , need only be wide-sense stationary. This is done by taking  $\bar{\xi}$  to be a general wide-sense cyclo-stationary process and calculating  $\langle U^2 \rangle$ . One then finds that the secular terms contain only the wide-sense stationary component of  $\bar{\xi}$  and its (cyclo-stationary) correlation with  $\xi$ . We therefore need only seek a wide-sense stationary process  $\bar{\xi}$  to replace  $g\xi$ . We can construct such a process by defining our “slow noise” process,  $\bar{\xi}$ , as a low-pass filtering of  $g\xi$ . Thus, we take

$$\dot{U}_i(y, t) = g_{ij}(y, t)\xi_j(t) - \bar{\xi}_i(y, t), \quad (\text{B.11})$$

$$\bar{\xi}_i(y, t) = \int_{-\infty}^{\infty} h(t - t')g_{ij}(y, t')\xi_j(t') dt', \quad (\text{B.12})$$

where  $h(t)$  is the time-domain filtering function, the filter's ‘impulse response’. Note that equation (B.12) defines the simplified noise  $\bar{\xi}$  as a functional of the original process,  $\xi$ . Thus, in principle, the statistics of  $\bar{\xi}$  may be calculated for non-white and/or non-Gaussian  $\xi$ . The definition of this coordinate transformation, however, does not require a causal filtering function and so we are free to choose  $h(t) \neq 0$  for  $t < 0$ . By a proper choice of the filter we can make  $\bar{\xi}$  wide-sense stationary. For example, we may choose an ideal low-pass filter with appropriate cut-off frequency. Our filter may also be characterized by the frequency domain filtering function,

$$H(\omega) = \int_{-\infty}^{\infty} h(t)e^{-i\omega t} dt. \quad (\text{B.13})$$

For an ideal low-pass filter, this is simply a rectangular pulse, in  $\omega$  space, centered zero. We now wish to show that  $U$  remains bounded, at least with high probability. To do this, we demonstrate that  $\langle U_i^2 \rangle$  is bounded for every  $i$ . For this to be so, the tails of the probability distribution for  $U(y, t)$  should decay sufficiently fast and so the probability for  $U$  to be very large is very small. In order to facilitate the calculation, it is convenient to first calculate the second moment of  $\bar{\xi}$  and its correlator with  $\xi$ . From equation (B.12) we find

$$\langle \xi_j(t) \bar{\xi}_i(y, s) \rangle = \sum_n \frac{1}{2\pi} \int_{-\infty}^{\infty} G_{ik}^{(n)} R_{kj}(\omega) H(\Omega_n - \omega) e^{i\omega(t-s)} e^{i\Omega_n s} d\omega, \quad (\text{B.14})$$

and

$$\begin{aligned} \langle \bar{\xi}_i(y, t) \bar{\xi}_j(y, s) \rangle &= \sum_{n,m} \frac{1}{2\pi} \int_{-\infty}^{\infty} G_{ik}^{(n)} G_{jl}^{(m)} R_{k\ell}(\omega) H(\Omega_n - \omega) H(\Omega_m + \omega) \\ &\quad \times e^{i\omega(s-t)} e^{i\Omega_n t} e^{i\Omega_m s} d\omega. \end{aligned} \quad (\text{B.15})$$

Equation (B.15) is of particular importance since it is the autocorrelation of the slow noise,  $\bar{\xi}$ . From this equation we can see how the oscillations of  $g$  select the noise around the frequencies  $\Omega_n$ . The oscillating function  $g$  modulates components of the noise  $\xi$  down to baseband. These low frequency components of the modulated noise are then selected by the low-pass filter. Moreover, we see that if  $H(\Omega_m - \omega)$  and  $H(\Omega_n + \omega)$  are orthogonal, except in the case  $m = -n$ , then the slow noise  $\bar{\xi}$  is wide-sense stationary. Returning to the ideal low-pass example, suppose  $H(\omega)$  is a rectangular window centered at  $\omega = 0$  and with width less than the minimum distance between any pair of frequencies  $\Omega_n$  and  $\Omega_m$ , ( $m \neq n$ ). In this case, only the wide-sense stationary terms in equation (B.15) survive.

It remains to show that our choice of  $\dot{U}$  in equation (B.11) is valid. To do this we

will calculate  $\langle U^2 \rangle$  and show that it remains bounded in time. Thus, from equation (B.11), we take

$$U_i = \int_{-\infty}^t g_{ij}(y, t') \xi_j(t') - \bar{\xi}_i(y, t') dt', \quad (\text{B.16})$$

and calculating the variance gives

$$\begin{aligned} \langle U_i^2 \rangle = & \int_{-\infty}^t \int_{-\infty}^t \left[ g_{ij}(y, t') g_{ik}(y, s') \langle \xi_j(t') \xi_k(s') \rangle - g_{ij}(y, t') \langle \xi_j(t') \bar{\xi}_i(y, s') \rangle \right. \\ & \left. - g_{ij}(y, s') \langle \xi_j(s') \bar{\xi}_i(y, t') \rangle + \langle \bar{\xi}_i(y, t') \bar{\xi}_i(y, s') \rangle \right] dt' ds'. \end{aligned} \quad (\text{B.17})$$

Applying equations (B.14) and (B.15) and moving into the frequency domain yields

$$\begin{aligned} \langle U_i^2 \rangle = & \sum_{n,m} \frac{1}{2\pi} \int_{-\infty}^{\infty} d\omega G_{ij}^{(n)} G_{ik}^{(m)} R_{kj}(\omega) \left( 1 - 2H(\Omega_m - \omega) \right. \\ & \left. + H(\Omega_m - \omega) H(\Omega_n + \omega) \right) e^{i(\Omega_n + \Omega_m)t} \\ & \times \int_{-\infty}^0 \int_{-\infty}^0 e^{i(\Omega_n + \omega)t'} e^{i(\Omega_m - \omega)s'} ds' dt'. \end{aligned} \quad (\text{B.18})$$

The time integrals over  $t'$  and  $s'$  can be understood as Fourier transforms of the unit step,

$$\int_{-\infty}^0 e^{iat'} dt' = \frac{1}{ia} + \pi\delta(a). \quad (\text{B.19})$$

Now, the secular terms in equation (B.18) are those for which  $m = -n$ . In these terms the poles and delta functions double up to make the integration over  $\omega$  unbounded. However, these terms are removed by the filtering on the condition that  $H(0) = 1$ .

This can be assumed without any restriction on the approach, in which case we find

$$\langle U_i^2 \rangle = \sum_{\substack{n,m \\ m \neq -n}} \frac{e^{i(\Omega_n + \Omega_m)t}}{i(\Omega_n + \Omega_m)} G_{ij}^{(n)} G_{ik}^{(m)} R_{kj}(-\Omega_n) \left(1 - H(\Omega_n + \Omega_m)\right), \quad (\text{B.20})$$

$$= \sum_{n \neq 0} \frac{e^{in\Omega t}}{in\Omega} \left(1 - H(n\Omega)\right) \left(\sum_m G_{ij}^{(m)} G_{ik}^{(n-m)} R_{kj}(-m\Omega)\right). \quad (\text{B.21})$$

Thus, we find that  $\langle U_i^2 \rangle$  is given by a Fourier series and it is bounded so long as this series converges. For example, if  $G_{ij}^{(n)}$  diminish sufficiently fast with large  $n$ .

### B.3 Stochastic Averaging Part II: $\mathcal{O}(\epsilon)$

With the choice of  $U(y, t)$  derived in the previous section, we now move onto the selection of the deterministic term  $V(y, t)$ . With our selection of  $U(y, t)$  equation (B.10) now becomes

$$\dot{y}_i = \epsilon^{1/2} \bar{\xi}_i(y, t) + \epsilon \left( f_i(y, t) + \eta_i(y, t) + d_i(y, t) - \dot{V}_i(y, t) \right) + \dots, \quad (\text{B.22})$$

where  $\eta + d$  is the  $\mathcal{O}(\epsilon)$  noise,  $\eta$  is the fluctuating part and  $d$  is the expectation, given by

$$\eta_i(y, t) = \frac{\partial g_{ij}}{\partial y_k} U_k \xi_j - \frac{\partial U_i}{\partial y_j} \bar{\xi}_j - d_i(y, t), \quad (\text{B.23})$$

$$d_i(y, t) = \left\langle \frac{\partial g_{ij}}{\partial y_k} U_k \xi_j - \frac{\partial U_i}{\partial y_j} \bar{\xi}_j \right\rangle. \quad (\text{B.24})$$

We have explicitly separated  $d$  from  $\eta$  because  $\eta$  will be dropped when we scale time (in the next section), but  $d$ , the term of interest, will be retained.

In order to simplify equation (B.22) as much as possible, understanding that  $\eta$

will be dropped, we take

$$\dot{V}_i(y, t) = f_i - \bar{f}_i + d_i - \bar{d}_i, \quad (\text{B.25})$$

$$\bar{f}_i(y) = \int_{-\infty}^{\infty} h(t - t') f_i(y, t') dt', \quad (\text{B.26})$$

$$\bar{d}_i(y, t) = \int_{-\infty}^{\infty} h(t - t') d_i(y, t') dt', \quad (\text{B.27})$$

where  $h$  is the filter function from the previous section. It is clear that  $V$  will remain bounded since it is the integral of oscillating functions with their low frequency components removed by the filter. We are therefore satisfied that this choice of  $V$  is valid and proceed to calculate  $\bar{d}$ . Evaluating the two parts of equation (B.24) gives

$$\left\langle \frac{\partial g_{ij}}{\partial y_k} U_k \xi_j \right\rangle = \sum_{n,m} \int_{-\infty}^{\infty} d\omega \frac{\partial G_{ij}^{(m)}}{\partial y_k} G_{k\ell}^{(n)} R_{\ell j}(\omega) \frac{1 - H(\Omega_n - \omega)}{2\pi i(\Omega_n - \omega)} e^{i(\Omega_n + \Omega_m)t}, \quad (\text{B.28})$$

and

$$\begin{aligned} \left\langle \frac{\partial U_i}{\partial y_j} \bar{\xi}_j \right\rangle &= \sum_{n,m} \int_{-\infty}^{\infty} d\omega \frac{\partial G_{ij}^{(m)}}{\partial y_k} G_{k\ell}^{(n)} R_{\ell j}(\omega) H(\Omega_n - \omega) \\ &\quad \times \frac{1 - H(\Omega_m + \omega)}{2\pi i(\Omega_m + \omega)} e^{i(\Omega_n + \Omega_m)t}. \end{aligned} \quad (\text{B.29})$$

Subtracting equation (B.29) from equation (B.28) and then filtering the difference gives the expression for  $\bar{d}$ ,

$$\begin{aligned} \bar{d}_i(y, t) &= \sum_{n,m} \int_{-\infty}^{\infty} d\omega \frac{\partial G_{ij}^{(m)}}{\partial y_k} G_{k\ell}^{(n)} R_{\ell j}(\omega) H(\Omega_n + \Omega_m) \left[ \frac{1 - H(\Omega_n - \omega)}{2\pi i(\Omega_n - \omega)} \right. \\ &\quad \left. - H(\Omega_n - \omega) \frac{1 - H(\Omega_m + \omega)}{2\pi i(\Omega_m + \omega)} \right] e^{i(\Omega_n + \Omega_m)t}. \end{aligned} \quad (\text{B.30})$$

Equation (B.30) simplifies significantly if  $H(\Omega_n + \Omega_m) = \delta_{m,-n}$ . In this case we have

$$\bar{d}_i(y, t) = \sum_n \int_{-\infty}^{\infty} d\omega \frac{\partial G_{ij}^{(-n)}}{\partial y_k} G_{k\ell}^{(n)} R_{\ell j}(\Omega_n - \omega) \frac{1 - |H(\omega)|^2}{2\pi i \omega}. \quad (\text{B.31})$$

If  $R_{\ell j}$  is even and real  $\bar{d}_i(y, t)$  becomes

$$\bar{d}_i(y, t) = \sum_{n=1}^{\infty} \text{Im} \left[ \frac{\partial G_{ij}^{(-n)}}{\partial y_k} G_{k\ell}^{(n)} \right] \int_{-\infty}^{\infty} d\omega R_{\ell j}(\omega - \Omega_n) \frac{1 - |H(\omega)|^2}{\pi \omega}. \quad (\text{B.32})$$

From equation (B.31) or (B.32) it is easy to see that  $\bar{d}$  is the contribution to the slow dynamics produced by the noise away from the frequencies  $\Omega_n$ . For white noise, for which  $R_{\ell j} = \text{const}$ , the weights are all zero and so  $\bar{d}$  is zero. In the more general case, however, it may nonzero.

## B.4 Time Scaling

With the coordinate transformation chosen, we scale time to put all important terms at  $\mathcal{O}(1)$ . Thus, we introduce the slow time  $\tau$ ,

$$\tau = \epsilon t. \quad (\text{B.33})$$

Assuming we have removed all oscillating components by the coordinate transformation, the equation of motion for  $y$  now takes the form

$$\frac{dy_i}{d\tau} = \bar{f}_i(y) + \bar{d}_i(y) + \epsilon^{-1/2} \bar{\xi}_i(y, \epsilon^{-1} \tau) + \eta_i(y, \epsilon^{-1} \tau) + \mathcal{O}(\epsilon^{1/2}). \quad (\text{B.34})$$

We replace the noise terms  $\bar{\xi}$  and  $\eta$  with noises defined in the new time  $\tau$  as follows.

Let

$$\zeta_i(y, \tau) \equiv \epsilon^{-1/2} \bar{\xi}_i(y, \epsilon^{-1} \tau), \quad (\text{B.35})$$

$$\hat{\eta}_i(y, \tau) \equiv \epsilon^{-1/2} \eta_i(y, \epsilon^{-1} \tau). \quad (\text{B.36})$$

We introduce the factor of  $\epsilon^{1/2}$  to that  $\zeta$  and  $\hat{\eta}$  maintain the same spectral magnitude. The signal power, however, increases. This can be understood by imagining that the noises appear to be ‘more white’ over the long time scale  $\tau$ . To see this, consider the spectrum,  $S_\zeta$ ,

$$\langle \zeta(y, t) \zeta(y, t + \tau) \rangle = \frac{1}{2\pi\epsilon} \int_{-\infty}^{\infty} d\omega' S_{\bar{\xi}}(y, \omega') e^{i\omega' \epsilon^{-1} \tau}, \quad (\text{B.37})$$

$$S_\zeta(y, \omega) = \int_{-\infty}^{\infty} d\tau \langle \zeta(y, t) \zeta(y, t + \tau) \rangle e^{-i\omega \tau}, \quad (\text{B.38})$$

$$= \frac{1}{2\pi\epsilon} \int_{-\infty}^{\infty} \int_{-\infty}^{\infty} d\omega' d\tau S_{\bar{\xi}}(y, \omega') e^{i(\epsilon^{-1} \omega' - \omega) \tau}, \quad (\text{B.39})$$

$$= \int_{-\infty}^{\infty} d\omega' S_{\bar{\xi}}(y, \omega') \delta(\omega' - \epsilon\omega), \quad (\text{B.40})$$

$$S_\zeta(y, \omega) = S_{\bar{\xi}}(y, \epsilon\omega). \quad (\text{B.41})$$

Thus the spectrum of  $\zeta$  is the stretched spectrum of  $\bar{\xi}$ . It is similar for  $\eta$ . In this way, we keep the spectral strength of the noise processes at a unit level, and let the coefficients multiplying these processes capture their scale. Accordingly, the process  $\eta$  becomes  $\epsilon^{1/2} \hat{\eta}$  with the scaling of time, and is thus deemed small in comparison to the other terms. We therefore drop  $\hat{\eta}$ .

The resulting averaged equations are

$$\frac{dy_i}{d\tau} = \bar{f}_i(y) + \bar{d}_i(y) + \zeta_i(y, \tau) + \mathcal{O}(\epsilon^{1/2}), \quad (\text{B.42})$$

where  $\bar{f} + \bar{d}$  are the deterministic parts of the approximate system, defined in equations (B.26) and (B.31), and  $\zeta$  is a non-Markovian stochastic process, for which the relevant equations are (B.12), (B.15), (B.35), and (B.41).

Since our coordinate transformation remains well ordered, and the neglected terms are small, a solution of (B.42) should remain close to our original system, (B.1), for some time until the neglected terms in  $\dot{y}$  build up. This time is expected to be  $\mathcal{O}(\epsilon^{-1/2})$ . Moreover, again since the coordinate transformation is well ordered, a stationary distribution of (B.42) is expected to be  $\mathcal{O}(\epsilon^{1/2})$  close to a stationary distribution of (B.1).

## B.5 Approximation by a Markov Process

Now the averaged equation (B.42) contains a non-Markovian process,  $\zeta$ , and so  $y$  is also non-Markovian. However, in some cases we may be able to approximate  $y$  as Markovian. If we suppose the cut-off frequency of the filter  $H(\omega)$  used to generate equation (B.42) is given by  $\omega_C$ , then  $\zeta$  might be uncorrelated over times  $\Delta \gg 2\pi\epsilon/\omega_C$ . For example, suppose that  $R(\omega)$  is flat around the frequencies  $\Omega_n$ , so that  $\zeta$  is a band-limited white noise. In this case its autocorrelation is given by

$$\langle \zeta_i(\tau) \zeta_j(\tau + \Delta) \rangle \propto \frac{\omega_C}{\epsilon\pi} \text{sinc} \left( \frac{\omega_C \Delta}{\epsilon} \right). \quad (\text{B.43})$$

Since  $\epsilon$  is small, this is a sharp delta-like function which goes approximately to zero for times of  $\mathcal{O}(\epsilon^{1/2})$ , over which the system state  $y$  has changed very little. We can therefore approximate  $y$  as a Markov process. We can describe this Markov process by its Kramers-Moyal coefficients. These coefficients are the moments of an infinitesimal



step of the process defined for a process  $z(t)$  as

$$\mathcal{D}^{(n)} = \lim_{\tau \rightarrow 0} \frac{1}{n! \tau} \langle (z(t + \tau) - z(t))^n \rangle \Big|_{z(t)=z}. \quad (\text{B.44})$$

In this section we will calculate the first two coefficients. These are all that is required for a Gaussian noise. For a non-Gaussian noise all coefficients are required for a complete description. However, it may be that higher-order coefficients are higher-order in  $\epsilon$ . This suggests that in the limit of small  $\epsilon$ , the noise may become Gaussian as well as white, which in turn suggests a type of central limit result. This can be viewed in a discrete sense, noting that for very small  $\epsilon$ , each step in coordinate results from the sum of many noise pulses, and the central limit theorem says such a sum should have a Gaussian distribution.

Returning to our calculation, in our approximation of  $y$  as Markovian, we cannot take the limit to zero as was done in equation (B.44), but rather we must take it to a small time of  $\mathcal{O}(\epsilon^{1/2})$ . Thus, to approximate  $\mathcal{D}^{(n)}$ , we must first calculate  $y(\tau + \epsilon^{1/2}\Delta) - y(\tau)$  given  $y(\tau) = y^{(0)}$ . We do this by the method of successive integration. We first integrate equation (B.42)

$$y_i(\tau + \epsilon^{1/2}\Delta) - y_i^{(0)} = \int_{\tau}^{\tau + \epsilon^{1/2}\Delta} \left( \bar{f}_i(y(t')) + \bar{d}_i(y(t')) + \zeta_i(y(t'), t') \right) dt', \quad (\text{B.45})$$

and then expand the integrand in a Taylor series in  $y$  about  $y^{(0)}$ . For example, for  $\bar{f}$ ,

$$\bar{f}_i(y(t')) \approx \bar{f}_i(y^{(0)}) + \frac{\partial \bar{f}_i(y^{(0)})}{\partial y_j} (y_j(t') - y_j^{(0)}), \quad (\text{B.46})$$

and similarly for the other terms. We then insert expression (B.45) into equation

(B.46) and repeat the Taylor series expansion. This process yields

$$\begin{aligned}
y_i(\tau + \epsilon^{1/2}\Delta) - y_i^{(0)} &= \epsilon^{1/2}\Delta \left( \bar{f}_i(y^{(0)}) + \bar{d}_i(y^{(0)}) \right) + \int_{\tau}^{\tau + \epsilon^{1/2}\Delta} \zeta_i(y^{(0)}, t') dt' \\
&+ \int_{\tau}^{\tau + \epsilon^{1/2}\Delta} dt' \int_{\tau}^{t'} dt'' \frac{\partial \zeta_i(y^{(0)}, t')}{\partial y_j} \zeta_j(y^{(0)}, t'') + \mathcal{O}(\epsilon). \quad (\text{B.47})
\end{aligned}$$

The first Kramers-Moyal coefficient, the drift coefficient is thus approximated by

$$\mathcal{D}_i^{(1)} \approx \frac{1}{\epsilon^{1/2}\Delta} \langle y_i(\tau + \epsilon^{1/2}\Delta) - y_i(\tau) \rangle \Big|_{y(\tau)=y} \quad (\text{B.48})$$

$$\begin{aligned}
&= \bar{f}_i(y) + \bar{d}_i(y) + \sum_n \frac{\partial G_{ij}^{(-n)}}{\partial y_k} G_{k\ell}^{(n)} \int_{-\infty}^{\infty} d\omega R_{\ell j}(\epsilon\omega + \Omega_n) H(\epsilon\omega) \quad (\text{B.49}) \\
&\quad \times \frac{1 + i\epsilon^{1/2}\Delta\omega - e^{i\epsilon^{1/2}\Delta\omega}}{2\pi\epsilon^{1/2}\Delta\omega^2}.
\end{aligned}$$

Since we asserted that  $R(\omega)$  is approximately constant around the frequencies  $\Omega_n$ , we have

$$\begin{aligned}
\mathcal{D}_i^{(1)} &\approx \bar{f}_i(y) + \bar{d}_i(y) + \sum_n \frac{\partial G_{ij}^{(-n)}}{\partial y_k} G_{k\ell}^{(n)} R_{\ell j}(\Omega_n) \\
&\quad \times \int_{-\omega_c/\epsilon}^{\omega_c/\epsilon} d\omega \frac{1 + i\epsilon^{1/2}\Delta\omega - e^{i\epsilon^{1/2}\Delta\omega}}{2\pi\epsilon^{1/2}\Delta\omega^2}. \quad (\text{B.50})
\end{aligned}$$

Moreover, at the limits of integration, the integrand in equation (B.50) is  $\mathcal{O}(\epsilon^{3/2})$ .

We therefore extend the limits to  $\pm\infty$  and the value of the integration is  $1/2$ . Thus, we find

$$\mathcal{D}_i^{(1)} \approx \bar{f}_i(y) + \bar{d}_i(y) + \frac{1}{2} \sum_n \frac{\partial G_{ij}^{(-n)}}{\partial y_k} G_{k\ell}^{(n)} R_{\ell j}(\Omega_n). \quad (\text{B.51})$$

The second Kramers-Moyal coefficient is approximated by

$$\mathcal{D}_{ij}^{(2)} \approx \frac{1}{2\epsilon^{1/2}\Delta} \left\langle (y_i(\tau + \epsilon^{1/2}\Delta) - y_i(\tau))(y_j(\tau + \epsilon^{1/2}\Delta) - y_j(\tau)) \right\rangle \bigg|_{y(\tau)=y} \quad (\text{B.52})$$

$$\approx \frac{1}{2} \sum_n G_{ik}^{(n)} G_{j\ell}^{(-n)} R_{k\ell}(\Omega_n) \int_{-\omega_c\epsilon}^{\omega_c/\epsilon} \frac{1 - \cos(\epsilon^{1/2}\Delta\omega)}{\pi\epsilon^{1/2}\Delta\omega^2} d\omega. \quad (\text{B.53})$$

Again, we let the integration limits go to  $\pm\infty$  and the integration evaluates to 1, resulting in

$$\mathcal{D}_{ij}^{(2)} \approx \frac{1}{2} \sum_n G_{ik}^{(n)} G_{j\ell}^{(-n)} R_{k\ell}(\Omega_n). \quad (\text{B.54})$$

Note that when the noise in the original equation is white, then  $\bar{d} = 0$  and the drift and diffusion coefficients are simply those belonging to the original equation averaged over one period. Other cases are significantly more challenging.

# Appendix C

## Derivation of Equation (2.65)

In this appendix we derive equation (2.65), the stochastic normal form for the pitchfork bifurcation arising from parametric resonance. Our main source for this development is reference [62]. We start with the equation for a parametrically forced resonator,

$$\ddot{z} + 2\Gamma\dot{z} + \omega_0^2(1 + \delta_1 + \delta_1 \cos 2\omega t)z + \gamma(1 + \delta_3 + \delta_3 \cos 2\omega t)z^3 = \xi(t), \quad (\text{C.1})$$

$$\langle \xi(t) \rangle = 0, \quad \langle \xi(t)\xi(t') \rangle = 2D\delta(t - t'). \quad (\text{C.2})$$

In principle this equation could include all terms of the form  $(\delta_n + \delta_n \cos 2\omega t)x^n$  for  $n = 0, 1, 2, 3$ , but only the  $n = 1, 3$  terms survive the averaging, and so only these are included here. We first transform this equation into a form amenable for stochastic averaging. We begin by rescaling time as

$$\tau = \Gamma t, \quad (\text{C.3})$$

$$\langle \xi(\tau)\xi(\tau') \rangle = 2D\Gamma\delta(\tau - \tau'), \quad (\text{C.4})$$

which gives the rescaled equation

$$\begin{aligned} \Gamma^2 z'' + 2\Gamma^2 z' + \omega_o^2(1 + \delta_1 + \delta_1 \cos(2\omega\tau/\Gamma))z \\ + \gamma(1 + \delta_3 + \delta_3 \cos(2\omega\tau/\Gamma))z^3 = \xi(\tau), \end{aligned} \quad (\text{C.5})$$

where  $(\cdot)' = d(\cdot)/d\tau$ . Next, the system is transformed into scaled Cartesian coordinates  $(a, b)$  that rotate with  $\omega/\Gamma$ , defined via

$$z = \sqrt{\frac{8\omega\Gamma}{3|\gamma|}}(a \cos(\omega/\Gamma\tau) + b \sin(\omega/\Gamma\tau)), \quad (\text{C.6})$$

$$z' = \sqrt{\frac{8\omega\Gamma}{3|\gamma|}}(-a\omega/\Gamma \sin(\omega/\Gamma\tau) + b\omega/\Gamma \cos(\omega/\Gamma\tau)). \quad (\text{C.7})$$

Applying this substitution and solving for  $a'$  and  $b'$  gives

$$\begin{aligned} \begin{bmatrix} a' \\ b' \end{bmatrix} = \sqrt{\frac{3|\gamma|}{8\omega^3\Gamma^3}} \begin{bmatrix} -\sin(\omega/\Gamma\tau) \\ \cos(\omega/\Gamma\tau) \end{bmatrix} \left( -2\Gamma^2 z' + \omega^2 z - \omega_o^2(1 + \delta_1 \right. \\ \left. + \delta_1 \cos(2\omega\tau/\Gamma))z - \gamma(1 + \delta_3 + \delta_3 \cos(2\omega\tau/\Gamma))z^3 + \xi(\tau) \right). \end{aligned} \quad (\text{C.8})$$

In appendix B we showed that the slow time drift and diffusion coefficients for a system like (C.8) can be approximated by their time-average. The averaged drift and

diffusion coefficients are

$$\bar{\mathcal{D}}_1^{(1)} = -a - \left( \frac{\omega^2 - \omega_o^2 - \delta_1 \omega_o^2}{2\omega\Gamma} + \frac{\delta_1 \omega_o^2}{4\omega\Gamma} \right) b + \text{sgn}(\gamma) b (a^2 + b^2) \quad (\text{C.9})$$

$$+ \text{sgn}(\gamma) \delta_3 b \left( a^2 + \frac{1}{3} b^2 \right),$$

$$\bar{\mathcal{D}}_2^{(1)} = -b + \left( \frac{\omega^2 - \omega_o^2 - \delta_1 \omega_o^2}{2\omega\Gamma} - \frac{\delta_1 \omega_o^2}{4\omega\Gamma} \right) a - \text{sgn}(\gamma) a (a^2 + b^2) \quad (\text{C.10})$$

$$- \text{sgn}(\gamma) \delta_3 a \left( \frac{5}{3} a^2 + b^2 \right),$$

$$\bar{\mathcal{D}}_{11}^{(2)} = \frac{3D|\gamma|}{16\omega^3\Gamma^2}, \quad (\text{C.11})$$

$$\bar{\mathcal{D}}_{12}^{(2)} = 0, \quad (\text{C.12})$$

$$\bar{\mathcal{D}}_{21}^{(2)} = 0, \quad (\text{C.13})$$

$$\bar{\mathcal{D}}_{22}^{(2)} = \frac{3D|\gamma|}{16\omega^3\Gamma^2}. \quad (\text{C.14})$$

To simplify the expressions for the drift coefficient, we define the nondimensional parameters

$$\alpha = \frac{\omega^2 - \omega_o^2(1 + \delta_1)}{2\omega\Gamma}, \quad (\text{C.15})$$

$$\beta = \frac{\delta_1 \omega_o^2}{4\omega\Gamma}. \quad (\text{C.16})$$

The parameter  $\alpha$  is the renormalized detuning, accounting for the shift in the resonant frequency from  $\delta_1$ .  $\beta$  is the effective parametric pump strength and  $|\beta| = 1$  is the minimum parametric pump required to induce parametric resonance. For the next several steps it is convenient to work with the Langevin description of the system. We therefore write a Langevin system that gives the drift and diffusion coefficients above. In addition, we now use the overdot to denote derivatives w.r.t.  $\tau$ . The

averaged Langevin equations are

$$\dot{a} = -a - (\alpha + \beta)b + \text{sgn}(\gamma)b(a^2 + b^2) + \text{sgn}(\gamma)\delta_3 b \left( a^2 + \frac{1}{3}b^2 \right) + \xi_1(\tau), \quad (\text{C.17})$$

$$\dot{b} = -b + (\alpha - \beta)a - \text{sgn}(\gamma)a(a^2 + b^2) - \text{sgn}(\gamma)\delta_3 a \left( \frac{5}{3}a^2 + b^2 \right) + \xi_2(\tau), \quad (\text{C.18})$$

$$\langle \xi_i \rangle = 0, \quad \langle \xi_i(\tau)\xi_j(\tau') \rangle = \frac{3D|\gamma|}{8\omega^3\Gamma^2} \delta_{ij} \delta(\tau - \tau'), \quad (\text{C.19})$$

which describe the evolution of  $(a, b)$  in convenient form. Next, we reduce the dimension of this system by restricting it to the slow invariant manifold that exists near the bifurcation point. We begin by applying a linear change of coordinates to the eigendirections. The linear deterministic part of this system is

$$\dot{a} = -a - (\alpha + \beta)b, \quad (\text{C.20})$$

$$\dot{b} = (\alpha - \beta)a - b, \quad (\text{C.21})$$

which has eigenvalues  $\lambda_{\pm} = -1 \pm \sqrt{\beta^2 - \alpha^2}$  and eigenvectors

$$v_+ = \left( -\frac{1}{\beta} \sqrt{\frac{\beta(\beta + \alpha)}{2}}, \sqrt{\frac{\beta - \alpha}{2\beta}} \right), \quad (\text{C.22})$$

$$v_- = \left( \frac{1}{\beta} \sqrt{\frac{\beta(\beta + \alpha)}{2}}, \sqrt{\frac{\beta - \alpha}{2\beta}} \right). \quad (\text{C.23})$$

This motivates the linear coordinate transformation,

$$u = \frac{\beta}{\sqrt{2\beta(\beta + \alpha)}}a + \sqrt{\frac{\beta}{2(\beta - \alpha)}}b, \quad a = \frac{1}{\beta} \sqrt{\frac{\beta(\beta + \alpha)}{2}}(u - v), \quad (\text{C.24})$$

$$v = -\frac{\beta}{\sqrt{2\beta(\beta + \alpha)}}a + \sqrt{\frac{\beta}{2(\beta - \alpha)}}b, \quad b = \sqrt{\frac{\beta - \alpha}{2\beta}}(u + v), \quad (\text{C.25})$$

that will render the linear part of the equation in normal form. The full equations in these coordinates are given by

$$\dot{u} = (-1 - \sqrt{\beta^2 - \alpha^2})u - \frac{\text{sgn}(\gamma)}{3\beta\sqrt{\beta^2 - \alpha^2}} \left( (3\alpha\beta + \delta_3(\alpha^2 + \beta^2 + 3\alpha\beta))u^3 \right. \quad (\text{C.26})$$

$$\begin{aligned} & - (6\alpha\beta\delta_3 + 6\alpha^2(1 + \delta_3) + 3\beta^2(1 + \delta_3))u^2v \\ & + (3\alpha^2\delta_3 + 3\beta^2\delta_3 + 9\alpha\beta(1 + \delta_3))uv^2 \\ & \left. - \beta(2\alpha\delta_3 + 3\beta(1 + \delta_3))v^3 \right) + \frac{\beta}{\sqrt{2\beta(\beta + \alpha)}}\xi_1(\tau) + \sqrt{\frac{\beta}{2(\beta - \alpha)}}\xi_2(\tau), \end{aligned}$$

$$\dot{v} = (-1 + \sqrt{\beta^2 - \alpha^2})v - \frac{\text{sgn}(\gamma)}{3\beta\sqrt{\beta^2 - \alpha^2}} \left( \beta(2\alpha\delta_3 + 3\beta(1 + \delta_3))u^3 \right. \quad (\text{C.27})$$

$$\begin{aligned} & - (3\alpha^2\delta_3 + 3\beta^2\delta_3 + 9\alpha\beta(1 + \delta_3))u^2v \\ & + (6\alpha\beta\delta_3 + 6\alpha^2(1 + \delta_3) + 3\beta^2(1 + \delta_3))uv^2 \\ & \left. - (3\alpha\beta + \delta_3(\alpha^2 + \beta^2 + 3\alpha\beta))v^3 \right) - \frac{\beta}{\sqrt{2\beta(\beta + \alpha)}}\xi_1(\tau) + \sqrt{\frac{\beta}{2(\beta - \alpha)}}\xi_2(\tau). \end{aligned}$$

As is typical, the linear terms are uncoupled, but at the expensive of more complicated nonlinear terms. We will need the deterministic center manifold  $u = h(v)$ , determined from the equation  $\dot{u}|_h = \frac{\partial h}{\partial v}\dot{v}|_h$  with  $\xi_1$  and  $\xi_2$  set to zero. This gives, to leading order,

$$u = \frac{\text{sgn}(\gamma)(3\beta + \delta_3(2\alpha + 3\beta))}{12(\beta^2 - \alpha^2) - 6\sqrt{\beta^2 - \alpha^2}}v^3. \quad (\text{C.28})$$



Next we write the Fokker-Planck equation for the system in  $(u, v)$  coordinates. For ease of notation, let

$$\dot{u} = F_1(u, v) + \hat{g}_1 \zeta_1(\tau) + \hat{g}_2 \zeta_2(\tau), \quad (\text{C.29})$$

$$\dot{v} = F_2(u, v) - \hat{g}_1 \zeta_1(\tau) + \hat{g}_2 \zeta_2(\tau), \quad (\text{C.30})$$

$$\hat{g}_1 = \beta \sqrt{\frac{3D|\gamma|}{32\omega^3\Gamma^2} \frac{1}{\beta(\beta + \alpha)}}, \quad (\text{C.31})$$

$$\hat{g}_2 = \sqrt{\frac{3D|\gamma|}{32\omega^3\Gamma^2} \frac{\beta}{\beta - \alpha}}, \quad (\text{C.32})$$

$$\langle \zeta_1(\tau) \rangle = \langle \zeta_2(\tau) \rangle = \langle \zeta_1(\tau) \zeta_2(\tau') \rangle = 0, \quad (\text{C.33})$$

$$\langle \zeta_1(\tau) \zeta_1(\tau') \rangle = \langle \zeta_2(\tau) \zeta_2(\tau') \rangle = 2\delta(\tau - \tau'), \quad (\text{C.34})$$

and the  $F_i$ 's are the deterministic part of the equations. Moreover, by defining

$$g_1 = \hat{g}_1^2 + \hat{g}_2^2, \quad (\text{C.35})$$

$$g_2 = 2(\hat{g}_2^2 - \hat{g}_1^2). \quad (\text{C.36})$$

the Fokker-Planck equation for the probability distribution of  $u$  and  $v$ , denoted as  $\mathcal{P}$ , is given by

$$\frac{\partial \mathcal{P}}{\partial \tau} = -\frac{\partial}{\partial u}(F_1 \mathcal{P}) - \frac{\partial}{\partial v}(F_2 \mathcal{P}) + g_1 \frac{\partial^2 \mathcal{P}}{\partial u^2} + g_2 \frac{\partial^2 \mathcal{P}}{\partial u \partial v} + g_1 \frac{\partial^2 \mathcal{P}}{\partial v^2}. \quad (\text{C.37})$$

To restrict the system to be near the suspended center manifold, we assume that  $\mathcal{P}$  is confined to a narrow strip around  $u = h(v)$ , specifically,  $\mathcal{P}$  is taken to be a narrow tube distribution with mean along the deterministic center manifold and Gaussian

cross section, as follows,

$$\mathcal{P} = p(u, \tau|v)P(v, \tau), \quad (\text{C.38})$$

$$p(u, \tau|v) = \sqrt{\frac{\Lambda(v)}{\pi}} \exp\left[-\Lambda(v)[u - h(v)]^2\right]. \quad (\text{C.39})$$

To formulate the FP equation for  $P$  we will need the partial derivatives of  $p(u, \tau|v)$  up to second order. These are

$$\frac{\partial p}{\partial u} = -2\Lambda(u - h)p, \quad (\text{C.40})$$

$$\frac{\partial p}{\partial v} = \frac{\Lambda'}{2\Lambda}p + (u - h)p(2\Lambda h' - \Lambda'(u - h)), \quad (\text{C.41})$$

$$\frac{\partial^2 p}{\partial u^2} = -2\Lambda p + 4\Lambda^2(u - h)^2p, \quad (\text{C.42})$$

$$\frac{\partial^2 p}{\partial u \partial v} = 2\Lambda h'p + (u - h)p\left[2\Lambda\Lambda'(u - h)^2 - 3\Lambda' - 4\Lambda^2h'(u - h)\right], \quad (\text{C.43})$$

$$\begin{aligned} \frac{\partial^2 p}{\partial v^2} = & -2\Lambda h'^2p - \frac{\Lambda'^2}{4\Lambda^2}p + \frac{\Lambda''}{2\Lambda}p + (u - h)p\left\{6\Lambda'h' - (u - h)\frac{\Lambda'^2}{\Lambda} \right. \\ & \left. + (u - h)[2\Lambda h' - (u - h)\Lambda']^2 + 2\Lambda h'' - (u - h)\Lambda''\right\}. \end{aligned} \quad (\text{C.44})$$

Substitution of the form of  $\mathcal{P}$  given in equation (C.38) into the Fokker-Planck equation gives

$$\begin{aligned} p\frac{\partial P}{\partial \tau} = & -p\frac{\partial}{\partial u}(F_1P) - F_1P\frac{\partial p}{\partial u} - p\frac{\partial}{\partial v}(F_2P) - F_2P\frac{\partial p}{\partial v} + \\ & \left(p\frac{\partial^2 P}{\partial u^2} + 2\frac{\partial p}{\partial u}\frac{\partial P}{\partial u} + P\frac{\partial^2 p}{\partial u^2}\right)g_1 + \left(p\frac{\partial^2 P}{\partial v^2} + 2\frac{\partial p}{\partial v}\frac{\partial P}{\partial v} + P\frac{\partial^2 p}{\partial v^2}\right)g_1 \\ & + \left(p\frac{\partial^2 P}{\partial u \partial v} + \frac{\partial p}{\partial u}\frac{\partial P}{\partial v} + \frac{\partial p}{\partial v}\frac{\partial P}{\partial u} + P\frac{\partial^2 p}{\partial u \partial v}\right)g_2. \end{aligned} \quad (\text{C.45})$$

To get an equation for  $P(v, \tau)$ , we integrate this equation over  $u$ , treating  $p(u, \tau|v)$  like a  $\delta(u - h(v))$ . This yields

$$\begin{aligned} \frac{\partial P}{\partial \tau} = & \left[ -P \frac{\partial F_1}{\partial u} - \frac{\partial}{\partial v}(F_2 P) - \frac{\Lambda'}{2\Lambda} F_2 P - 2\Lambda g_1 P + g_1 \frac{\partial^2 P}{\partial v^2} + \frac{\Lambda'}{\Lambda} g_1 \frac{\partial P}{\partial v} \right. \\ & \left. - 2\Lambda h'^2 g_1 P - \frac{\Lambda'^2}{4\Lambda^2} g_1 P + \frac{\Lambda''}{2\Lambda} g_1 P + 2\Lambda h' g_2 P \right]_{u=h}. \end{aligned} \quad (\text{C.46})$$

Next, we assume  $\Lambda = \Lambda_0 + \Lambda_1 v + \Lambda_2 v^2$ , and use scaling arguments to greatly simplify this equation. For notational ease, we also express  $F_1$  and  $F_2$  as

$$F_1 = a_1 u + b_1 u^3 + c_1 u^2 v + d_1 u v^2 + e_1 v^3, \quad (\text{C.47})$$

$$F_2 = a_2 v + b_2 u^3 + c_2 u^2 v + d_2 u v^2 + e_2 v^3. \quad (\text{C.48})$$

The scaling employed is motivated by proximity to the bifurcation point and weak noise, and is given by

$$v \rightarrow \epsilon v, \quad (\text{C.49})$$

$$a_2 \rightarrow \epsilon^2 a_2, \quad (\text{C.50})$$

$$g_i \rightarrow \epsilon^4 g_i, \quad (\text{C.51})$$

$$\Lambda_i \rightarrow \epsilon^{-4} \Lambda_i. \quad (\text{C.52})$$

Keeping terms up to  $\epsilon^2$  gives

$$\begin{aligned} \frac{\partial P}{\partial \tau} = & \epsilon^2 \left\{ -\frac{\partial}{\partial v}[(a_2 v + e_2 v^3)P] + g_1 \frac{\partial^2 P}{\partial v^2} \right\} + P \left( -2\Lambda_0 g_1 - a_1 - 2\epsilon \Lambda_1 g_1 v \right. \\ & \left. + \epsilon^2 (-d_1 v^2 + 6\Lambda_0 a_3 g_2 v^2 - 2\Lambda_2 g_1 v^2) \right). \end{aligned} \quad (\text{C.53})$$

To ensure that the  $P$  equation represents a conservation of probability along the center manifold, it is necessary that all terms proportional to  $P$  vanish. Accordingly,

we take

$$\Lambda_0 = -\frac{a_1}{2g_1}, \quad (\text{C.54})$$

$$\Lambda_1 = 0, \quad (\text{C.55})$$

$$\Lambda_2 = \frac{6\Lambda_0 a_3 g_2}{2g_1} - \frac{d_1}{2g_1}. \quad (\text{C.56})$$

The resulting Fokker-Planck equation is given by

$$\frac{\partial P}{\partial \tau} = -\frac{\partial}{\partial v} \left[ \left( a_2 v + e_2 v^3 \right) P \right] + g_1 \frac{\partial^2 P}{\partial v^2}, \quad (\text{C.57})$$

which corresponds with the Langevin equation

$$\dot{v} = a_2 v + e_2 v^3 + \sqrt{g_1} \xi(\tau). \quad (\text{C.58})$$

We scale this according to

$$q = \frac{\sqrt{e_2}}{2} v, \quad (\text{C.59})$$

resulting in

$$\dot{q} = a_2 q + 4q^3 + \sqrt{\frac{e_2 g_1}{4}} \xi(\tau). \quad (\text{C.60})$$

Substitution of the values of  $a_2$ ,  $e_2$ , and  $g_1$  into the above gives the final normal form, expressed as

$$\dot{q} = (-1 + \sqrt{\beta^2 - \alpha^2})q + 4q^3 + \sqrt{\frac{D\gamma}{64\omega^3\Gamma^2} \frac{\alpha\beta^2(3+2\delta_3)+\delta_3\beta(\beta+\alpha)^2}{(\beta^2-\alpha^2)^{3/2}}} \xi(\tau), \quad (\text{C.61})$$

$$\langle \xi \rangle = 0, \quad \langle \xi(\tau) \xi(\tau') \rangle = 2\delta(\tau - \tau'). \quad (\text{C.62})$$

## Bibliography

# BIBLIOGRAPHY

- [1] Milton Abramowitz and Irene A. Stegun. *Handbook of Mathematical Functions: with Formulas, Graphs, and Mathematical Tables*. Dover, 1965.
- [2] J.S. Aldridge and A.N. Cleland. Noise-enabled precise measurements of a duffing nanomechanical resonator. *Phys Rev Lett*, 94:156403, 2005.
- [3] D. Allan, H. Hellwig, P. Kartaschoff, J. Vanier, J. Vig, G.M.R. Winkler, and N.F. Yannoni. Standard terminology for fundamental frequency and time metrology. In *Frequency Control Symposium, 1988., Proceedings of the 42nd Annual*, pages 419–425, June 1988.
- [4] Vinay Ambegaokar and B. I. Halperin. Voltage due to thermal noise in the dc josephson effect. *Phys Rev Lett*, 22:1364–1366, 1969.
- [5] A. D. Armour. Current noise of a single-electron transistor coupled to a nanomechanical resonator. *Phys. Rev. B*, 70:165315, 2004.
- [6] A. D. Armour, M. P. Blencowe, and Y. Zhang. Classical dynamics of a nanomechanical resonator coupled to a single-electron transistor. *Phys Rev B*, 69:125313, 2004.
- [7] D. A. Bagrets and Yu. V. Nazarov. Full counting statistics of charge transfer in coulomb blockade systems. *Phys. Rev. B*, 67:085316, 2003.
- [8] Nils Berglund and Barbara Gentz. Pathwise description of dynamic pitchfork bifurcations with additive noise. *Probability Theory and Related Fields*, 122:341–388, 2002.
- [9] Nils Berglund and Barbara Gentz. *Noise-Induced Phenomena in Slow-Fast Dynamical Systems: A Sample-Paths Approach*. Springer, 2006.
- [10] Lora Billings, M. I. Dykman, Marie McCrary, and Ira B. Schwartz. Switching barrier scaling near bifurcation points for non-gaussian noise. *Phys. Rev. Lett.*, 104:140601, September 2010.

- [11] Lora Billings, Mark I. Dykman, and Ira B. Schwartz. Thermally activated switching in the presence of non-gaussian noise. *Phys. Rev. E.*, 78:051122, 2008.
- [12] Lora Billings, Ira B. Schwartz, Marie McCrary, A. N. Korotkov, and M. I. Dykman. Switching exponent scaling near bifurcation points for non-gaussian noise. *Phys. Rev. Lett.*, 104:140601, 2010.
- [13] G. Binnig, Ch. Gerber, E. Stoll, T. R. Albrecht, and C. F. Quate. Atomic resolution with atomic force microscope. *Europhysics Letters*, 3:1281–1286, 1987.
- [14] G. Broggi, A. Colombo, L. A. Lugiato, and Paul Mandel. Influence of white noise on delayed bifurcations. *Physical Review A*, 33:3635–3637, 1986.
- [15] Eyal Buks and Bernard Yurke. Mass detection with a nonlinear nanomechanical resonator. *Physical Review E*, 74:046619, 2006.
- [16] C. B. Burgner, K. L. Turner, N. J. Miller, and S. W. Shaw. Parameter sweep strategies for sensing using bifurcations in mems. In *Proceedings of the 13th Hilton Head Solid State Sensors and Actuators Conference, June 6-10, SC, USA*, 2010.
- [17] Christopher Burgner, William Snyders, and Kimberly Turner. Control of mems on the edge of instability. In *IEEE Transducers, Beijing, China, June*, 2011.
- [18] Paul F. Byrd and Morris D. Friedman. *Handbook of Elliptic Integrals for Engineers and Physicists*. Springer-Verlag / Berlin, 1954.
- [19] J. Carr. *Applications of Centre Manifold Theory*. Springer; 1 edition, 1981.
- [20] H. B. Chan, M. I. Dykman, and C. Stambaugh. Paths of fluctuation induced switching. *Phys Rev Lett*, 100:130602, 2008.
- [21] H. B. Chan, M. I. Dykman, and C. Stambaugh. Switching-path distribution in multidimensional systems. *Physical Review E*, 78:051109, 2008.
- [22] Shui-Nee Chow and Hao-Min Zhou. An analysis of phase noise and fokker-planck equations. *J. Differential Equations*, 234:391–411, 2007.
- [23] A. N. Cleland and M. R. Geller. Superconducting qubit storage and entanglement with nanomechanical resonators. *Phys Rev Lett*, 93:070501, 2004.
- [24] A. N. Cleland and M. R. Geller. Mechancial quantum resonators. *Electronic Properties of Novel Nanostructures: XIX International Winter-school/Euroconference on Electronic Properties of Novel Materials. AIP Conference Proceedings*, 786:396–400, 2005.
- [25] A. N. Cleland and M. L. Roukes. Noise processes in a nanomechanical resonators. *Journal of Applied Physics*, 92:2758–2769, 2002.

- [26] Andrew N. Cleland. *Foundations of Nanomechanics*. Springer-Verlag, 2003.
- [27] Alper Demir, Amit Mehrotra, and Jaijeet Roychowdhury. Phase noise in oscillators: A unifying theory and numerical methods for characterization. *IEEE Transactions on circuits and systems - I: Fundamental Theory and Applications*, 47:655–674, 2000.
- [28] Michel H. Devoret, Daniel Esteve, John M. Martinis, Andrew Cleland, and John Clarke. Resonant activation of a brownian particle out of a potential well: Microwave-enhanced escape from the zero-voltage state of a josephson junction. *Phys. Rev. B.*, 36(1):58–73, July 1987.
- [29] O. K. Dudko, A. E. Filippov, J. Klafter, and M. Urbakh. Beyond the conventional description of dynamic force spectroscopy of adhesion bonds. *PNAS September 30*, 100:11378–11381, 2003.
- [30] M. Dykman. Quantum measurements with dynamically bistable systems. In Visarath In, Patrick Longhini, and Antonio Palacios, editors, *Applications of Nonlinear Dynamics*, volume 35 of *Understanding Complex Systems*, pages 367–378. Springer Berlin / Heidelberg, 2009.
- [31] M. I. Dykman. Poisson-noise induced escape from a metastable state. *Phys. Rev. E*, 81:051124, 2010. (in press).
- [32] M. I. Dykman, B. Golding, L. I. McCann, V. N. Smelyanskiy, D. G. Luchinsky, R. Mannella, and P. V. E. McClintock. Activated escape of periodically driven systems. *Chaos*, 11:587–594, 2001.
- [33] M. I. Dykman, M. Khasin, J. Portman, and S.W. Shaw. Spectrum of an oscillator with jumping frequency and the interference of partial susceptibilities. *Phys. Rev. Lett*, 105:230601, 2010.
- [34] M. I. Dykman and M. A. Krivoglaz. Classical theory of nonlinear oscillators interacting with a medium. *Phys. Stat. Sol. (b)*, 48:497–512, 1971.
- [35] M. I. Dykman and M. A. Krivoglaz. Theory of fluctuational transistions between stable states of a nonlinear oscillator. *Sov. Phys. JETP*, 50:30–37, 1979.
- [36] M. I. Dykman and M. A. Krivoglaz. Theory of nonlinear oscillator interacting with a medium. *Sov. Sci. Rev. A Phys.*, 5:265–442, 1984.
- [37] M. I. Dykman, C. M. Maloney, V. N. Smelyanskiy, and M. Silverstein. Fluctuational phase-flip transitions in parametrically driven oscillators. *Phys Rev E*, 57:5202–5212, 1998.
- [38] M. I. Dykman, R. Mannella, P. V. E. McClintock, S. M. Soskin, and N. G. Stocks. Noise-induced narrowing of peaks in the power spectra of underdamped nonlinear oscillators. *Phys Rev A*, 42:7041–7049, 1990.



- [39] Albert Einstein. *Investigations on the theory of the Brownian Movement*. Dover Publications, 1956.
- [40] K. L. Ekinici, X. M. H. Huang, and M. L. Roukes. Ultrasensitive nanoelectromechanical mass detection. *App. Phys. Lett.*, 84:4469 – 4471, 2004.
- [41] K. L. Ekinici and M. L. Roukes. Nanoelectromechanical systems. *Review of Scientific Instruments*, 76:061101, 2005.
- [42] K. L. Ekinici, Y. T. Yang, and M. L. Roukes. Ultimate limits to inertial mass sensing based upon nanoelectromechanical systems. *Journal of Applied Physics*, 95:2682–2689, 2004.
- [43] Kilho Eom, Harold S. Park, Dae Sung Yoon, and Taeyun Kwon. Nanomechanical resonators and their applications in biological/chemical detection: Nanomechanics principles. *Physics Reports*, 503:115–163, 2011.
- [44] Mykhaylo Evstigneev. Statistics of forced thermally activated escape events out of a metastable state: Most probable escape force and escape-force moments. *Phys. Rev. E*, 78:011118, 2008.
- [45] X.L. Feng, C.J. White, A. Hajimiri, and M.L. Roukes. A self-sustaining ultrahigh-frequency nanoelectromechanical oscillator. *Nature Nanotechnology*, 3:342–346, 2008.
- [46] Richard P. Feynman and Albert R. Hibbs. *Quantum Mechanics and Path Integrals: Emended Edition (Dover Books on Physics)*. Dover Publications, 2010.
- [47] T. A. Fulton and L. N. Dunkleberger. Lifetime of the zero-voltage state in josephson tunnel junctions. *Phys Rev B*, 9:4760, 1974.
- [48] Anupam Garg. Escape-field distribution for escape from a metastable potential well subject to a steadily increasing bias field. *Phys. Rev. B*, 51(21):15592–15595, June 1995.
- [49] Cevat Gökçek. Tracking the resonance frequency of a series rlc circuit using a phase locked loop. *Control Applications, 2003. CCA 2003. Proceedings of 2003 IEEE Conference on*, 1:609 – 613, 2003.
- [50] Herbert Goldstein. *Classical Mechanics, Second Edition*. Addison-Wesley, 1980.
- [51] A. C. R. Grayson, R. S. Shawgo, A. M. Johnson, N. T. Flynn, Li Yawen, M. J. Cima, and R. Langer. A biomems review: Mems technology for physiologically integrated devices. *Proceedings of the IEEE*, 92:6–21, 2004.
- [52] J. Guckenheimer and P. Holmes. *Nonlinear Oscillations, Dynamical Systems, and Bifurcations of Vector Fields*. Springer-Verlag New York, 1983.

- [53] S. Gustavsson, R. Leturcq, B. Simović, R. Schleser, T. Ihn, P. Studerus, K. Ensslin, D. C. Driscoll, and A. C. Gossard. Counting statistics of single electron transport in a quantum dot. *Phys Rev Lett*, 96:076605, 2006.
- [54] Peter Hanggi. Escape from a metastable state. *Journal of Statistical Physics*, 42:105–148, 1986.
- [55] Tero T. Heikkilä, Pauli Virtanen, Göran Johansson, and Frank K. Wilhelm. Measuring non-gaussian fluctuations through incoherent cooper-pair current. *Phys. Rev. Lett.*, 93:247005, 2004.
- [56] B. Huard, H. Pothier, Norman O. Birge, D. Esteve, X. Waintal, and J. Ankerhold. Josephson junctions as detectors for non-gaussian noise. *Ann. Phys. (Leipzig)*, 16(10-11):736–750, 2007.
- [57] G. Hummer and A. Szabo. Kinetics from nonequilibrium single-molecule pulling experiments. *Biophysical Journal*, 85:5–15, 2003.
- [58] L. D. Jackel, W. W. Webb, J. E. Lukens, and S. S. Pei. Measurement of the probability distribution of thermally excited fluxoid quantum transitions in a superconducting ring closed by a josephson junction. *Phys Rev B*, 9:115, 1974.
- [59] Kalvis M. Jansons and G. D. Lythe. Stochastic calculus: Application to dynamic bifurcations and threshold crossings. *Journal of Statistical Physics*, 90:227–251, 1998.
- [60] N.G. Van Kampen. *Stochastic Processes in Physics and Chemistry*. Elsevier Academic Press, 2007.
- [61] Peter E. Kloeden and Eckhard Platen. *Numerical Solution of Stochastic Differential Equations*. Springer, 3rd edition, 1999.
- [62] E. Knobloch and K. A. Wiesenfeld. Bifurcations in fluctuating systems: The center-manifold approach. *J. of Stat. Phys.*, 33(3):611–637, 1983.
- [63] R. H. Koch, G. Grinstein, G. A. Keefe, Yu Lu, P. L. Trouilloud, and W. J. Gallagher. Thermally assisted magnetization reversal in submicron-sized magnetic thin films. *Phys Rev Lett*, 84:5419, 2000.
- [64] H. A. Kramers. Brownian motion in a field of force and the diffusion model of chemical reactions. *Physica VII*, 7(4):284–304, 1940.
- [65] I. N. Krivorotov, N. C. Emley, A. G. F. Garcia, J. C. Sankey, S. I. Kiselev, D. C. Ralph, and R. A. Buhrman. Temperature dependence of spin-transfer-induced switching of nanomagnets. *Phys. Rev. Lett.*, 93:166603, 2004.

- [66] Vijay Kumar, J. William Boley, Yushi Yang, Hendrik Ekowaluyo, Jacob K. Miller, George T.-C. Chiu, and Jeffery F. Rhoads. Bifurcation-based mass sensing using piezoelectrically actuated microcantilevers. *App. Phys. Lett.*, 98:1, 2011.
- [67] Juhani Kurkijärvi. Intrinsic fluctuations in a superconducting ring closed with a josephson junction. *Phys. Rev. B*, 6(3):832–835, August 1972.
- [68] M. D. LaHaye, J. Suh, P. M. Echternach, K. C. Schwab, and M. L. Roukes. Nanomechanical measurements of a superconducting qubit. *Nature*, 459:960–964, 2009.
- [69] L. D. Landau and E. M. Lifshitz. *Mechanics, Third Edition: Course of Theoretical Physics Volume 1*. Elsevier Academic Press, 2008.
- [70] Q. Le Masne, H. Pothier, Norman O. Birge, C. Urbina, and D. Esteve. Asymmetric noise probed with a josephson junction. *Phys. Rev. Lett.*, 102:067002, January 2009.
- [71] Sangwoo Lee, Sangjun Park, Jongpal Kim, Sangchul Lee, and Dong il (Dan) Cho. Surface/bulk micromachined single-crystalline-silicon micro-gyroscope. *Microelectromechanical Systems, Journal of*, 9:557–567, 2000.
- [72] Thomas H. Lee and Ali Hajimiri. Oscillator phase noise: A tutorial. *IEEE Journal of Solid-State Circuits*, 35:326–336, 2000.
- [73] R. Lifshitz and M. C. Cross. Nonlinear dynamics of nanomechanical and micromechanical resonators. In *Reviews of Nonlinear Dynamics and Complexity*. Wiley-VCH Verlag GmbH & Co. KGaA, Weinheim, Germany., 2009.
- [74] Ron Lifshitz and M. L. Roukes. Thermoelastic damping in micro- and nanomechanical systems. *Phys Rev B*, 61:5600–5609, 2000.
- [75] Chang Liu. *Foundations of MEMS*. Pearson Education, 2006.
- [76] A. Lupascu, S. Saito, T. Picot, P. C. De Groot, C. J. P. M. Harmans, and J. E. Mooij. Quantum non-demolition measurement of a superconducting two-level system. *nature physics*, 3:119–123, 2007.
- [77] I. Mahboob, C. Froitier, and H. Yamaguchi. A symmetry-breaking electromechanical detector. *App. Phys. Lett.*, 96:213103, 2010.
- [78] Francois Mallet, Florian R. Ong, Agustin Palacios-Laloy, Francois Nguyen, Patrice Bertet, Denis Vion, and Daniel Esteve. Single-shot qubit readout in circuit quantum electrodynamics. *Nature Physics*, 5:791–795, 2009.
- [79] C. Meunier and A. D. Verga. Noise and bifurcations. *Journal of Statistical Physics*, 50:345–375, 1988.

- [80] Jeff Moehlis. On the precision of noisy oscillators. Department of Mechanical Engineering, University of California, Santa Barbara, CA, Preprint, 2012.
- [81] P. Mohanty, D. A. Harrington, K. L. Ekinici, Y. T. Yang, M. J. Murphy, and M. L. Roukes. Intrinsic dissipation in high-frequency micromechanical resonators. *Phys Rev B*, 66:085416, 2002.
- [82] F. Mohd-Yasin, D. J. Nagel, and C. E. Korman. Noise in mems. *Measurement Science and Technology*, 21:012001, 2010.
- [83] Martin H. Müser, Michael Urbakh, and Mark O. Robbins. Statistical mechanics of static and low-velocity kinetic friction. In I. Prigogine and Stuart A. Rice, editors, *Advances in Chemical Physics*, volume 126, pages 187–272. John Wiley & Sons Inc., 2003.
- [84] E. B. Myers, F. J. Albert, J. C. Sankey, E. Bonet, R. A. Buhrman, and D. C. Ralph. Thermally activated magnetic reversal induced by a spin-polarized current. *Phys Rev Lett*, 89:196801, 2002.
- [85] N. Sri Namachchivaya. Stochastic bifurcation. *Applied Mathematics and Computation*, 38:101–159, 1990.
- [86] N. Sri Namachchivaya and Y. K. Lin. Method of stochastic normal forms. *International Journal of Non-Linear Mechanics*, 26:931–943, 1991.
- [87] Anatoly Neishtadt. On stability loss delay for dynamical bifurcations. *Discrete and Continuous Dynamical Systems Series S*, 2:897–909, 2009.
- [88] Tomáš Novotný. Josephson junctions as threshold detectors of full counting statistics: open issues. *Journal of Statistical Mechanics: Theory and Experiment*, 2009:P01050, 2009.
- [89] L. A. Oropeza-Ramos, C. B. Burgner, and K. L. Turner. Robust micro-rate sensor actuated by parametric resonance. *Sensors and Actuators A: Physical*, 152(1):80–87, 2009.
- [90] H.W.C. Postma, I. Kozinsky, A. Husain, and M.L. Roukes. Dynamic range of nanotube- and nanowire-based electromechanical systems. *Applied Physics Letters*, 86:223105, 2005.
- [91] Michael V. Requa and Kimberly L. Turner. Precise frequency estimation in a microelectromechanical parametric resonator. *App. Phys. Lett.*, 90:173508, 2007.
- [92] Jeffery F. Rhoads, Steven W. Shaw, and Kimberly L. Turner. Nonlinear dynamics and its applications in micro- and nanoresonators. *Journal of Dynamic Systems, Measurement, and Control*, 132:034001, 2010.

- [93] H. Risken. *The Fokker-Planck Equation: Methods of Solution and Applications*. Springer, 2nd edition, 1996.
- [94] M. L. Roukes. Nanoelectromechanical systems face the future. *Physics World*, 14:25–31, 2001.
- [95] Y. Sang, M. Dubé, and M. Grant. Thermal effects on atomic friction. *Phys Rev Lett*, 87:174301, 2001.
- [96] I. Serban, M. I. Dykman, and F. K. Wilhelm. Relaxation of a qubit measured by a driven duffing oscillator. *Phys. Rev. A*, 81:022305, 2010.
- [97] I. Siddiqi, R. Vijay, M. Metcalfe, E. Boaknin, L. Frunzio, R. J. Schoelkopf, and M. H. Devoret. Dispersive measurements of superconducting qubit coherence with a fast latching readout. *Phys Rev B*, 73:054510, 2006.
- [98] I. Siddiqi, R. Vijay, F. Pierre, C. M. Wilson, M. Metcalfe, C. Rigetti, L. Frunzio, and M. H. Devoret. Rf-driven josephson bifurcation amplifier for quantum measurement. *Phys Rev Lett*, 93:207002, 2004.
- [99] J. Sieber, A. Gonzalez-Buelga, S. A. Neild, D. J. Wagg, and B. Krauskopf. Experimental continuation of periodic orbits through a fold. *Phys. Rev. Lett.*, 100:244101, 2008.
- [100] V. N. Smelyanskiy, M. I. Dykman, H. Rabitz, and B. E. Vugmeister. Fluctuations, escape, and nucleation in driven systems: Logarithmic susceptibility. *Phys Rev Lett*, 79:3113–3116, 1997.
- [101] S. M. Soskin, R. Mannella, and P. V. E. McClintock. Zero-dispersion phenomena in oscillatory systems. *Physics Reports*, 373:247–408, 2003.
- [102] Michael J. Stephen. Noise in a driven josephson oscillator. *Physical Review*, 186:393–397, 1969.
- [103] N. G. Stocks, R. Mannella, and P. V. E. McClintock. Influence of random fluctuations on delayed bifurcations: The case of additive white noise. *Phys Rev A*, 40:5361–5369, 1989.
- [104] N. G. Stocks, R. Mannella, and P. V. E. McClintock. Influence of random fluctuations on delayed bifurcations. ii. the cases of white and colored additive and multiplicative noise. *Phys Rev A*, 42:3356–3362, 1990.
- [105] Eugene V. Sukhorukov and Andrew N. Jordan. Stochastic dynamics of a josephson junction threshold detector. *Phys Rev Lett*, 98:136803, 2007.
- [106] J. Z. Sun, J. C. Slonczewski, P. L. Trouilloud, D. Abraham, Ian Bacchus, W. J. Gallagher, J. Hummel, Yu Lu, and G. Wright. Thermal activation-induced sweep-rate dependence of magnetic switching astroid. *App. Phys. Lett.*, 78(25):4004–4006, 2001.

- [107] Masuo Suzuki. Anomalous fluctuation and relaxation in unstable systems. *Journal of Statistical Physics*, 16:477–504, 1977.
- [108] Masuo Suzuki. Scaling theory of non-equilibrium systems near the instability point. iii. *Progress of Theoretical Physics*, 57:380–392, 1977.
- [109] J. Tobiska and Yu. V. Nazarov. Josephson junctions as threshold detectors for full counting statistics. *Phys Rev Lett*, 93:106801, 2004.
- [110] M. C. Torrent and M. San Miguel. Stochastic-dynamics characterization of delayed laser threshold instability with swept control parameter. *Phys Rev A*, 38:245–251, 1988.
- [111] M. C. Torrent, F. Sagués, and M. San Miguel. Dynamics of sweeping through an instability: Passage-time statistics for colored noise. *Phys Rev A*, 40:6662–6672, 1989.
- [112] A. V. Tsukanov. Nanoelectromechanical systems and quantum information processing. *Russian Microelectronics*, 40:254–267, 2011.
- [113] Michael Urbakh, Joseph Klafter, Delphine Gourdon, and Jacob Israelachvili. The nonlinear nature of friction. *Nature*, 430:525–528, 2004.
- [114] D. F. Urban and Hermann Grabert. Feedback and rate asymmetry of the josephson junction noise detector. *Phys. Rev. B*, 79:113102, 2009.
- [115] R. H. Victora. Predicted time dependence of the switching field for magnetic materials. *Phys Rev Lett*, 63:457–460, 1989.
- [116] R. Vijay, M. H. Devoret, and I. Siddiqi. Invited review article: The josephson bifurcation amplifier. *Review of Scientific Instruments*, 80:111101, 2009.
- [117] D. Vion, M. Gotz, P. Joyez, D. Esteve, and M. H. Devoret. Thermal activation above a dissipation barrier: Switching of a small josephson junction. *Phys Rev Lett*, 77(16):3435–3438, 1996.
- [118] Philip S. Waggoner and Harold G. Craighead. Micro- and nanomechanical sensors for environmental, chemical, and biological detection. *Lab on a Chip*, 7:1238–1255, 2007.
- [119] W. Wernsdorfer, M. Murugesu, A. J. Tasiopoulos, and G. Christou. Field-sweep-rate dependence of the coercive field of single-molecule magnets: A classical approach with applications to the quantum regime. *Phys. Rev. B*, 72:212406, 2005.
- [120] W. Wernsdorfer, E. Bonet Orozco, K. Hasselbach, A. Benoit, B. Barbara, N. Demoncy, A. Loiseau, H. Pascard, and D. Mailly. Experimental evidence of the nel-brown model of magnetization reversal. *Phys Rev Lett*, 78:1791–1794, 1997.

- [121] Y. T. Yang, C. Callegari, X. L. Feng, K. L. Ekinici, and M. L. Roukes. Zeptogram-scale nanomechanical mass sensing. *Nano Letters*, 6:583586, 2006.
- [122] H. Zeghlache and Paul Mandel. Influence of noise on delayed bifurcations. *Phys Rev A*, 40:286–294, 1989.